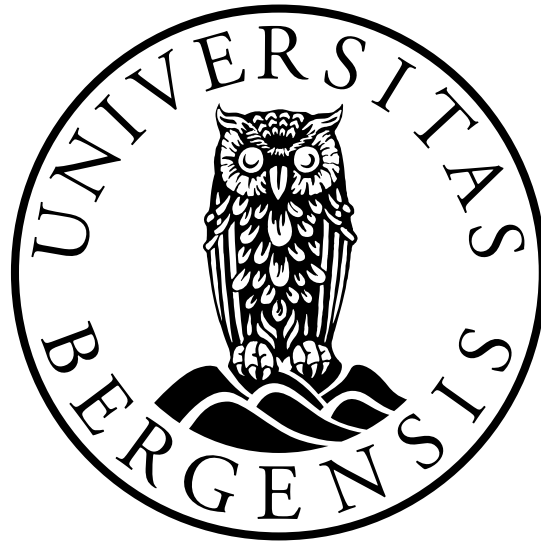# UNIVERSITY OF BERGEN

Department of Physics and Technology

MASTER'S THESIS IN OCEAN TECHNOLOGY

Digital twin of a hydraulic accumulator for virtual detection of subsea leaks

---

By Otto Andreas Moe

June 3, 2019

Abstract

In cooperation with OneSubsea, this thesis investigates the reasons behind a sudden pressure drop occurring in hydraulic systems during operation of hydraulic accumulators. The thesis also addresses the challenge of detecting and locating leaks in hydraulic systems.

A hydraulic system that is located topside on a floating production storing offloading vessel (FPSO) delivers barrier fluid to a subsea processing facility. Hydraulic pumps pressurize the hydraulic fluid, and the pressure energy is stored in high-pressure accumulators. This high-pressure system then delivers hydraulic fluid to a low-pressure system through a valve. From here the hydraulic fluid is stored in low-pressure accumulators, and hydraulic fluid is continuously delivered through an umbilical to a subsea system.

As it follows from industrial experience, after pressure charging of the low-pressure accumulators, when the supply valve is being closed, a sudden pressure drop occurs in the corresponding pipeline. This issue has been investigated.

In this project, the accumulator has been modeled with the use of Computational Fluid Dynamics (CFD) where the piston-fluid interaction has been accounted for. This has been done by using the overset mesh technique together with Dynamic Fluid Body Interaction method (DFBI) Rotation and Translation, which is embedded in the CFD software Simens Simcenter STAR-CCM+. In a sensitivity analysis, simulation results have been compared with measured data, and a virtual digital twin has been developed, with an average discrepancy of 1.06 % compared with measured pressure data set 3. This virtual digital twin with a smooth friction shift has been seen as the best alternative to be taken further for leak detection assignments.

This thesis closes with a summary of the conducted simulations, and suggestions for future work to improve the virtual model.

Preface

This thesis is the result of a Master of Science project at the Department of Physics and Technology (IFT) at the University of Bergen (UiB). The master thesis is an obligatory part of the study program worth 60 credit points (ECTS) to obtain a Master of Science degree in Ocean Technology, Marine Installations. The problem in question was provided by OneSubsea Processing AS.

I thank my supervisor Professor Boris V. Balakin at the Department of Mechanical and Marine Engineering (IMM) at Western Norway University of Applied Sciences (HVL), for his guidance through the project. I am truly thankful for his availability and his interest in numerical modeling and computational fluid dynamics.

I express my grattitude to Gleb Pisarev and OneSubsea Processing AS for assigning this project to me. I am truly grateful to Gleb Pisarev, who have provided me with support, information, and measured data regarding the system of interest.

Special thanks are given to the accumulator company Hydroll for their help in providing information and drawings of the Hydroll accumulator. I also express my gratitude to the hydraulic company HAWE for providing information regarding the orifice, to the Shell Lubricants distributor in Norway Univar for providing information regarding the barrier fluid, and Aratron Hydraulikk AS and Wandfluh for providing information regarding the solenoid valve.

Last but not least, I would like to thank Professor Bjørn Tore Hjertaker at IFT who has provided advice and support through the whole master degree, his dedication in measurement technology has been a great inspiration.

Bergen, June 3, 2019

Otto Andreas Moe

Contents

List of Tables

List of Figures

Nomenclature

Abbrevations

CAD   Computer-aided Design
CFD   Computational Fluid Dynamics
DFBI   Dynamic Fluid Body Interaction
FPSO   Floating Production Storage Offloading vessel
HPU   Hydraulic Power Unit
HP   High pressure
LP   Low pressure
MEG   Monoethylene Glycol
VOF   Volume of fluid method

Roman symbols

Cv   Ball valve flow coefficient imperial
E Total energy [J]
F_{app} Applied force [N]
F_C Coulomb friction force [N]
F_R Friction force [N]
F_S Maximum static friction [N]
F_v Viscous friction force [N]
F_x Force in x-direction [N]
$\vec{F}$ Force vector [N]

H	Height [m]
K	Valve coefficient
Kv	Ball valve flow coefficient metric
N	Normal force [N]
Q	Volume flow [m^3/s]
$\vec{S}$	Surface area [m^2]
T	Absolute Temperature [K]
T_0	Ambient temperature [K]
T_{Cr}	Crtitical temperature [Pa]
T_R	Reduced temperature
$\vec{V}$	Velocity vector [m/s]
$V\!\!\!/$	Volume [m^3]
$V\!\!\!/_0$	Precharge volume [m^3]
$V\!\!\!/_1$	Initial volume [m^3]
a_x	acceleration in x-direction [m/s^2]
$\vec{a}$	Acceleration vector [m/s^2]
d	Diameter [m]
e	Internal energy per unit mass [J/kg]
f_x	Body force on fluid element in x-direction per unit mass [N/kg]
k	Thermal conductivity [W/m·K]
k_{tanh}	Slope constant for the Coulomb tanh friction function
k_v	Viscous friction coefficient
m	Mass [kg]
p	Pressure [Pa]
p_0	Precharge pressure [Pa]
p_1	Initial pressure [Pa]
p_2	full charge pressure [Pa]
p_{Cr}	Critical pressure [Pa]
p_{HP}	Pressure in high pressure system [Pa]
p_{LP}	Pressure in low pressure system [Pa]
p_R	Reduced pressure
Δp	pressure loss [Pa]
$\dot{q}$	Rate of volumetric heat addition per unit mass [J/kg·s]
t	Time [s]
u	x-component of the velocity [m/s]
$v = \dot{x}$	Velocity [m/s^2]
v_m	Mean velocity [m/s]
v_S	Sliding speed coefficient
$\frac{V^2}{2}$	Kinetic energy per unit mass [J/kg]

Greek symbols

ϵ	Pipe roughness [m]
ρ	Density [kg/m^3]
ζ	Loss coefficient
λ	Pipe coefficient of friction
μ	friction coefficient
$\hat{\mu}$	Orifice flow coefficient
τ_{xx}	Normal stress [N/m^2]
τ_{yx}	Shear stress [N/m^2]
τ_{zx}	Shear stress [N/m^2]
∇	Vector differential operator

Chapter 1

Introduction

It is estimated that 47 % of all the remaining hydrocarbon resources on the Norwegian shelf is undiscovered, and of this, more than 60 % are expected to lie in the Barents Sea. This estimate from the Norwegian Petroleum Directorate in 2018 shows that the remaining undiscovered resources could provide the basis for oil and gas production over several decades to come [7]. When meeting the harsh and untouched nature in the Arctic, the existing production systems must be adapted to encounter the cold conditions and strict regulations. A significant part of these production systems will then be stationed subsea.

These subsea installations are operated by hydraulic systems that control hydraulically operated parts and hydraulic actuators such as valves, chokes, and manifolds. In these components the pressure exceeds ambient, and in case of a crack, hole or porosity, leakage is possible. The hydraulic system used in subsea processing usually uses a water-based hydraulic fluid that is environmentally non-hazardous. Early leak detection for hydraulic systems that control components such as multiphase pumps, blowout preventers, and production manifolds could still prevent serious deviations that could cause severe failures that potentially would lead to substantial repair costs and present a high risk for the environment. In addition to this, a leak also represents unnecessary consumption of control fluid that goes to waste, which also leads to further financial losses. Other systems that are used in the industry, such as Monoethylene Glycol (MEG) injection, boosting, and compression systems use toxic and hardly bio-degradable organic fluids [8]. A Leakage from such equipment is not tolerable, not only due to the enormous capital losses related to potential failures but especially regarding marine pollution. The harsh environment of the Arctic may complicate mitigation of such leaks, and it is questionable if water-based control fluids can be used in Arctic environments.

According to statistics from the Norwegian Petroleum Directorate [9], the annual degree of marine pollution by petroleum-related chemicals represents 152 000 ton, from where

up to 6 % are addressed to leaks from technological equipment. These losses of industrial fluids, considering the cost price of fluid, as well as all regulatory, operational, and reputational cost, stands for huge expenses even at the present state. An increase in the use of subsea installations will probably not improve this situation, but somewhat additionally complicate the control of the leaks. New research and technology are required to detect and locate these leaks.

In an article from Teknisk Ukeblad [10], the development of a leak detection device is presented. Primarily developed for the water distribution systems, this technology requires significant domestic improvements before it can be used in the oil and gas industry.

In collaboration with OneSubsea, this master project is to be conducted in the field of hydraulics and fluid dynamics with the use of computational methods. The project is aimed towards hydraulic accumulators and centrifugal pumps in a hydraulic system, and the main goal is to develop a virtual digital twin of a piston accumulator that can be used for leak detection assessment. A second goal of the project is to use the digital twin to understand a phenomenon that occurs in the charging process of hydraulic systems. Observations made by OneSubsea shows a sudden pressure drop just after the charging process of a hydraulic system consisting of two piston accumulators. When the pressure has reached the specified level, and the inlet valve closes, a pressure drop occurs during the first ∼ 30 seconds. It is desired to investigate the underlying causes of this pressure drop.

In a thesis by Hiis [11], the predecessor to a closely related project, a model of an accumulator is described. The Hiis model was developed in computational fluid dynamics (CFD) to be used to get a better understanding of the accumulator discharge process. The accumulator model that was developed in this project did not include a solid piston, and the thesis concluded with the recommendation to create a more realistic accumulator geometry, where the piston should be included, and friction could be added [11]. A similar model of an accumulator was developed in a research paper published at the Scandinavian International Conference on Fluid Power [12]. This model was used to study the thermodynamic processes involved in the operation of hydraulic accumulators. The model presented in this conference paper from 2017 introduced a solid piston by using three main physical regions that correspond to the liquid, gas, and solid regions. However, in this model, gravity was neglected, and the friction force was not mentioned. Therefore it is desired to develop a functioning model that also can model the friction forces that acts on the piston.

1.1 Project objective

The master project aims to analyze the industrial hydraulic system that is required to operate the OneSubsea subsea multiphase pump. The focus has been directed towards the Hydraulic Power Unit (HPU) and umbilical in the hydraulic system, and the instance where a hydraulic accumulator has been pressurized to a specific level and further acts as the main driver in the system. As it follows from industrial experience, during pressure charging, and when the inlet valve is being closed, a sudden pressure drop occurs in the system. This process lasts for ~ 30 seconds. The problem statement has been to look at and search for the reason leading to this pressure drop. It is desired to develop a virtual digital twin of the system using computational fluid dynamics (CFD), and run simulations that can be compared with existing measured data. This digital twin can then later be used in further CFD analysis, to search for potential leaks in the system.

1.2 The hydraulic system

The system that is in focus is a hydraulic system that delivers barrier fluid to a subsea multiphase pump. The hydraulic system and its main components have been shown in Fig. 1.1, to get an overview of the hydraulic system.
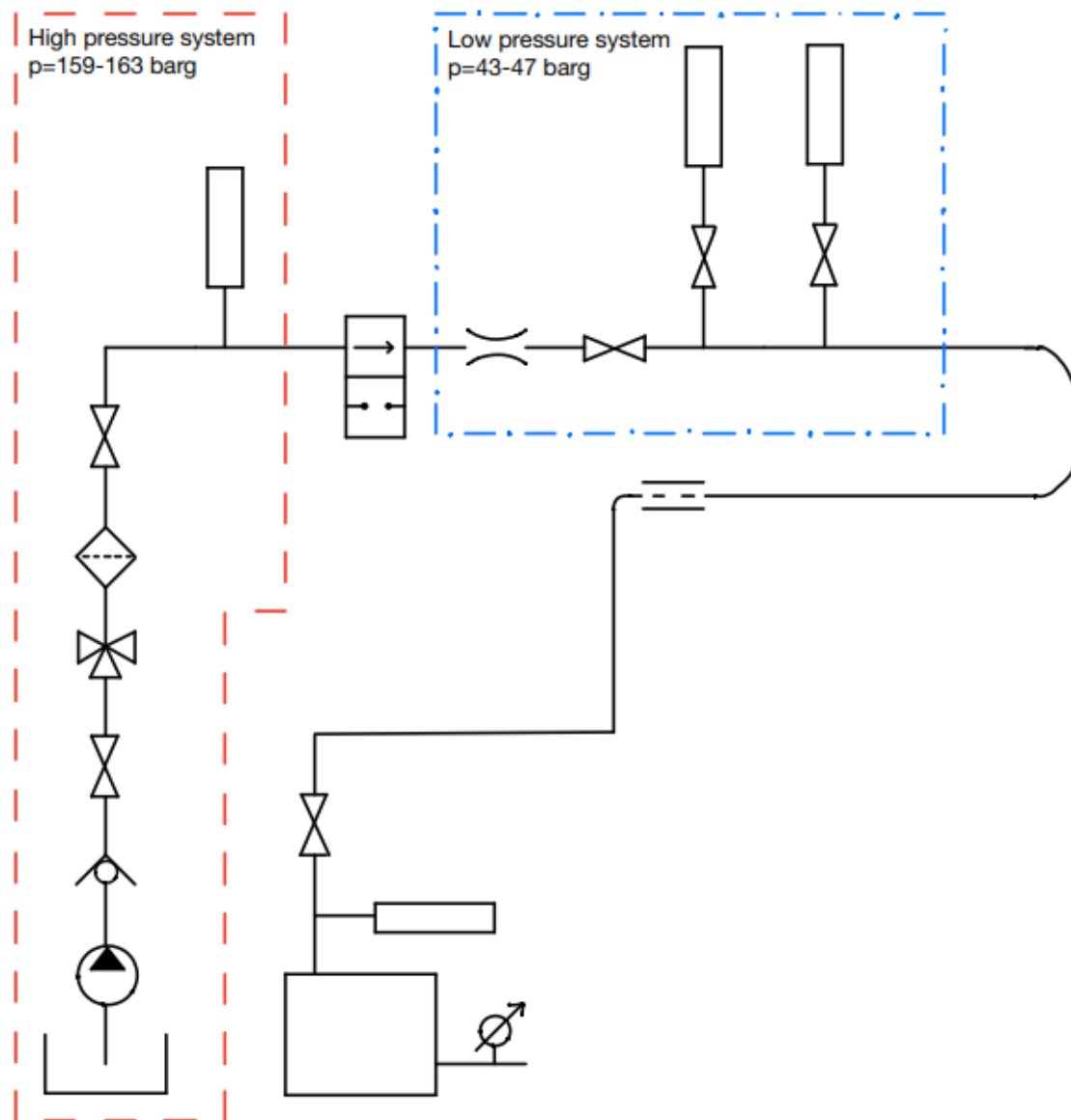
Figure 1.1: Schematics of the hydraulic system divided into a high pressure system and a low pressure system.

Fig. 1.1 shows the main components of the HPU that is located topside on the floating production storage offloading vessel (FPSO). The HPU main components consist of reservoirs, hydraulic pumps, valves, accumulators, piping, and umbilical. The umbilical delivers the barrier fluid down subsea to a multiphase pump.

As shown in Fig. 1.1, the system is divided into a high pressure (HP) system on the left

and low pressure (LP) system on the right. The pressure in the HP system varies between 159-163 barg and is maintained by the use of pumps and two pieces 15 l high-pressure accumulators precharged with 144 barg to store pressure. Flow is delivered from the HP system to the LP system through a valve. In the LP system, two pieces 10 l low-pressure accumulators precharged with 39 barg and 55 barg store the pressure. The pressure in the LP system varies between 43-47 barg. The solenoid valve separating the HP and LP systems is opened when the pressure reduces to 43 barg and closes when the pressure has reached 47 barg.

A block diagram can be used to simplify and visualize the hydraulic system, as shown below:
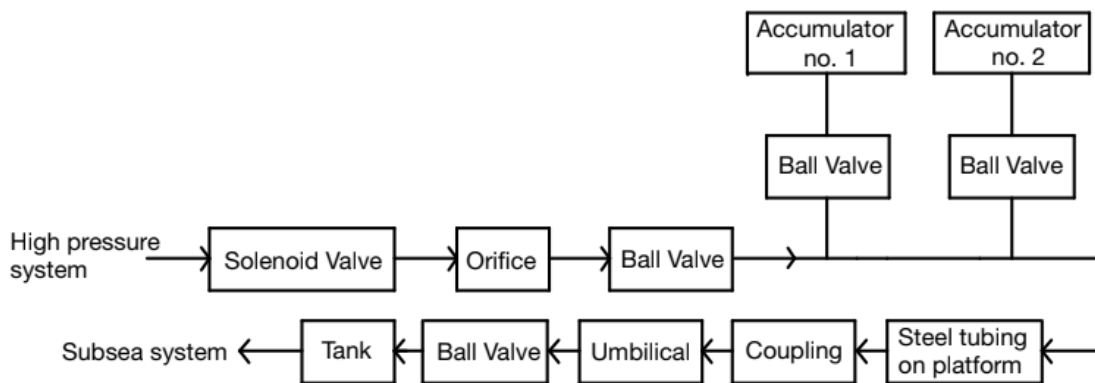
Figure 1.2: Block diagram of the hydraulic system.

The block diagram in Fig. 1.2 shows the direction of flow from the high-pressure system through the different components of the system. The accumulators no. 1 and no. 2 stores pressure, to continuously deliver barrier fluid to the subsea system.

The situation of interest is the charging process of the two accumulators, and Fig. 1.3 shows a plot of acquired measured pressure data from the LP system for the situation of interest. All graphs presented in this thesis have been made in Matlab, and the scripts are shown in Appendix B.
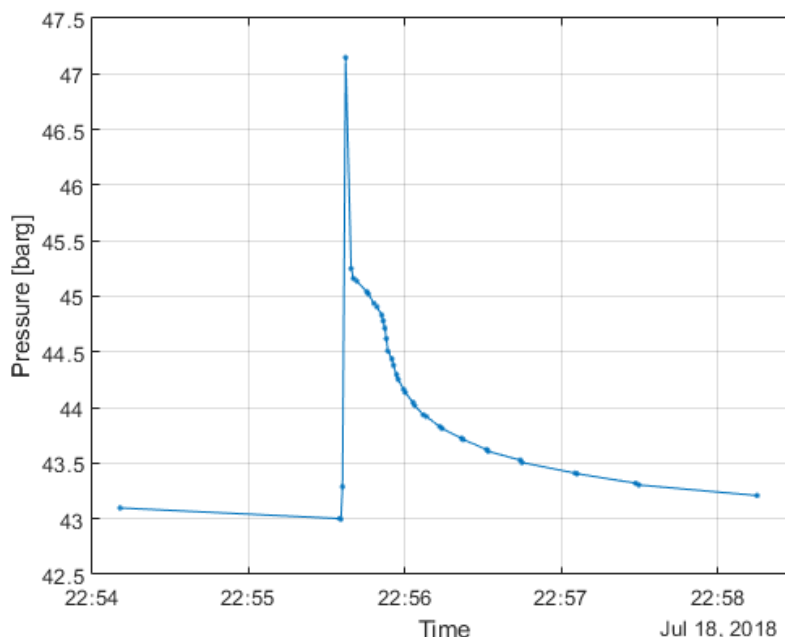
Figure 1.3: Plot of the measured pressure data in the LP system.

In Fig. 1.3 the charging process can be seen where the pressure starts to rise when the pressure has decreased to 43 barg. The pressure then increases until the pressure has reached 47.15 barg, where the solenoid valve closes, and the charging of the accumulators is stopped. At this point, the pressure suddenly drops down about 2 bar before a smooth discharge can be seen.

In this project, the two accumulators in the LP system, have been modeled with the CFD software Simcenter STAR-CCM+, and the components that are relevant for the system have been presented more in detail in Chapter 3.

1.3   Virtual Digital Twin

A digital twin is a virtual representation of a physical product or process, that can be used to understand and predict the physical counterpart's performance characteristics. The virtual digital twin use measured data from sensors that are installed on the physical twin to model the physical behavior of the system accurately. With the help of this data, the digital twin can evolve and continuously update to reflect any changes that are made to the physical twin [13].

1.4 Subsea multiphase pump

The subsea multiphase pump is developed to add pressure energy to fluid consisting of a mixture of water, oil, gas, and sand. The pump is based on rotodynamic principle, as found in centrifugal pumps, and consists of several stages of impellers and diffusers, that increases the pressure to the fluid [14].

The rotation of an impeller transfers mechanical work to the fluid by the centrifugal force, and increases the pressure and absolute velocity of pump fluid. In the pump channel there is friction that decrease the relative velocity due to friction, and this also contributes to a pressure increase. The increase in absolute velocity caused by the rotation of the impeller is not wanted, depending on the shape of the volute casing or diffuser, this absolute velocity energy can be transformed into pressure energy and increase the pressure even further [15].

1.5 Barrier fluid

The barrier fluid is a hydraulic oil that secures the integrity of the subsea multiphase pump by pressurizing the motor casing, which prevents produced fluid in the pump from getting into the electrical parts. The barrier fluid also lubricates and cools the motor and pump bearings.

1.6 Hydraulic accumulator

A Hydraulic accumulator is a type of high-pressure vessel, that is developed to store and release pressure energy. This pressure energy is usually stored in a gas, a spring, or weight. Accumulators serves many purposes as it can serve as pressure delivery when a pump is decoupled for maintenance, it can function as an additional source to handle peak load, it can maintain the pressure in a closed system where leakages or temperature variations cause volume changes, it can equalize pressure fluctuations, and absorb instant pressure shocks [16].

1.7 Thesis outline

This thesis is divided into five chapters. The first chapter gives a brief introduction to the background of the project and why it is of interest. Chapter 2 describes the theory that has been used for modeling, and Chapter 3 describes the model setup. Chapter 4 presents the results and discussion regarding each simulation that have been carried out. The conclusion and ideas for future work are presented in Chapter 5.

Chapter 2

Theoretical Background

2.1   Governing equations of CFD

The CFD software that is used for this project is Simcenter STAR-CCM+, which can be used to model physics phenomena like fluid dynamics, solid mechanics, heat transfer, electromagnetism, and chemical reactions. STAR-CCM+ models the materials as a continua on a macroscopic scale, and the physics of the continua are described with a set of mathematical models derived from fundamental laws that express conservation principles. In continuum mechanics, the behavior of the continua is studied in response to mechanical forces, and the equations that express the fundamental laws that govern the mechanics of fluids are the continuity, momentum, and energy equations which describes the conservation of mass, conservation of momentum, and conservation of energy respectively [3].

By applying these equations to an infinitesimal volume element of a flowing fluid, a set of partial differential equations are obtained which, completely describe the three-dimensional flow field, this in the form of the continuity and Navier-Stokes equations. In general, these equations, cannot be solved analytically, but only solved numerically [17].

The conservation laws can be expressed using an Eulerian approach or a Lagrangian approach. In the Eulerian approach, space is represented with a given volume where the material can flow through. The Lagrangian approach usees a given volume to represent a small portion of the material, and this material then moves through space [3]. By either looking at a control volume fixed in space with the fluid moving through it or by looking at a moving control volume that always contains the same fluid particles, one can obtain the conservation form and the non-conservation form respectively [2]. STAR-CCM+ use both these approaches, and use the most convenient to model the given field of physics.

In the following the fundamental laws and equations that govern the mechanics of fluids

have been discussed to give an introduction to the equations that are solved in the CFD software STAR-CCM+.

2.1.1   Continuity equation

The continuity equation expresses the balance of mass through a control volume. If considering a finite control volume that is fixed in space, as seen in Fig. 2.1 the conservation form of the continuity equation can be obtained.
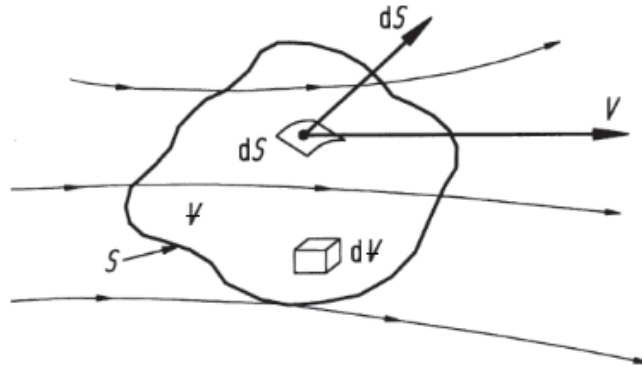
Figure 2.1: Finite control volume fixed in space [2].

In Fig. 2.1, $\vec{V}$ is the flow velocity at a point on the control surface, $d\vec{S}$ is the elemental surface area, and $d\Psi$ is the elemental volume inside the finite control volume [2].
The principle that mass is conserved applies to the control volume as follows:

$$\begin{Bmatrix} \text{Net mass flow out} \\ \text{of control volume} \\ \text{through surface} \end{Bmatrix} = \begin{Bmatrix} \text{Time rate of decrease} \\ \text{of mass inside control} \\ \text{volume} \end{Bmatrix} \tag{2.1.1}$$

For the left side of Eqn.(2.1.1) the net mass of the control volume across the area S, can be expressed as a surface integral as shown below.

$$\oiint_S \rho \vec{V} \cdot \vec{d}S \tag{2.1.2}$$

In Eqn.(2.1.2), $\vec{d}S$ is the area of the elemental mass that by convention always points in an outward direction of the control volume. Hence, the outflow is defined as positive.

For the right hand side of Eqn.(2.1.1) the total mass m that is contained inside the control volume Ψ is expressed as in the following equation.

$$\oiiint_\Psi \rho \, d\Psi \tag{2.1.3}$$

From the expression for total mass as in Eqn.(2.1.3), the time rate of decrease of mass inside $V\!\!\!\!/$ then becomes:

$$-\frac{\partial}{\partial t} \oiiint_{V\!\!\!\!/} \rho \, \mathrm{d}V\!\!\!\!/ \tag{2.1.4}$$

Eqn.(2.1.2) and Eqn.(2.1.4) is substituted into Eqn.(2.1.1) and the equation is rearranged to get the integral form of the continuity equation in conservation form:

$$\frac{\partial}{\partial t} \oiiint_{V\!\!\!\!/} \rho \, \mathrm{d}V\!\!\!\!/ + \oiint_{S} \rho \vec{V} \cdot \vec{\mathrm{d}}S = 0 \tag{2.1.5}$$

The limits of integration are constant since the control volume is fixed in space. Therefore, Eqn.(2.1.5) can be written with the time derivative inside the integral as in the following equation.

$$\oiiint_{V\!\!\!\!/} \frac{\partial}{\partial t} \rho \, \mathrm{d}V\!\!\!\!/ + \oiint_{S} \rho \vec{V} \cdot \vec{\mathrm{d}}S = 0 \tag{2.1.6}$$

The divergence theorem states that the surface integral in Eqn.(2.1.6) can be expressed as a volume integral, which when simplified yields:

$$\oiiint_{V\!\!\!\!/} \left[\frac{\partial}{\partial t} \rho + \nabla \cdot (\rho \vec{V}) \right] \mathrm{d}V\!\!\!\!/ = 0 \tag{2.1.7}$$

Eqn.(2.1.7) must hold for any domain in the fluid. The only way the integral can be equal to zero is when the integrand is equal to zero, and this has to be true for every point within the control volume. Hence Eqn.(2.1.7) can be written as follows.

$$\frac{\partial}{\partial t} \rho + \nabla \cdot (\rho \vec{V}) = 0 \tag{2.1.8}$$

Eqn.(2.1.8) is the continuity equation in conservation form.

2.1.2   Momentum equation

Newton's second law states that the rate of change of momentum of a body is directly proportional to the force applied. This change in momentum takes place in the direction of the applied force. The law can further be expressed in terms of the acceleration of the object as shown in Eqn.(2.1.9).

$$\vec{F} = m\vec{a} \tag{2.1.9}$$

Eqn.(2.1.9) is a vector relation and can be split into scalar relations along x, y, and z-direction. Fig. 2.2 shows a model of a moving fluid element, considering the scalar x-component.
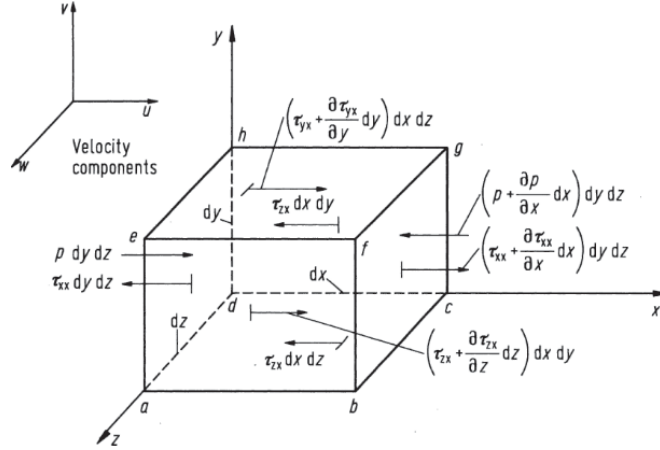
Figure 2.2: Infinitesimally small, moving fluid element. Only forces in the x-direction are shown [2].

When only looking at forces in the x-direction, the Eqn.(2.1.9) can be written in scalar form as follows:

$$F_x = ma_x \tag{2.1.10}$$

In Eqn.(2.1.10), F_x is the force in x-direction, and a_x is the acceleration in x-direction. For the left-hand side of this equation, two types of forces are acting, the body forces and the surface forces. The body forces are forces that act directly on the fluid element, such as gravitational, magnetic, and electric forces. The surface forces act directly on the surface of the fluid element, in the form of pressure distribution acting on the surface caused by the surrounding fluid, and shear and normal stress distributions that acts on the surface due to friction from the surrounding fluid [2].

By applying these forces to Eqn.(2.1.10), the momentum equation in the x-direction, also known as the Navier-Stokes equation can be derived. The Navier-Stokes equation in conservation form are shown in the following equation.

$$\frac{\partial(\rho u)}{\partial t} + \nabla \cdot (\rho u \vec{V}) = -\frac{\partial p}{\partial x} + \frac{\partial \tau_{xx}}{\partial x} + \frac{\partial \tau_{yx}}{\partial y} + \frac{\partial \tau_{zx}}{\partial z} + \rho f_x \tag{2.1.11}$$

The right hand side of Eqn.(2.1.11), is due to the body and surface forces, where τ_{xx} is the normal stress, τ_{yx} and τ_{zx} represents the shear stress, and ρf_x is the body force on the fluid element acting in x-direction. The left hand side of Eqn.(2.1.11) represents the ma_x therm from Eqn.(2.1.10) [2]. The Navier-Stokes equations for y, and z-direction are shown in Eqn.(2.1.12), and Eqn.(2.1.13) respectively.

$$\frac{\partial(\rho v)}{\partial t} + \nabla \cdot (\rho v \vec{V}) = -\frac{\partial p}{\partial y} + \frac{\partial \tau_{xy}}{\partial x} + \frac{\partial \tau_{yy}}{\partial y} + \frac{\partial \tau_{zy}}{\partial z} + \rho f_y \tag{2.1.12}$$

$$\frac{\partial(\rho w)}{\partial t} + \nabla \cdot (\rho w \vec{V}) = -\frac{\partial p}{\partial z} + \frac{\partial \tau_{xz}}{\partial x} + \frac{\partial \tau_{yz}}{\partial y} + \frac{\partial \tau_{zz}}{\partial z} + \rho f_x \tag{2.1.13}$$

2.1.3 The energy equation

The first law of thermodynamics states the principle that energy is conserved. This law applies to a moving fluid element as described in the following equation:

$$
\left\{ \begin{array}{c} \text{Rate of change of} \\ \text{energy inside the} \\ \text{fluid element} \\ \text{(a)} \end{array} \right\} = \left\{ \begin{array}{c} \text{Net heat flux} \\ \text{into} \\ \text{the element} \\ \text{(b)} \end{array} \right\} + \left\{ \begin{array}{c} \text{Rate of work done on} \\ \text{the element due to body} \\ \text{and surface forces} \\ \text{(c)} \end{array} \right\} \quad (2.1.14)
$$

In Eqn.(2.1.14), the last therm (c) describes the body forces $\rho \vec{f} \cdot \vec{V}(dxdydz)$, and the surface forces as shown in Fig. 2.3.
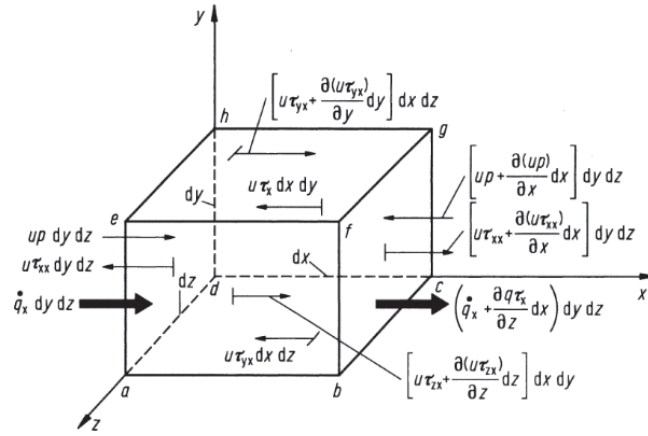
Figure 2.3: Energy fluxes associated with an infinitesimally small, moving fluid element. For simplicity, only the fluxes in the x direction are shown [2]

As shown in Fig. 2.3 for the x-direction, the surface forces is the x-component of the velocity u, multiplied with the forces due to pressure and shear forces. The (b) therm in Eqn.(2.1.14), refers to the volumetric heating e.g. absorption or emission of radiation, and the heat transfer over the surface due to temperature gradients. The (a) therm is the time rate of the energy in the fluid element.

The conservation form of the energy equation is shown in the following equation [2].

$$
\frac{\partial}{\partial t}\left[\rho\left(e + \frac{V^2}{2}\right)\right] + \nabla\left[\rho\left(e + \frac{V^2}{2}\vec{V}\right)\right] =
$$
$$
\rho\dot{q} + \frac{\partial}{\partial x}\left(k\frac{\partial T}{\partial x}\right) + \frac{\partial}{\partial y}\left(k\frac{\partial T}{\partial y}\right) + \frac{\partial}{\partial z}\left(k\frac{\partial T}{\partial z}\right)
$$
$$
-\frac{\partial(up)}{\partial x} - \frac{\partial(vp)}{\partial y} - \frac{\partial(wp)}{\partial z} + \frac{\partial(u\tau_{xx})}{\partial x} + \frac{\partial(u\tau_{yx})}{\partial y} + \frac{\partial(u\tau_{zx})}{\partial z} +
$$
$$
\frac{\partial(v\tau_{xy})}{\partial x} + \frac{\partial(v\tau_{yy})}{\partial y} + \frac{\partial(v\tau_{zy})}{\partial z} + \frac{\partial(w\tau_{xz})}{\partial x} + \frac{\partial(w\tau_{yz})}{\partial y} + \frac{\partial(w\tau_{zz})}{\partial z} + \rho\vec{f}\cdot\vec{v}
$$

$$(2.1.15)$$

As seen in Eqn.(2.1.15), the total energy E is represented by the term $e + \frac{V^2}{2}$, where e is the contribution from the internal energy per unit mass and $\frac{V^2}{2}$ is the kinetic energy per unit mass. On the right-hand side of the equation, $\dot{q}$ is the rate of volumetric heat addition per unit mass, k is the thermal conductivity, and $\vec{f}$ is the total body force acting on the fluid element per unit mass [2].

2.2   Discretization

When solving the governing equations discussed in the previous section of this chapter, numerically methods are used, which only gives answers at discrete points in the domain. These points are called grid points and shown in Fig. 2.4
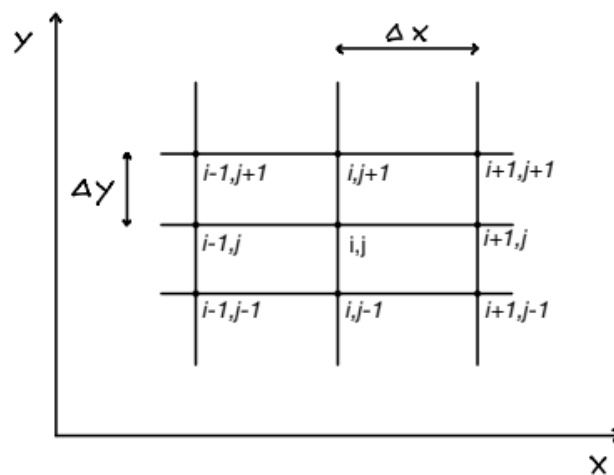
Figure 2.4: Discrete grid points

As seen in Fig. 2.4 these grid points are labeled with an index of i and j that runs in x and y-direction respectively, and the grid points are separated with a spacing of δx and δy. The discretization is used to replace the partial derivatives (or integrals) in the governing equations with discrete numbers. The discretization of the governing equations in partial differential form is called finite differences, and discretization in the integral form is called finite volumes [2]. The Navier Stokes-equations are normally solved on staggered grid where the pressure and the velocity are computed on different nodes, this to prevent a non physical situation.

2.3   Meshing

A mesh is the discretized representation of a geometric domain and is defined by a set of grid points, that forms a grid. This grid or mesh can be classified from its structure, shape, orthogonality, and other distinct features.

The mesh structure can be classified into either structured or unstructured type. The differences between the two are the way the cells are ordered, the structured grid has a consistent geometrical regularity, whereas the unstructured grid has grid points that are placed in an irregular pattern. The unstructured mesh has the advantage with its ability to fit complex geometry [2], and the advantage of the structured mesh is the easy connectivity between the cell neighbors.

Apart from the cell structure, there are also different cell shapes used in a mesh, which is controlled by a meshing model. The three most common meshing models include Tetrahedral, Polyhedral, and trimmed mesher [3]:

- The tetrahedral mesher use the tetrahedral cell shape to build the core mesh. It is the fastest of these three models, and it uses the least amount of memory for a given number of cells.

- The polyhedral mesher uses an arbitrary polyhedral cell shape to build the core mesh. It requires the same amount of surface preparation as the tetrahedral mesh, and hence relatively easy and efficient to build. In addition to this, it contains five times fewer cells than a tetrahedral mesh.

- The trimmed mesh is constructed by a template mesh of hexahedral cells that are trimmed or cut from the starting input surface. This meshing model is robust and efficient and can produce high-quality grid for simple and complex mesh geometries.

2.3.1   Prism layer mesher

The prism layer mesher creates an orthogonal prismatic volume mesh next to wall surfaces and boundaries and improves the accuracy of the flow solution. Parameters that define the prism layer are the thickness of the prism layer, number of layers, the distribution of size throughout the prism layer, and the function that generates the distribution [3].

2.3.2   Overset mesh

The overset mesh technique is a useful method when working with multiple or moving bodies. The technique is used to discretize a computational domain that can include different meshes that arbitrarily overlap each other. An example of the can be seen in the following figure.
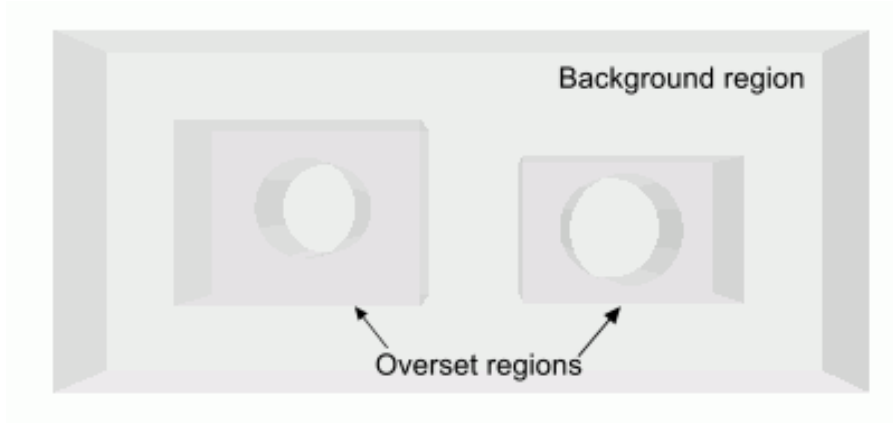
Figure 2.5: Example of overset mesh, on top of a background mesh [3].

Fig. 2.5 shows two overset regions that each surrounds a potentially moving body placed in a background region. The two overset meshes will move with the corresponding body, and the boundaries of these overset meshes are connected with the background mesh to complete the computational domain. The overset mesh consists of three different cells, active, inactive or acceptor cells, and the status of the cells changes depending on the movement of the overset mesh. The acceptor cells couples the background mesh and the overset mesh, and the discretized fundamental governing equations are solved in the active cells [3].

2.4   Dynamic Fluid Body Interaction (DFBI)

The DFBI is used to simulate the motion of a rigid body due to forces exerted by the physics continuum, or to any additional forces that have been defined. Examples of these additional forces include gravity force, friction force, and damping force. In STAR-CCM+ the body resultant force and moment is calculated, and the equations of motion are solved to find the new position of the body [3].

For DFBI there are two types of bodies. The continuum body and the mechanical body. The continuum body is used in situations where the body interacts with a physics continuum, and a mechanical body is a rigid structure that has no interaction with a physics continuum except the gravity [3].

When setting up a continuum body for DFBI, it is not necessary to model the interior of the body, only the interaction between the DFBI body and the physics continuum has to be set. For situations where heat transfer between the rigid body and the fluid is relevant, a solid region can be set for the rigid body. Other parameters to be set is the mass of the object, release time, ramp time, and body motion [3].

The release time is the time before the calculation of the motion of the body begins. It is recommended to allow some time for the fluid flow to initialize, that for an unsteady model the release time typically would be 10 to 50 time-steps. If the time-step is set to 0.01 s, then 50 time-steps would amount to 0.5 s. When the release time is reached, the forces and moments are applied, and this can cause a shock effect. The ramp time helps to get a more robust solution by reducing the oscillation. When the ramp time is set, forces and moments are applied proportionally across the interval to reduce the shock effects. The value for ramp time is typically ten times the release time [3]. Various body motions can be selected in the DFBI. The default motion type is the free body motion, where it can be decided which directions the motion should be calculated for, and which to leave locked [3].

2.5 Volume of fluid method (VOF)

The volume of fluid method (VOF) is an interface-capturing method that predicts the distribution and movement of the interface of immiscible phases [3]. This method treats the flow of the fluid with equivalent parameters, where the density, viscosity, and thermal properties of the fluid are set proportional to the volume fractions of the components (gas and liquid), while their transport is modeled with separate scalar transport equations. The distribution of the phases and the position of the interface are described by field functions in STAR-ccm+.

2.6   Friction force

Friction appears in all mechanical systems where surfaces are in contact. There exist many different friction models that each are suited for different situations. Generally, the friction is divided into four regimes, as shown in the following figure:
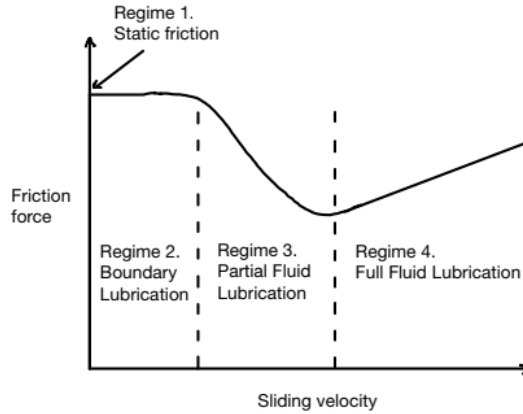
Figure 2.6: A generalized Stribeck curve, showing friction as a function of velocity for low velocities [4].

As seen in Fig. 2.6, the first regime consists of static friction, where the friction is independent of velocity. The second regime is where the velocity is very low and not sufficient to build a fluid film between the surfaces. The third regime is when the lubrication is being drawn in between the surfaces, and the thickness of the fluid film increases with rising velocity and greater viscosity. The fourth regime is when the fluid film has fully developed, and a rise in velocity will increase the magnitude of viscous friction force [4].

The Coulomb friction model is one of the most commonly used friction models and can be formulated as:

$$F_R = \begin{cases} F_C, & \text{if } v > 0 \\ F_{app}, & \text{if } v = 0 \text{ and } F_{app} < F_C \end{cases} \tag{2.6.1}$$

Where F_R is the friction force, $v = \dot{x}$ the sliding velocity, $F_C = \mu N$ is the Coulomb sliding friction force, μ is the friction coefficient, N normal force and F_{app} is the applied force.

The Coulomb friction model is often used to model dry friction but is also used for the boundary and mixed lubricated contacts. The equation of motion becomes strongly non-linear with the Coulomb friction model, and hence a viscous friction model is often used instead [5]:

$$F_v = k_v \cdot v \tag{2.6.2}$$

In Eqn.(2.6.2) F_v is the viscous friction force, k_v the viscous coefficient and v the sliding

velocity. The viscous friction model is considerably easier to simulate than the Coulomb friction model, and for some cases as with full film contacts, the viscous model may offer the best representation of the real friction behavior. The model does not always validate with the real friction behavior, but for particular running conditions, when tuning the viscous coefficient, the model can represent such things as damping quite well [5].

The Coulomb friction model and the viscous friction model can be combined to get a smoother transition when the direction of friction changes, as for oscillating motions. In the following figure, the Coulomb friction force, together with the viscous friction, are shown in graphs, both separately and combined.
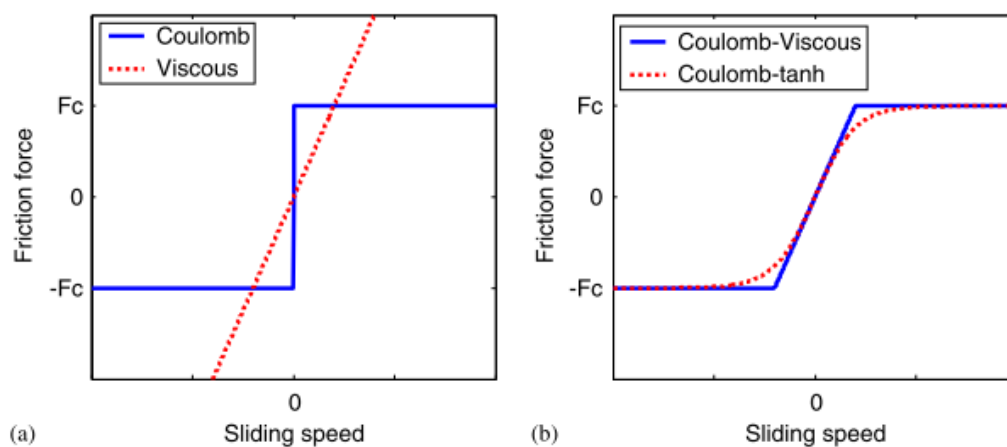
Figure 2.7: (a) Coulomb and viscous friction forces as function of sliding speed, (b) combined Coulomb and viscous friction and combined Coulomb and tanh friction as function of sliding speed [5].

In Fig.(2.7, b), the Coulomb-tanh function gives a smooth transition between positive and negative direction of friction. The Coulomb-tanh friction function can be written as in the following equation:

$$F_R = F_C \cdot tanh(k_{tanh} \cdot v) \tag{2.6.3}$$

In Eqn.(2.6.3), k_{tanh} is a constant to to control the slope. The combined Coulomb and viscous friction model, and the combined Coulomb and tanh friction model both have the disadvantage that they assume a friction force that is zero when the sliding speed is zero. Due to this, the friction force will only exist when motion is taking place, and this can cause inaccuracy in the final position [5].

Another friction model is the Stribeck friction model. In the generalized friction model, as shown in Fig. 2.6, it can be seen that for lubricated sliding contacts, the friction force will vary with the velocity of the sliding object. The magnitude of the friction force depends on whether the interacting contact surfaces are in the regime of the boundary, mixed or full film lubrication. For a lubricated sliding contact, the friction decreases with

increasing sliding speed until a full film situation is obtained, after which the friction either becomes constant, increase, or decrease with the increasing sliding velocity due to viscous and thermal effects [5]. The Stribeck friction is written as:

$$F_R = \left(F_C + (F_S - F_C) \exp\left(-\left(\frac{|v|}{v_s} \right)^i \right) \right) \text{sign}(v) + k_v \cdot v \tag{2.6.4}$$

In Eqn.(2.6.4) F_R is the Friction force, F_C is the Coulomb friction, F_s is the maximum static friction, v is the sliding velocity, v_s is the sliding speed coefficient, k_v is the viscous friction coefficient, and i is an exponent. This friction model can provide a good representation of the dynamic friction, and it covers both the Coulomb friction and the viscous friction as well [5].
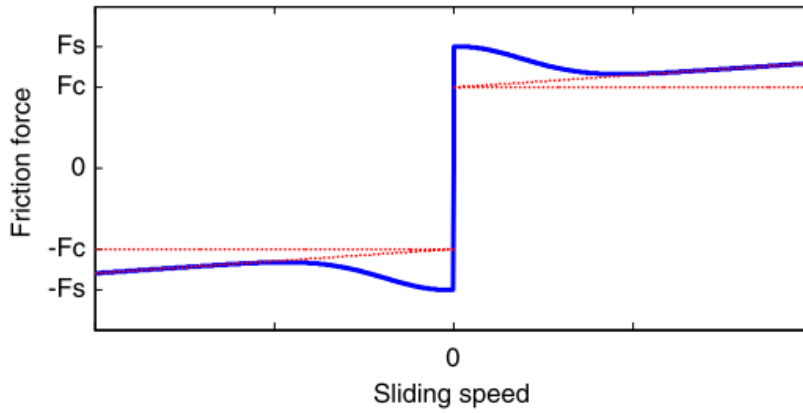
Figure 2.8: Graph showing the relation between friction force and sliding speed according to the Stribeck friction model, The red horizontal line represents the Coulomb friction, the top of the blue line represents the static friction, and the red angled line represents the viscous friction. [5].

As seen in Fig. 2.8, the blue line connects the Coulomb friction, the static friction, and the viscous friction into one model. The model does have the same problem as the Coulomb friction model when the sliding direction is changed. Therefore it is recommended to use a modified version of Eqn.(2.6.4) where the sign function is replaced with a tanh function [5]. Hence, the modified version of Eqn.(2.6.4) becomes:

$$F_R = \left(F_C + (F_S - F_C) \exp\left(-\left(\frac{|v|}{v_s} \right)^i \right) \right) \tanh(k_{\text{tanh}} \cdot v) + k_v \cdot v \tag{2.6.5}$$

In Eqn.(2.6.5), F_C is the Coulomb friction force, F_s is the maximum static friction force, k_{tanh} is a coefficient that determines how fast the tanh function changes from -1 to 1, k_v is the viscous damping force, v_s is the sliding speed coefficient, i an exponent. These parameters can all be determined from a dynamic friction test [5].

2.7 Accumulator thermodynamics

For the process of compression and expansion in an accumulator system, some basic thermodynamics is applied and is described in this section.

2.7.1 Basics of gas thermodynamics

In a quasi-equilibrium process where the system changes at a sufficiently slow rate to allow the system to adjust and remain infinitesimally close to equilibrium at all times, the ideal gas equation can be used as shown below.

$$p = \frac{RT}{V} \qquad (2.7.1)$$

Where p is the pressure, T the absolute temperature, and R the gas constant that varies for each gas. Nitrogen has a gas constant of $R = 0.2968$ kJ/kg·K. Many gases can be treated as ideal gases with minimal error, e.g., air, nitrogen, oxygen, hydrogen, helium, and argon [18]. The gas constant remains the same for a gas in any situation, and therefore the ideal gas law can be solved for the gas constant R to connect two different situations of the same system, as shown in the following equation:

$$\frac{p_1 \cdot V_1}{T_1} = \frac{p_2 \cdot V_2}{T_2} \qquad (2.7.2)$$

Eqn.(2.7.2) gives a relation between two situations (1), and (2). Often an isotherm version of this equation is used, where the process changes slowly and constant temperature can be assumed $T_1 = T_2$. If the state of a gas is close to the saturation region, the gas does not behave as an ideal gas. To determine if the ideal gas equation can be used the reduced temperature and reduced pressure are defined in the next two equations:

$$T_R = \frac{T}{T_{Cr}} \qquad (2.7.3)$$

In Eqn.(2.7.3) T_R is the reduced temperature, T the measured absolute temperature, and T_{Cr} the critical temperature.

$$p_R = \frac{p}{p_{Cr}} \qquad (2.7.4)$$

In Eqn.(2.7.4) p_R is the reduced pressure, p is the measured pressure, and p_{Cr} is the critical pressure.

All gases behave approximately the same way for the same T_R and p_R and when pressures are very low $p_R \ll 1$, gases behaves as ideal gases regardless of temperature. Also, at high temperatures $T_R > 2$, gases can be assumed to be ideal with good accuracy regardless of pressure except when $p_R \gg 1$ [18].

During actual compression and expansion process of gasses, the pressure and volume are described through the relation known as a polytropic process. Here the pressure and volume are related by:

$$p V^n = C \qquad (2.7.5)$$

In Eqn.(2.7.5), n is the polytropic exponent, C is a constant, p the pressure, and V the gas volume. For nitrogen the polytropic exponent $n = 1.2$ [16].

For a process where the change is fast, and there is not enough time for heat exchange to happen, the polytropic process is turned to an adiabatic process. An adiabatic process is a process where no heat transfer occurs and applies to situations where a system is at the same temperature as the surrounding temperature, or when a system is insulated so well that the heat transfer can be neglected. For an adiabatic process, the polytropic index $n = k$, where k is the adiabatic index defined as follows:

$$k = \frac{c_p}{c_v} \qquad (2.7.6)$$

In Eqn.(2.7.6) c_p and c_v are the specific heat at constant pressure and volume respectively. For nitrogen the adiabatic index $k = 1.4$ [16]. Eqn.(2.7.5) can be used to connect two different situations of the same system, as shown in the following equation:

$$p_1 V_1^n = p_2 V_2^n \qquad (2.7.7)$$

In Eqn.(2.7.7), $n = k$ for an adiabatic process.

Chapter 3

Modeling setup

In this chapter, system parameters that are relevant to the modeling of the system have been reviewed, and the model geometry has been described. In addition, the selections regarding mesh settings and the selected settings for physics conditions to the applicable situation has been described. The chapter closes with a section on changes and improvements that have been made to the different simulations. In the following, the system has been described more in detail.

For the modeling of the system, a drawing of the accumulator that is used in the system has been provided by the piston accumulator company Hydroll. Information regarding the barrier fluid has been provided by Univar AS, the Shell Lubricants distributor of Norway. Aratron Hydraulikk AS has provided information regarding the Wandfluh solenoid valve used in the system, and HAWE has provided information regarding the orifice used in the system. OneSubsea has provided additional information regarding piping layout, system components, pressure, and flow conditions.

As shown earlier in Fig. 1.1 in Chapter 1, the system that is looked at consists of a high-pressure system and a low-pressure system that are separated with a solenoid valve, an orifice, and a ball valve. As seen in Fig. 3.1, a more detailed drawing of the system have been made to get an overview of the important information for the piping and components.
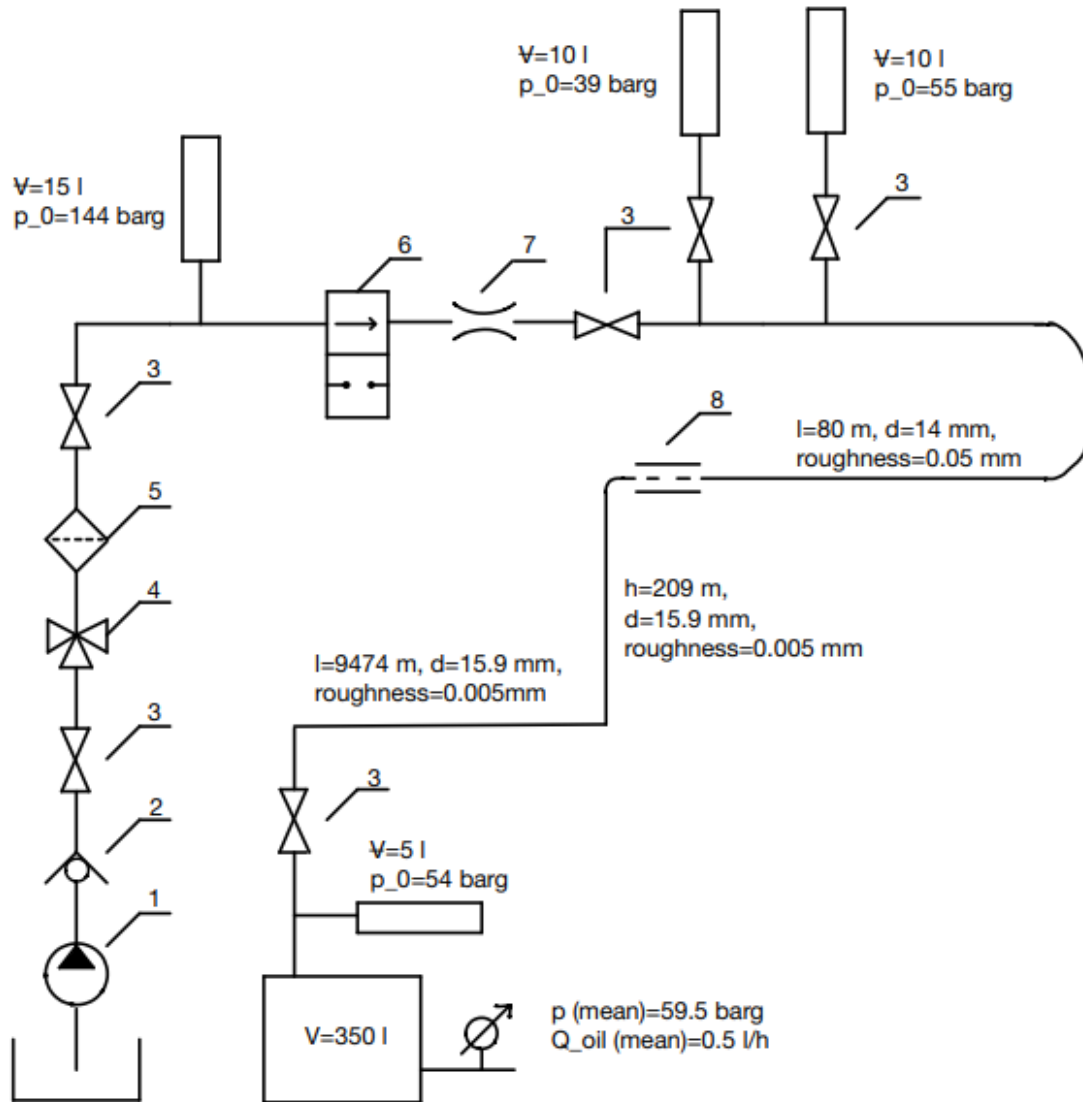
Figure 3.1: Drawing of the hydraulic system and its components.

As seen in Fig. 3.1, the different piping components have been numbered. The situation that is considered starts when the pressure in the LP system has decreased to $p_1 = 43$ barg, and the feed solenoid (nr. 6) opens to recharge the LP system. Barrier fluid flows from the HP system through the valve to charge two pcs. 10 l HPS11-350-140-0100 accumulators that has a precharge pressure of $p_0 = 39$ barg and $p_0 = 55$ barg with nitrogen. When the pressure in the low-pressure system reaches $p_2 = 47$ barg, the feed solenoid closes. The ambient temperature in the HPU is $T_0 = 300$ K throughout the process. The components and relevant parameters are listed in Table. 3.1.

Table 3.1: Dimensions of the piping and system components provided by OneSubsea

Nr.	Name	Parameter	Value
1	Radial piston pump		
2	Non return valve		
3	Ball valve[1]	Connection size	1/2" NPT
		Bore	10 mm
		Cv	4.2
		Kv	3.6
4, 6	Solenoid valve[2]		
5	Filter		
7	Orifice SOLEX jet M5-1.0[3]	Bore	1mm
	Steel tubing on platform	App.Length	80 m
		Internal diameter	14 mm
		Roughness	0.05 mm
8	Coupling upstream umbilical	Dimension	5/8"
	Umbilical (FPSO to seabed)	Length	209 m
		Internal diameter	15.9 mm
		Roughness	0.005 mm
	Umbilical (seabed)	Length	9474 m
		Internal diameter	15.9 mm
		Roughness	0.005 mm

[1,2,3] Additional information have been provided in the Appendix

In Table. 3.1, the system parameters have been listed. These parameters, together with the data sheets found in the Appendix, have been used in the different model calculations in this chapter.

3.1   Barrier fluid

The barrier fluid that is used in the hydraulic system is Shell Morlina S2 BL 5, an oil with special low viscosity that provides extended performance for machines operating at high speeds. The properties from its technical data sheet are presented in Table 3.2 [1].

Table 3.2: Properties of the barrier fluid Morlina S2 BL 5 [1].

Property	Value
Density	869 kg/m^3
Kinematic Viscosity	5 mm^2/s
Thermal Conductivity[1]	0.152 W/m K
Specific heat capacity[2]	1670 J/kg K

[1,2] Parameters provided by OneSubsea

Another property of interest regarding the barrier fluid is the bulk modulus, that is a measure of how compressible a specific substance is. Univar, which is the Shell Lubricants distributor in Norway, have provided tables and data sheets. The closest measured data for bulk modulus they had available was for the Tellus Oil 10 (Pre-ISO name Tellus Oil 15), which should give a good approximation for the bulk modulus of Morlina S2 BL 5.

From the tables provided by Univar as shown in Appendix D, the isentropic tangent bulk modulus has been approximated to ≈ 1.73 GPa, for a temperature at 300 K and pressure at 45 barg.

3.2   Hydraulic accumulator

The accumulator that is used in the HPU on the production vessel is the 10 l piston accumulator HPS11-350-140-0100. The piston accumulator company Hydroll have provided a 1:2 scaled drawing of the accumulator. The dimensions of the accumulator have been listed in Table 3.3.

Table 3.3:   Dimensions of accumulator based on the drawing provided by Hydroll.

Parameter	Value
Accumulator inner length	693 mm
Accumulator inner diameter	140 mm
Fluid port threads[1]	G1/2
Fluid port inner diameter	19 mm
Fluid port total length	70 mm
Fluid port length to threads	48 mm
Piping on platform	14 mm
Piston geometry:	
Outer height	80 mm
Inner height	60 mm
Outer diameter	140 mm
Inner diameter	105 mm
Piston volume	0.000712 m^3
Piston mass	5.7 kg
Virtual Piston height	46 mm

[1] G1/2 is of British standard parallel pipe(BSPP) connection (ISO 228), with a bore of 19 mm, major diameter of 20.955 mm and minor diameter male thread of 18.631 mm

In Table 3.3, the mass of the piston, and a simplified piston shape have been estimated from the piston geometry. The mass of the piston has been estimated by using the density of steel $\rho = 8000 \text{ kg/m}^3$. From this the mass of the piston is, $m \approx 5.7$ kg. For the 3D-CAD model, the geometry of the piston has been simplified to a cylindrical shape, where the diameter of the piston equals the inner diameter of the accumulator of 0.14 m, and the height of the piston is $H_{\text{piston}} \approx 0.046$ m:

3.3   3D Geometry

Two different geometric models have been made to represent the physical system. One
model has been made as a single accumulator model, and one model has been made
as a double accumulator model. The geometries of the accumulator models have been
modeled in the 3D CAD software Creo Parametric based on the dimensions in Table 3.3.
In the CFD software STAR-CCM+, a replica of these models has been made. In this
section, the geometry of the single accumulator model has been described. The double
accumulator model is introduced in the last section of this chapter.

3.3.1   Single accumulator model

In STAR-CCM+ the geometry of the single accumulator model consists of four parts,
the background geometry (accumulator wall and piping), two parts that define the fluid
volume surrounding the piston shown referred to as overset meshes, and the piston. The
geometry of the accumulator is shown in Fig. 3.2. To make the model, first, the geometry
of the internal volume has been made by extruding a circle in a two-way extrude. The
piston has been modeled with the overset mesh technique, as described in Chapter 2. To
apply this technique, the fluid volume that is closest to the piston is represented with an
additional overlaying geometry, as shown in the following figure:
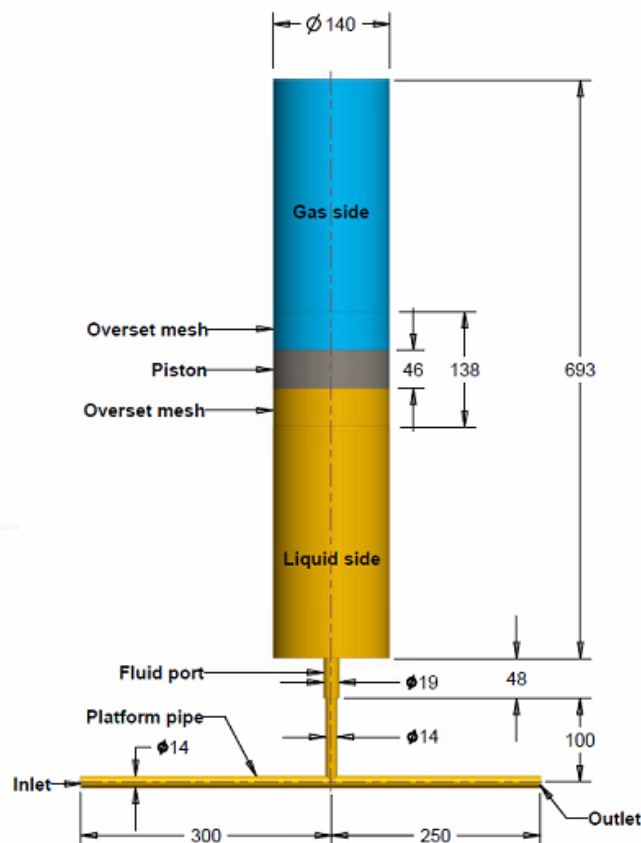
Figure 3.2: CAD model of the single accumulator, all dimensions are given in mm.

As can be seen in Fig. 3.2, the piston, and the overset regions were modeled in symmetry with the center of the accumulator. After the mesh generation, these regions were translated down to the initial position of the piston. The overset regions have the same diameter as the background geometry, and a height equal to the piston height of 46 mm. The diameter of the piping has been set to 14 mm, as shown in Table 3.1. The length of the inlet and outlet pipe have been set to 300 mm and 250 mm respectively, and the vertical pipe from the platform pipe to the fluid port of the accumulator has been set to 100 mm from the center of the platform pipe to the end of the threads in the fluid port.

3.3.2   Placement of piston

The accumulator is pre-charged with a pressure $p_0 = 39$ barg, and is charged from $p_1 = 43$ barg to $p_2 = 47$ barg, while the ambient temperature in the HPU is $T_0 = 300$ K.

To find the corresponding placements of the piston, the ideal gas equation of state as presented in Eqn.(2.7.1) has been used. To check if nitrogen can be treated as an ideal gas in this situation the reduced pressure and temperature is found and evaluated. The critical-point properties, $T_{Cr} = 126.2$ K and $p_{Cr} = 3.39$ MPa as listed in Table A1 of [18], are used to find the reduced pressure p_R and temperature T_R as shown in Eqn.(2.7.4) and (2.7.3). The critical temperature and pressure for the given situation have been found to $T_R \approx 2.4 > 2$, and $p_R \approx 1.4 \not\gg 1$. Hence for the given conditions nitrogen can be treated as an ideal gas.

It is assumed that the piston moves to the bottom wall during the pre-charging of the accumulator and this gives the nitrogen pre-charge volume, $V_0 \approx 9.956 \cdot 10^{-3}$ m^3. From this, the inner height of the pre-charge gas volume from the top of the piston to the top wall is found to be $H_0 \approx 0.647$ m.

The initial placement of the piston at $p_1 = 43$ barg have been found by using the ideal gas equation. Hence, the initial placement H_1 from top of the piston to top wall have been found to be $H_1 \approx 0.588$ m.

3.4   Region Layout

As described in the previous section, the geometry has been divided into four different parts; background region, two overset regions, and a piston region. These independent parts have been made to simulate the movement of the piston. In this section, the different regions with boundaries, and interfaces have been described, starting with the background region.

3.4.1   Background region

The system that the LP accumulators are connected to consists of an upstream delivery line, and a downstream platform piping and umbilical that transports the barrier fluid to the subsea system. The block diagram shown in Fig. 1.2 has been modified to visually show the model with its input and output and how the components are combined, as shown below.
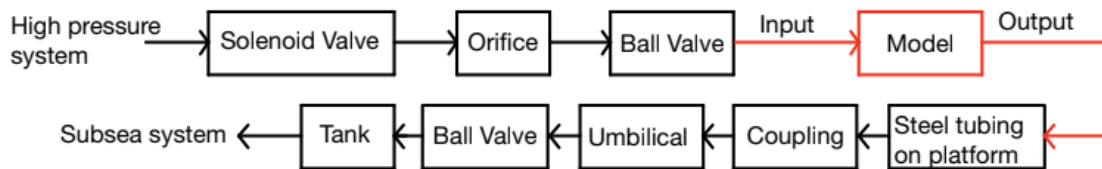
Figure 3.3: Block diagram of the hydraulic system and its components.

In Fig. 3.3, it is shown how the piping connects to the model through an inlet and outlet boundary. The inlet and outlet have been defined on the horizontal pipe of the model, and at these boundaries, the velocity or pressure is applied with the use of field functions. The dimensions and parameters related to the piping components were shown earlier in Table 3.1.

The inlet and outlet boundaries of the model have been set to velocity inlet and pressure outlet, respectively. Expressions for the inlet velocity and outlet pressure have been found as shown in the following sections.

3.4.2   Velocity inlet

At the inlet boundary, a field function has been applied to control the inlet velocity as shown in the following equation:

$$v_{\text{inlet}} = \frac{Q_{\text{inlet}}}{0.25 \cdot \pi \cdot 0.014^2} \tag{3.4.1}$$

In Eqn.(3.4.1), Q_{inlet} is the inlet volume flow that can be related to the pressure in the HP system, the pressure in the LP system and the pressure losses across the valves and orifice. The pressure balance can be written as in Eqn.(3.4.2).

$$p_{\text{LP}} = p_{\text{HP}} - \Delta p_{\text{Solenoidvalve}} - \Delta p_{\text{orifice}} - \Delta p_{\text{ballvalve1}} - \Delta p_{\text{ballvalve2}} \tag{3.4.2}$$

In Eqn.(3.4.2), p_{LP} is the pressure in the low-pressure system, and it has been monitored in the model at the bottom of the accumulator. As seen in Eqn.(3.4.2), this gives the pressure drop across the ball valve at the fluid port of the accumulator $\Delta p_{\text{ballvalve2}}$. Due to the flow splitting at the fluid port pipe, the pressure drop across the second ball valve has been estimated to be half the pressure drop of the first ball valve. This gives a combined pressure drop across the two valves of $1.5 \cdot \Delta p_{ballvalve}$. p_{HP} is the pressure in the high-pressure system, which can be estimated from measured pressure data that have been provided. Based on Table. 3.1, and the product data sheets as shown in the Appendix, expressions for the pressure losses have been found for the valves and orifice, according to pressure loss equations in ref. [16]. The coefficients for the different components have been estimated in Excel, as shown in Appendix C.

Pressure in high-pressure system

The pressure in the HP system p_{HP} as shown in Eqn.(3.4.2) has been estimated according to time data acquired from OneSubsea, and the pressure has been plotted as:
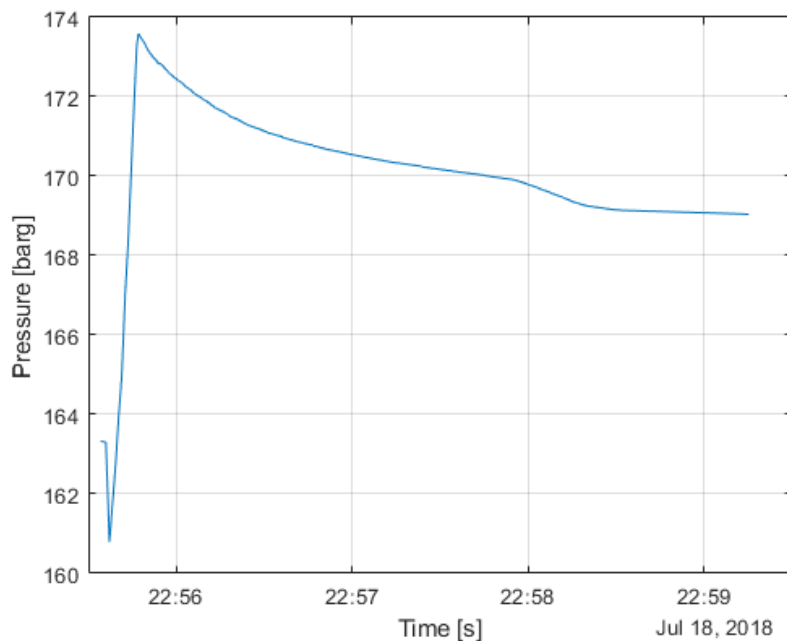
Figure 3.4: Plot of the pressure in the high pressure system

This measured data goes beyond the time it takes to charge the LP system, and only a small part of the graph is needed to set up a simulation of the charging process of the LP system. Fig. 3.5 shows a narrower plot, limited to the time when the valve is open. The start time at 0 s refers to the time when the solenoid opens.
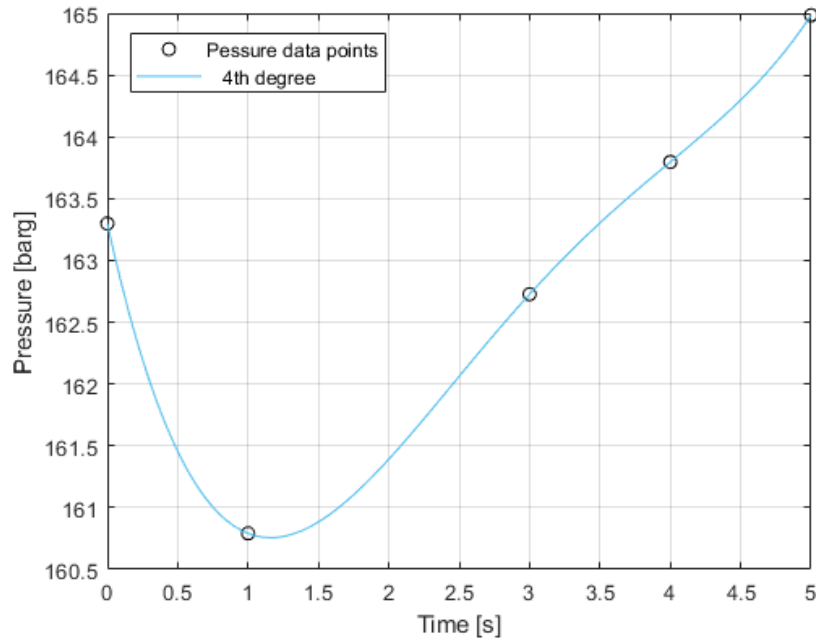
Figure 3.5: Plot of the pressure data points at high-pressure system during charging of LP system, Basic curve fitting in Matlab, with 4 th. degree polynomial.

From this curve fit, the expression for p_{HP} has been found as:

$$p_{HP} = (0.057 \cdot t^4 - 0.740 \cdot t^3 + 3.372 \cdot t^2 - 5.196 \cdot t + 164.300) \cdot 10^5 \text{ [Pa]} \tag{3.4.3}$$

Solenoid valve

The solenoid valve is of the type BEX2204041a-K9-S1788-g24/T4 Atex, PTB 01 ATEX 2129 X, stainless steel, manufactured by Wandfluh. The "pressure drop volume flow characteristics" from Appendix F, that shows the characteristics of the control valve has been shown in the following figure:
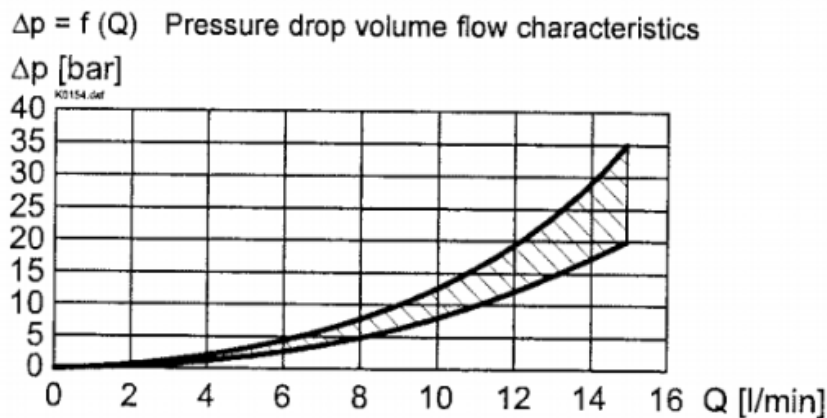
Figure 3.6: Figure showing the"pressure drop volume flow characteristics" of the solenoid valve used in the system

As seen in Fig. 3.6, $\Delta p = f(Q)$ is the Measured pressure loss across one control edge in function of the volume flow, and this pressure loss is measured as close to the valve as possible [19]. The valve in the system is either open or closed. An example of the pressure drop in a three position directional valve can be seen in Fig. 3.7.
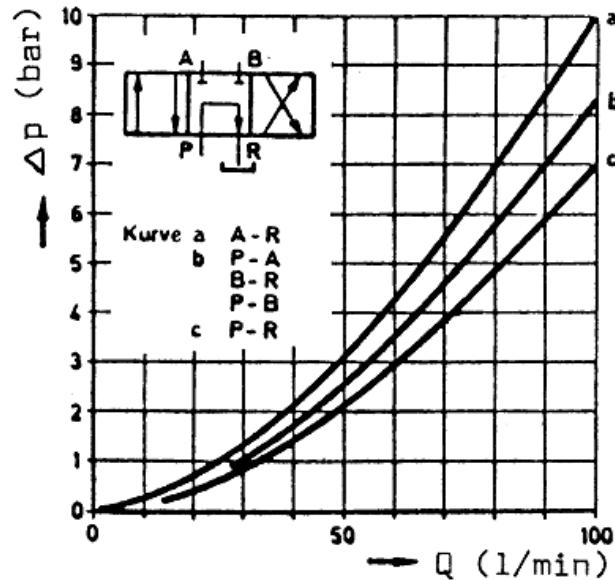
Figure 3.7: Figure showing pressure losses in a directional valve [6].

As seen in Fig. 3.7, the distribution of the curves corresponds to the different positions of the valve. For the case where the flow goes straight through the valve, curve (b) refers to the pressure drop across the valve. By using the average values in the hatched graph shown in Fig. 3.6, a set of individual valve coefficients have been found, and the average value of these gives the valve coefficient for the solenoid valve. The pressure and volume flow are related through the equation:

$$\Delta p = K \cdot Q^2 \tag{3.4.4}$$

From Eqn.(3.4.4) the general equation for the individual valve coefficients has been found to be:

$$K_i = \frac{\Delta p_i}{Q_i^2} \tag{3.4.5}$$

The valve coefficient for the solenoid valve $K_{\text{solenoidvalve}}$ has then been estimated as an average of all the individual coefficients found in Eqn.(3.4.5):

$$K_{\text{solenoid}} = K_{\text{average}} = \frac{\sum_{i=1}^{n} K_i}{n} \tag{3.4.6}$$

The average values for the pressure drop and the corresponding volume flows from the hatched graph in Fig.(3.6) have been listed In Table 3.4, and with the use of Eqn.(3.4.5) and Eqn.(3.4.6), the solenoid valve coefficient has been estimated as seen in Table 3.4.

Table 3.4: Estimate of the solenoid valve coefficient

i	Q [l/min]	Δp [bar]	K (SI)[1]
1	2	0.36	$3.24 \cdot 10^{13}$
2	4	1.43	$3.22 \cdot 10^{13}$
3	6	3.39	$3.39 \cdot 10^{13}$
4	8	5.71	$3.21 \cdot 10^{13}$
5	10	9.68	$3.48 \cdot 10^{13}$
6	12	15	$3.75 \cdot 10^{13}$
$n = 7$	14	22.07	$4.05 \cdot 10^{13}$
K_{average}			$3.58 \cdot 10^{13}$

[1] The valve coefficient K have been calculated in SI units

As seen in Table 3.4, the solenoid valve coefficient has been estimated, and this coefficient has been used in Eqn.(3.4.4) to give the expression for pressure loss across the solenoid valve.

Orifice

The orifice is of the type SOLEX jet M5-1.0 and manufactured by HAWE. HAWE have provided information regarding the orifice [20] see Appendix E.

The volume flow through the orifice can be written as:

$$Q_{\text{orifice}} = A\hat{\mu} \cdot \sqrt{\frac{2}{\rho} \cdot \Delta p_{\text{orifice}}} \tag{3.4.7}$$

Where A is the area of the orifice bore, $\hat{\mu}$ is the flow coefficient that accounts for the contraction coefficient and the friction coefficient as well as the impact from any change in pipe size from the two sides. For a short circular narrowing when $\frac{dRe}{l} > 50$, the flow coefficient $\hat{\mu}$ can be found as:

$$\hat{\mu} = \frac{1}{\sqrt{1.5 + 13.74 \sqrt{\frac{l}{d \cdot Re}}}} \tag{3.4.8}$$

Hence the pressure drop across the orifice can be written as:

$$\Delta p_{\text{orifice}} = \frac{\rho}{2} \cdot (A \cdot \hat{\mu})^2 \cdot Q_{\text{orifice}}^2 = K_{\text{orifice}} \cdot Q_{\text{orifice}}^2 \tag{3.4.9}$$

From this, a coefficient for the orifice is found, and the coefficient has been estimated in

Excel as seen in Appendix C:

$$K_{\text{orifice}} = \frac{\rho}{2} \cdot (A \cdot \hat{\mu})^2 = 1.27 \cdot 10^{15} \tag{3.4.10}$$

Ball valve

From the ball valve data sheet, as seen in Appendix G, the flow coefficients Cv and Kv are shown, where Kv is given in metric units and Cv in imperial units. This makes Kv slightly easier to work with, and Kv= 3.6 [m³·h⁻¹·bar⁻⁰·⁵] has been used as the flow coefficient.

$$Q = \text{Kv}\sqrt{\frac{\Delta p}{\text{SG}}} \tag{3.4.11}$$

In Eqn.(3.4.11), Q is the volume flow in m³/h, Δp is the pressure drop in bar, SG is the specific gravity of the fluid, and Kv is the flow coefficient. Eqn.(3.4.11) can be solved for the pressure drop across the ball valve in SI units as:

$$\Delta p = \frac{\text{SG}}{\text{Kv}^2}Q^2 \cdot 3600^2 \cdot 10^5 = K_{\text{ballvalve}} \cdot Q^2 \tag{3.4.12}$$

In Eqn.(3.4.12), Q is the volume flow in m³/s. The ball valve coefficient $K_{\text{ballvalve}}$ has been estimated to $8.69 \cdot 10^{10}$ Pa· s²/m⁶.

Eqn.(3.4.3), (3.4.4), (3.4.9), and (3.4.12), have been substituted into Eqn.(3.4.2), to achieve an expression for the inlet volume flow:

$$p_{\text{LP}} = p_{\text{HP}} - K_{\text{Solenoidvalve}} \cdot Q^2_{\text{inlet}} - K_{\text{orifice}} \cdot Q^2_{\text{inlet}} - 1.5 \cdot K_{\text{ballvalve}} \cdot Q^2_{\text{inlet}} \tag{3.4.13}$$

In Eqn.(3.4.13), $1.5 \cdot K_{\text{ballvalve}}$ represents both the ball valves. The equation is solved for Q_{inlet} to get the following:

$$Q_{\text{inlet}} = \sqrt{\frac{p_{\text{HP}} - p_{\text{LPreport}}}{K_{\text{Solenoidvalve}} + K_{\text{orifice}} + 1.5 \cdot K_{\text{ballvalve}}}} \tag{3.4.14}$$

Where p_{HP} is the pressure at the high pressure side, p_{LPreport} is the pressure at the sensor placed in the bottom of the accumulator, $K_{\text{Solenoidvalve}}$ is a coefficient for the solenoid valve. K_{orifice} is a coefficient for the orifice, and $K_{\text{ballvalve}}$ is a coefficient for the ball valve. Eqn.(3.4.14) is then substituted into the function for the inlet velocity Eqn.(3.4.1), and applied at the inlet boundary for the model in STAR-CCM+.

3.4.3   Pressure outlet

For the pressure outlet, a pressure balance was set up, starting with the subsea pressure and following the hydraulic pipeline upstream to the pressure outlet, and accounting for all components. Based on this, the outlet pressure is controlled by the scalar field function:

$$p_{\text{outlet}} = p_{\text{subsea}} - \Delta p_{\text{hyd}} + \Delta p_{\text{platform}} + \Delta p_{\text{umbilical}}$$
$$+ \Delta p_{\text{coupling}} + \Delta p_{\text{ballvalve}} + \Delta p_{\text{tank}}$$

(3.4.15)

In Eqn.(3.4.15) p_{subsea} is the pressure at the subsea pump that has a mean value of 59.5 barg. The hydro static pressure drop $\Delta p_{\text{hyd}} = \rho \cdot g \cdot h = 1781702$ Pa, $\Delta p_{\text{platform}}$ is the pressure loss in the piping on the platform, $\Delta p_{\text{umbilical}}$ is the pressure loss in the umbilical, $\Delta p_{\text{coupling}}$ is the pressure drop in the coupling between the platform pipe and the umbilical, $\Delta p_{\text{ballvalve}}$ is the pressure drop across the ball valve, and Δp_{tank} is the pressure loss when the fluid enters the 350 l tank. The pressure drop therms in the equation are found by using pressure drop equations from ref [16], together with the parameters and dimensions presented in table 3.1. The coefficients for the different components have been estimated in Excel, as shown in Appendix C.

Platform pipe and umbilical

The pressure loss in the platform pipe and umbilical can be found from the following equation:

$$\Delta p_{\text{loss}} = \sum \lambda \frac{l}{d} \rho \frac{v_m^2}{2}$$

(3.4.16)

In Eqn.(3.4.16), λ is the coefficient of friction, l the length of the pipe, d the diameter of the pipe, ρ the density of the fluid, and v_m the mean velocity of the fluid.
λ can be found from a Moody chart, knowing the roughness ϵ, and then the relative roughness $\frac{\epsilon}{d}$ in the pipe, together with Reynolds number Re. For this method, the coefficient of friction has to be found from the chart. Hence an alternative approach has been used, to automatically find the coefficient of friction. For a smooth pipe, the coefficient of friction λ follows the following relationship:

$$\lambda = \begin{cases} \frac{64}{\text{Re}}, & \text{for laminar flow Re} < 2300 \\ \frac{0.316}{\text{Re}^{0.25}}, & \text{for turbulent flow Re} > 2300 \end{cases}$$

(3.4.17)

For laminar flow, the roughness of the pipe has no visible effect, but for turbulent flow, the coefficient of friction depends on the roughness in the pipeline. This effect can be accounted for by introducing a coefficient that adjusts for the roughness. With an approximation, the coefficient of friction in the pipe with roughness $\epsilon = 0.05$ mm is about 1.3 times larger than that of a smooth pipe.

For the mean velocity v_m in Eqn.(3.4.16), the average velocity was measured in a plane located at the pressure outlet of the model. This velocity was used for the pressure loss in the platform pipe, and calculated to a mean volume flow Q_{Outlet} that was used to find the pressure loss in the downstream components of the outlet.

With these expressions inserted into Eqn.(3.4.16), the pressure losses in the platform pipe and umbilical has been found.

Ball valve

The ball valve on the umbilical is of the same type as the one used at the inlet, and therefore Eqn.(3.4.12) has been used.

Coupling and tank

The pressure loss in pipe bends, couplings, inlets and outlets are calculated according to Eqn.(3.4.18).

$$\Delta p = \zeta \rho \frac{v_m^2}{2} \tag{3.4.18}$$

In the above equation, ζ is the loss coefficient, and v_m is the incoming mean velocity before the pipe component. For a sudden increase in pipe diameter, the loss coefficient can be found:

$$\zeta = \left(1 - \left(\frac{d_1}{d_2}\right)^2\right)^2 \tag{3.4.19}$$

In Eqn.(3.4.19), d_1 and d_2 are the diameters at the two cross sections, that for this case are $d_1 = 14$ mm and $d_2 = 15.9$ mm. This equation has been used to estimate the loss coefficient for the coupling. For the outlet to the tank the loss coefficient $\zeta = 1$ was used.

The expressions shown in Eqn.(3.4.16), (3.4.12), (3.4.18), together with the subsea pressure and hydrostatic pressure have been substituted into Eqn.(3.4.15) to acquire a function for the outlet pressure. This function has been used at the outlet boundary in STAR-CCM+.

3.4.4   Overset and solid piston region

To simulate the movement of the piston, a region that defines the fluid volume surrounding the piston have been made, and the boundaries of this region have been defined. The areas next to the piston and accumulator wall have been defined as walls, and the area connecting the fluid volume in the overset region and background region has been defined as overset. An overset mesh interface has been made to connect the overset region and the background region. In the following figure, the overset regions and the piston region are shown separately with their associated interfaces.

(a) Overset region   **(b)** Solid part region
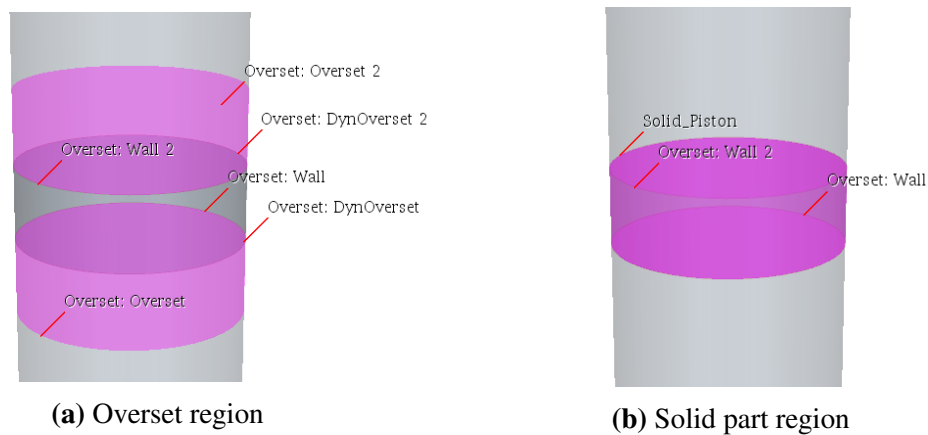
Figure 3.8: Scenes that shows the interfaces between the overset region and the background region, and between the solid part region and the overset region

To visualize the piston in the simulation, and to simulate heat exchange between the regions, a solid part region to represent the piston was made. The solid piston region and the overset region have been connected with an interface at top and bottom of the piston. In Fig. 3.8b the solid part region has been shown with the overset wall interfaces.

3.5   Mesh

The mesh has been made with the parts based meshing strategy, and it consists of a surface mesh and a volume mesh. The meshers that have been chosen for the model is the surface remesher and trimmed cell mesher. The surface remesher has been used to improve the surface mesh quality before the volume mesh was generated. The base size of the mesh has been set to 1/10 of the piston height, $4.6 \cdot 10^{-4}$ m.

The generated mesh is shown in Fig. 3.9, where the solid piston part region together with the overset region first was generated in the center of the accumulator and then translated down to the start position of the piston.
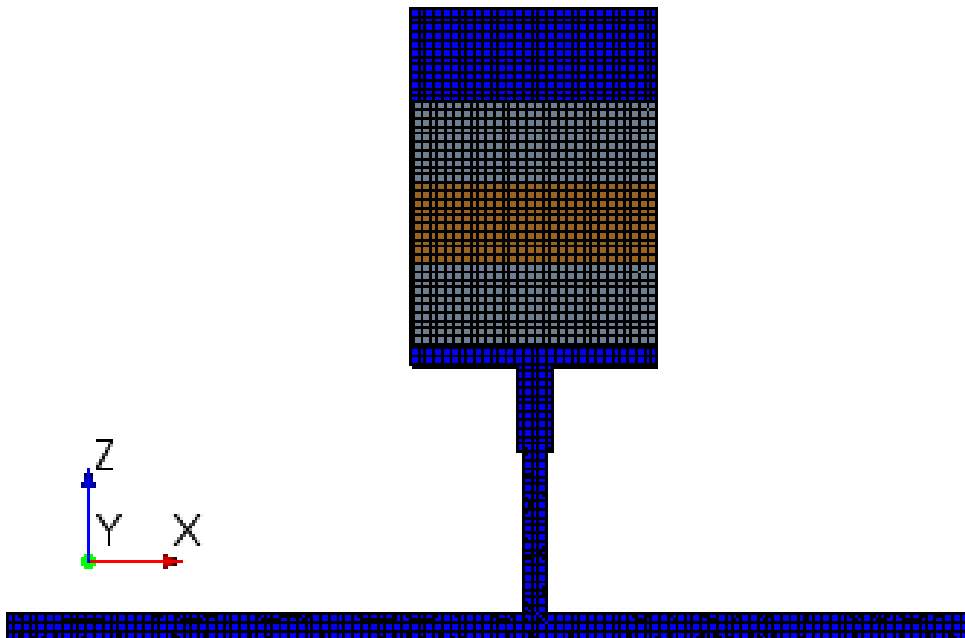
Figure 3.9: Detail of the bottom of the model mesh.

In Fig. 3.9, the mesh has been divided into three colors. The blue mesh is the background mesh, the two grey meshes, represents the overset meshes that lays on top of the background mesh, and the brown mesh represents the solid piston mesh, that lies between the two overset meshes. When the simulation is initialized, the overset mesh cuts into the background mesh to create one continuous mesh that transforms as the piston moves. Fig. 3.10, shows a set of scalar scenes set up in STAR-CCM+, that have been used to monitor and control the overset mesh for errors. These scenes have been shown together with a close view of the overset mesh initialized and imprinted in the background mesh.

(a) Piston, overset and background mesh.

(b) Overset mesh cell status.

(c) Overset mesh cell type.

(d) Overset error status.
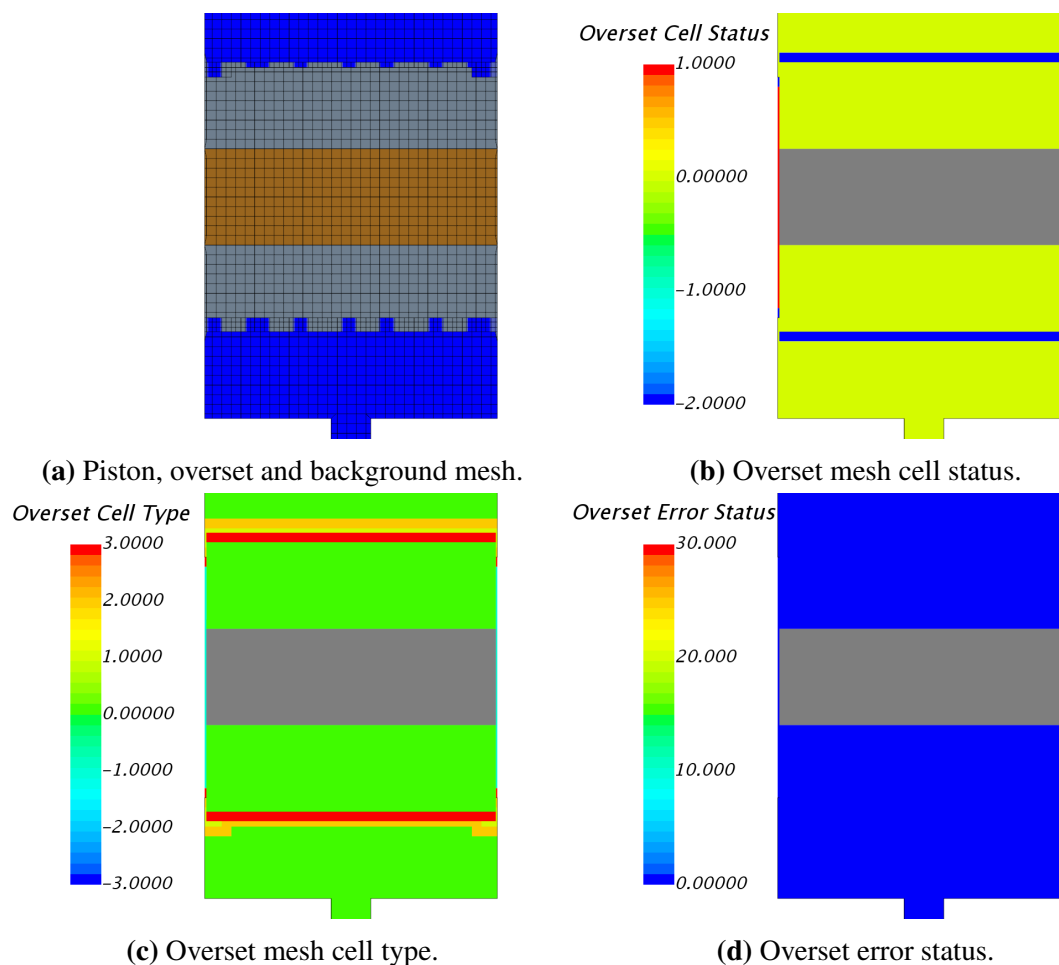
Figure 3.10: Details of the model mesh.

As described in the previous chapter, the overset mesh consists of three different cells, active, inactive, or acceptor cells, and these are shown in Fig. 3.10b that shows the status of the overset mesh. Fig. 3.10c shows in detail what type each of the cells are, and Fig. 3.10d indicates if there are cells that have an error.

3.6 Setting up the physics models

A set of models have been chosen to simulate the situation considered for the model. The process consists of two fluids, nitrogen and the Barrier fluid Morlina S2 BL5 that are separated with a piston. There is a volume flow of barrier fluid entering the velocity inlet and another volume flow of barrier fluid leaving the pressure outlet. The initial temperature in the system is 300 K, and the initial pressure is 43 barg. In this section, the chosen models have been described.

3.6.1 Continua

Two physics continua have been made to represent the different materials that are present in the simulation. One represents the fluid, and the other represents the solid piston. For the fluid, the following models have been selected:

The space of the continuum has been selected to Three Dimensional. The situation considered is transient, and therefore, the Implicit Unsteady time model has been selected. The material of the fluid continuum has been selected to Eulerian Multiphase as it consists of both nitrogen and barrier fluid. The Volume of Fluid model (VOF) and the Segregated flow model were chosen for the Eulerian Multiphase models. The nitrogen has been set up as a gas, whereas the barrier fluid Morlina S2 BL5 has been set up as a liquid with density changing with pressure.

For this system, the phases do not mix due to the piston that separates them. The volume fraction that defines the initial placement of the two fluids is controlled by the two field functions in STAR-CCM+ syntax, shown as follows:

$$\text{Initial\_distribution\_morlina} = (\$\$Position[2] <= -0.2645)?0.99 : 0.01$$

$$\text{Initial\_distribution\_nitrogen} = 1 - \$\text{Initial\_distribution\_morlina}$$

A turbulent flow regime was expected for the simulations. Hence the turbulent viscous regime model was selected, and Reynolds-Averaged Turbulence was selected to K-Epsilon Turbulence. From the optional models in STAR-CCM+, gravity was selected with a value of -9.81 m/s^2 applied in the z-direction. The initial pressure and the initial temperature for the fluid have been set to $43 \cdot 10^5$ Pa and 300 K respectively.

For the solid continua, the following models have been chosen; Three-dimensional space, Implicit unsteady time model, Solid material, Segregated solid Energy, Gradients, and constant density. The density of the solid was set to a constant value of 8000 kg/m^3, the specific heat was set to 500 J/kg·K, and thermal conductivity to 50.0 W/m·K. The initial static temperature of the solid piston was set to 300.0 K.

3.6.2 DFBI

To simulate the movement of the piston, dynamic fluid body interaction (DFBI) has been used, which is described in Chapter 2. A DFBI continuum body was set up with the overset region as the input parts. The body mass was set to 5.7 kg, as shown in Table. 3.3. The release time and ramp time was set to 0.002 s and 0.02 s respectively to prevent large oscillations at the start of the simulation. The body motion was set to *Free motion* and enabled in the z-direction. All initial values of the DFBI have been set to zero. For external forces and moments, the damping force had to be calculated, together with the friction force.

Friction

The friction force that is applied to the piston consists of the contact friction between the accumulator housing and the piston seals, and the viscous friction due to the movement of the piston. In Chapter 2 different friction models have been presented. The combined Coulomb and *tanh* friction model and the Stribeck friction model are the two models that have been seen as the most relevant for the simulations in this project, and the Stribeck friction model was the first to be tried out. The friction force was divided into two parts, static and kinetic friction when estimating the total friction force. The accumulator manufacturer Hydroll have provided information that the breakaway pressure-difference for the piston is approximately 1 bar. The diameter of the piston is 0.14 m, as presented in Table (3.3). Based on this, the static friction force has been calculated as follows:

$$F_{\text{static}} = p \cdot A = 10^5 \text{ Pa} \cdot \pi \cdot (0.07 \text{ m})^2 \approx 1540 \text{ N} \qquad (3.6.1)$$

In Eqn.(3.6.1), F_{static} is the static friction force. An assumption that the contact between the piston and inner accumulator wall is of type lubricated metal on metal gives the approximate friction coefficients, $\mu_s = 0.15$ for static friction, and $\mu_k = 0.06$ for kinetic friction [21]. In Eqn.(3.6.1) the static friction was estimated to 1540 N. By applying the friction coefficients, the kinetic friction is derived to 616 N.

The viscous friction force also needs to be considered, as shown in Chapter 2, it comes from the resistance against straight motion in an energy medium. This viscous damping force is linearly dependent on the velocity [22]. Hence this damping force can be defined as:

$$F_v = k_v \cdot v \qquad (3.6.2)$$

In Eqn.(3.6.2) F_v is the viscous damping force, k_v the damping coefficient, and v the sliding velocity.
The damping coefficient k_v for piston motion in a cylinder with fluid have been estimated

with the following equation [22]:

$$k_v = \pi \cdot \rho \cdot v \cdot \frac{d}{\delta} \cdot \frac{l}{d} \cdot d \qquad (3.6.3)$$

In Eqn.(3.6.3), ρ and v is the density and kinematic viscosity of the fluid respectively, d is the average diameter, δ the gap between piston and cylinder, and l the length of piston.

Based on Eqn.(3.6.3), the damping coefficent has been calculated to ≈ 0.15 Ns/m . The static, kinetic and viscous friction force can be combined as shown in Eqn.(2.6.5). This equation gives an estimate of the total friction force as a function of velocity by inserting the Coulomb friction $F_C = F_{kinetic} = 616$ N, the Stribeck friction $F_S = F_{static} = 1540$ N, and $k_v = 0.15$ Ns/m. For the coefficients, v_s, k_{tanh}, and the exponent i, parameter values were selected to provide a smooth function. In the following, these parameters have been inserted into Eqn.(2.6.5) to visualize the friction force in a graph:
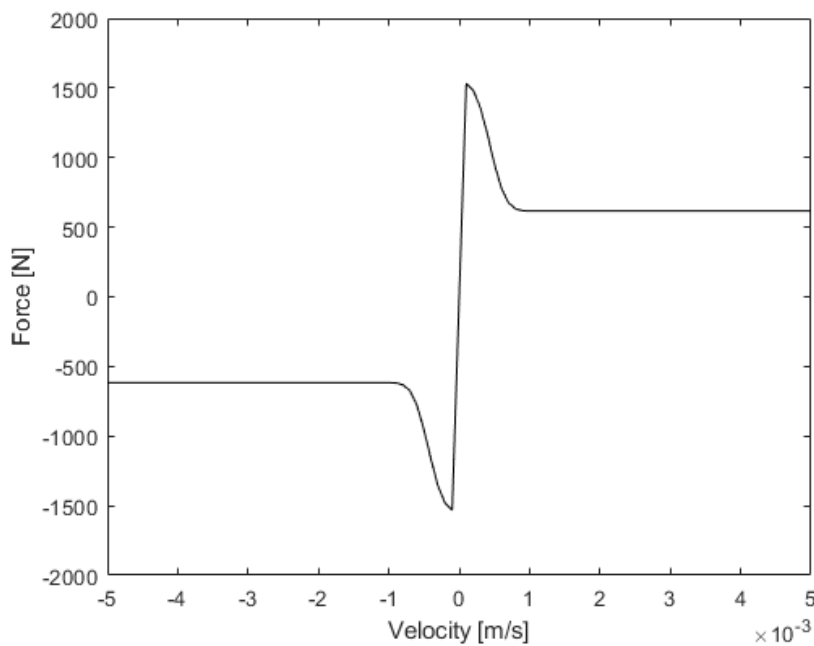
Figure 3.11: Plot of the total friction force based on the tanh modified Stribec function as in Eqn.(2.6.5), where $v_s = 0.0005$, $k_{tanh} = 100000$, and the exponent $i = 3$. These parameter values were selected to provide a smooth function.

This model is only dependent on the velocity of the piston, and not the displacement that is important at a static friction situation. Due to large oscillations of the velocity at the beginning of the simulation, this model was not brought any further. A micro-slip friction model such as a Dankowitcz friction model would account for small displacements [5], but for simplicity, a modified version of the combined Coulomb tanh friction function was considered as a better alternative for the simulations in this project. Therefore the Stribeck friction model was substituted by a constant friction force to achieve a more

stable simulation. With the assumption that the piston has static friction of 1540 N, the Coulomb friction of 616 N has been used as the constant friction force in the simulation.

$$F_{\text{R piston}} = 616 \text{ N} \tag{3.6.4}$$

Also, to smoothly change the direction of this friction force when the inlet valve is closed, and the accumulators are being discharged, a field function based on the *tanh* function have been used:

$$F_{\text{R piston}}(t) = \frac{F_{\text{R piston}} \cdot e^{\left(\frac{t-t_0}{w}\right)} - a \cdot F_{\text{R piston}} \cdot e^{\left(\frac{t_0-t}{w}\right)}}{e^{\left(\frac{t-t_0}{w}\right)} + e^{\left(\frac{t_0-t}{w}\right)}} \tag{3.6.5}$$

Where $F_{\text{R piston}}(t)$ is the friction force at time t that changes from a negative to positive friction value, w is a constant to control the slope of the function, and $F_{\text{R piston}}$ is the friction force. a is a constant that is either 1 or 3 depending on the type of friction shift. For $a = 1$ the function behaves as a *tanh* function, and t_0 represents the time of the turning point of the *tanh* function. For $a = 3$, the function represent an exponential friction shift, and t_0 is changed from the turning point of the function to the start point of the function. Eqn.(3.6.5), has been used in the DFBI model together with the damping constant $k_v = 0.15$ N.

3.6.3   Time step

For the simulation time step, different values in the range of 0.0002 s to 0.00008 s have been selected to get stable simulations and to be sure that for any time step, the overset mesh would only move by a distance smaller than the height of the smallest cell in the background region. A finer mesh would require an even smaller time step.

3.7 Changes to model parameters and model setup

After the first simulations, some of the model parameters have been changed to represent the physical system better.

3.7.1 Simulation 3: Single accumulator model 39 barg with 1540 N friction

The initial pressure in the nitrogen needed to be changed, and hence also the initial volume of the nitrogen needed to be changed. Based on the observations from the simulated pressure results, a sketch showing the pressure over time has been made:
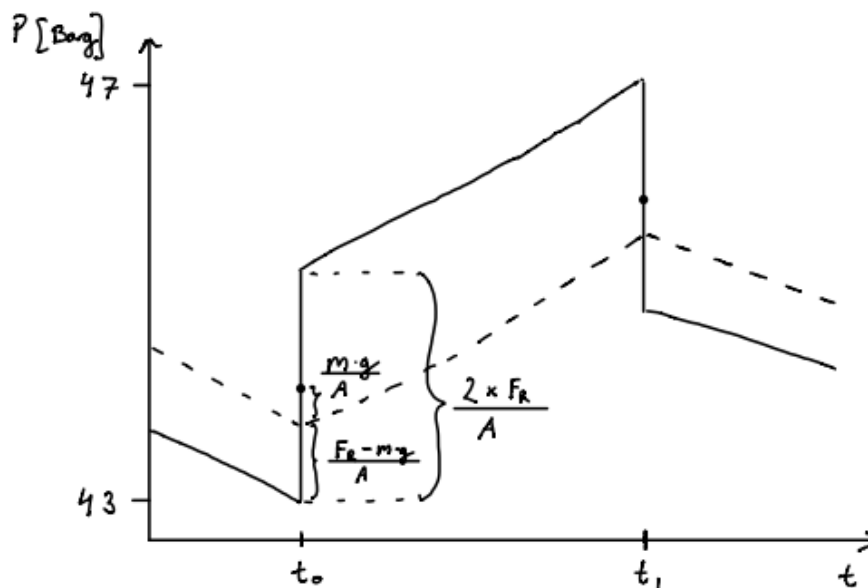
Figure 3.12: Sketch of pressure development in the gas (dashed line) and liquid (solid line) of the model.

From Fig. 3.12, it can be seen that the pressure in the upper part of the accumulator is higher then first assumed, when the charging process begins at t_0. The friction force was considered to be too low when comparing the first simulation results with the real pressure data. A new value for the friction force has been estimated to 1540 N, based on information from the accumulator company, and the pressure drop of about 2 bar observed from the measured presssure data. Also, based on the measured data set 1, the friction should change from negative to positive in about 2 s when the inlet valve is being closed. With the mass of the piston estimated to 5.7 kg, a new initial gas pressure has been estimated to $p_1 \approx 4496407.8$ Pa.

To find the new initial placement of the piston, the ideal gas equation of state was again used to find a new initial volume, and the inner height of the initial volume from the top of the piston to the top wall was thereafter found to be $H_1 \approx 0.575$ m.

The changes made to the initial pressures and placement of the piston are listed in Table 3.5.

Table 3.5: Changes to parameters for the accumulator precharged with 39 barg.

Parameter	Value
Initial pressure in liquid	$44 \cdot 10^5$ Pa
Initial pressure in gas	4496407.814 Pa
Initial volume of nitrogen	$8.86 \cdot 10^{-3}$ m^3
Initial placement of piston	575 mm

For this model heat transfer was also introduced through the walls of the accumulator and the piston. For the heat transfer through the walls of the accumulator, a heat transfer coefficient of 3.0 W/m$^2 \cdot$K was used, which is a typical value for natural convection of air at normal conditions. For the piston, a field function was applied at the boundary of the piston to transfer the heat between the fluid and steel, the thermal conductivity of the piston was chosen to 50 W/m·K.

3.7.2 Simulation 4: Double accumulator model

In the actual system, there are two accumulators, one precharged with 39 barg of pressure, and one with 55 barg of pressure. A second accumulator has been added to the model to see how this impacts the simulation. A 3D CAD model of the double accumulator has been made in Creo Parametric to show the dimensions of the model. This 3D model can be seen in Fig. 3.13.
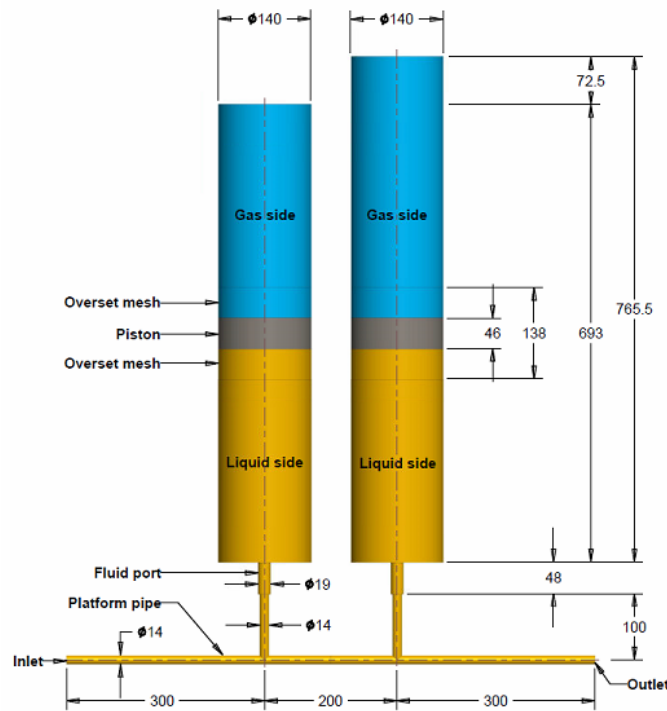
Figure 3.13: CAD model of the double accumulator, all dimensions are given in mm.

As can be seen from the model in Fig. 3.13, the accumulator to the right is 72.5 mm higher than the accumulator to the left. The reason for this is due to the position of the piston in the accumulator with 55 barg of pre-charge pressure. The initial position of the piston in the 55 barg accumulator is at the bottom of the accumulator, and this caused an issue with the connection between the overset mesh and the background when running the simulations. A virtual volume was then added to the bottom of the second accumulator, and the accumulator geometry had to be moved up corresponding to the height of this virtual volume. The virtual volume was set with a height of 72.5 mm, chosen to make the two pistons equally leveled at the initial placements.

3.7.3   Simulation 5: Improved simulation

For the last simulation, further improvements where made, to represent the real system even better. From the previous simulation results, it could be seen that the charging time was longer than that of the measured pressure data. In an attempt to increase the charging speed of the accumulator, the field function for the inlet pressure was changed to an average pressure value based on the pressure data required by OneSubsea. This average pressure was first calculated to $\approx$ 163 barg based on the initial pressure function, as shown in Fig. 3.5, and was then increased to 166 barg, to increase the inlet velocity.

Also the subsea pressure was changed, in an attempt to lower the outlet velocity. In the previous simulations, a constant pressure of 59.5 barg was used for the subsea pressure in the outlet pressure function described earlier in this chapter. When the pressure in the accumulator increases, the pressure down subsea should also increase, and this should lower the outlet velocity and thereby increase the charging speed. From the pressure data acquired from OneSubsea, the initial subsea pressure before the charging starts is around 58.8 barg, and when the charging of the accumulators starts the subsea pressure gradually builds up. In the following figure, measured data of the subsea pressure have been plotted, and curve fitting in Matlab has been used to estimate a function for the subsea pressure development.
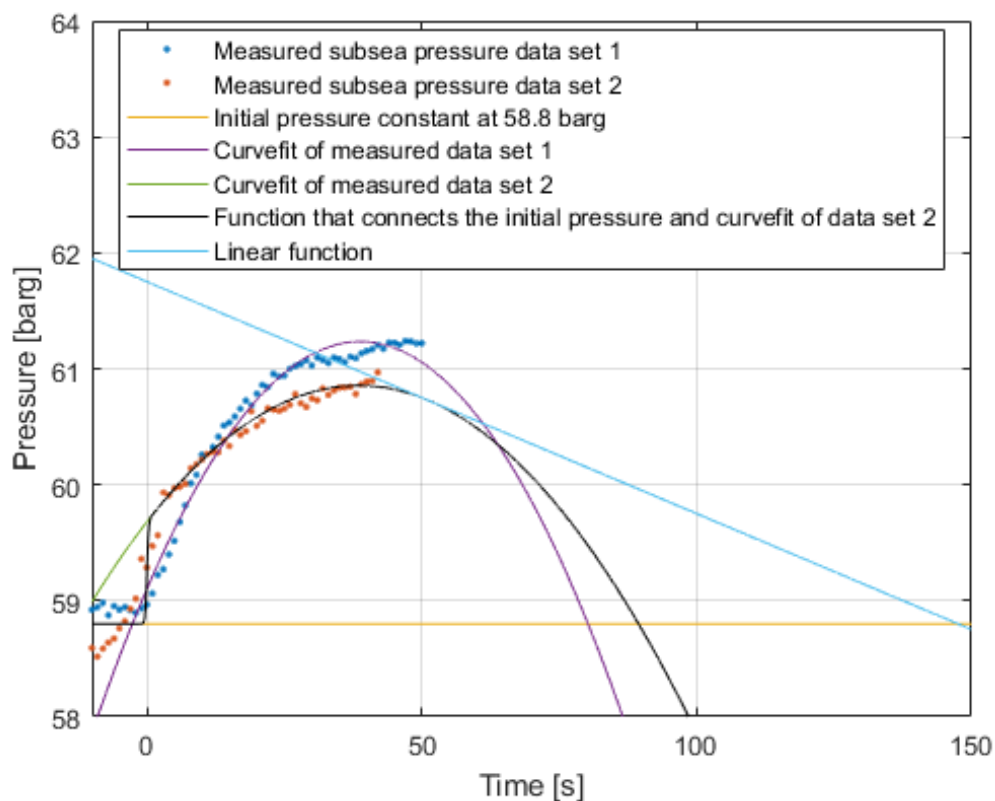
Figure 3.14: Plot of the estimate of a function that describes the subsea pressure development

As seen in Fig. 3.14, based on the measured data set 2, a field function was applied to the model to gradually increase from 58.8 barg to a quadratic function reaching 60.9 barg, and then slide over to a linear function bringing the pressure back down to 58.8 barg in around 150 s. It should be noted that the acquired measured pressure data stops at around 50 s, and the linear function is only an estimate. The subsea pressure may also vary due to slugs in the system, and inconsistent oil usage from the subsea pump.

Another modification that has been applied to this simulation is a gradually changing friction function at the start of the charging process. This is the same friction function that has been used for the earlier simulations in this project, to switch the direction of friction. This function has been modified and used at the start of the simulation as well. After this modification, the release time and ramp time in the DFBI was set to zero.

Chapter 4

Simulations

This chapter presents the simulations that have been run on the models. A sensitivity analysis has been set up to understand how the system model behaves. Many test simulations were run prior to these simulations to get a properly working model. The sensitivity analysis has been set up as follows:

1. Simulation of a single accumulator model without friction on the piston.

2. Simulation of a single accumulator model with constant friction of -616 N during charging and exponential change from negative to positive at the point of discharge.

3. Simulation of a single accumulator model with constant friction of -1540 N during charging, and from here, three different cases were set up:

   (a) Steep exponential change from negative to positive friction at the point of discharge in about 0.5 s.

   (b) Exponential change from negative to positive friction at the point of discharge in about 2 s.

   (c) Smooth change from negative to positive friction at the point of discharge in about 2 s.

4. Simulation of a double accumulator model with constant friction of 1540 N and exponential change same as 3b.

5. Improved simulation of a single accumulator model, modified with a friction shift at the start of the simulation, for this two cases were set up:

   (a) With exponential friction shift at the start and end of charging in 2 s, similar to 3b.

   (b) With smooth friction shift at the start and end of charging in 2 s, similar to 3c.

The first three simulations that are presented use a model with a single accumulator precharged with 39 barg. The fourth simulation use a model with two accumulators with the accumulators precharged with 39 barg and 55 barg respectively. In the sensitivity analysis, the causes that leads to the pressure drop have been investigated, and the different simulations have been compared to give an overview of how the model is affected by specific adjustments.

The following figure shows a closer look at the measured pressure data from the charging and discharging of the low-pressure system as presented in Fig. 1.3.
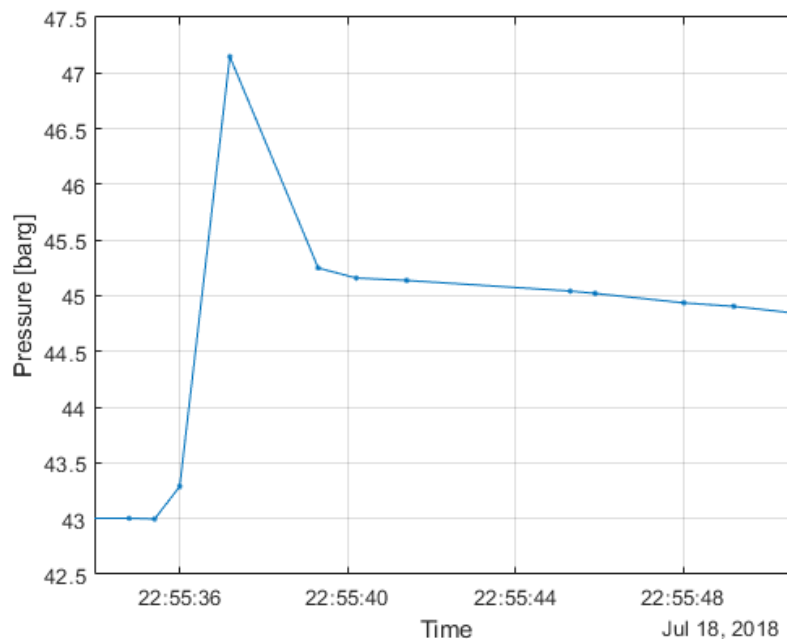
Figure 4.1: A close look at the measured pressure data, showing the charging process of the investigated low pressure system.

The measured data presented in Fig. 4.1, has been compared with the results from the different simulations in the sensitivity analysis, and the simulation results have been used to investigate the sudden pressure drop that occurs when the inlet valve is being closed.

Two more data sets were later provided by OneSubsea, and these data have also been included in the sensitivity analysis. The data sets have then been used to further, improve, and verify the model. All data sets have been plotted in one graph showing the first 12 s after the start of charging as shown in Figure 4.2.
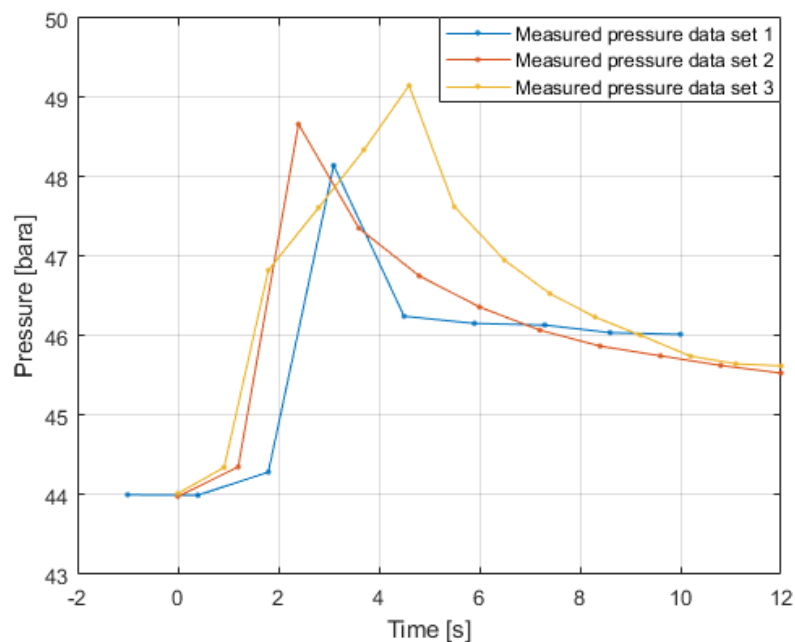
Figure 4.2: Three different measured data sets showing the pressure development during charging of the accumulators.

In the measured data sets that have been provided by OneSubsea, some of the measurements are spaced with one second, some occur within the same second, and some are spaced with two seconds. Further away from the interval of charging, the measurements have a longer sampling interval. Since the charging occurs in a short period, and the measurements have been sampled at an inconsistent sample interval, there are significant uncertainties related to the data sets.

In the graphs shown in Fig. 4.2, the interval from where the charging starts at zero seconds to around 12 seconds were equally distributed over the interval. Also, to better visualize the pressure curves, lines have been drawn between the points. It should be pointed out that what happens between the time of each sample is unknown.

4.1 Sensitivity analysis

This section presents the sensitivity analysis as described in the above. For all simulations, a scene representation has been set up to show the pressure, velocity, and temperature development in the system. This scene has then been recorded as images, and have been used to make animations of the simulations. An example of the recorded scene can be seen in Fig. 4.3.
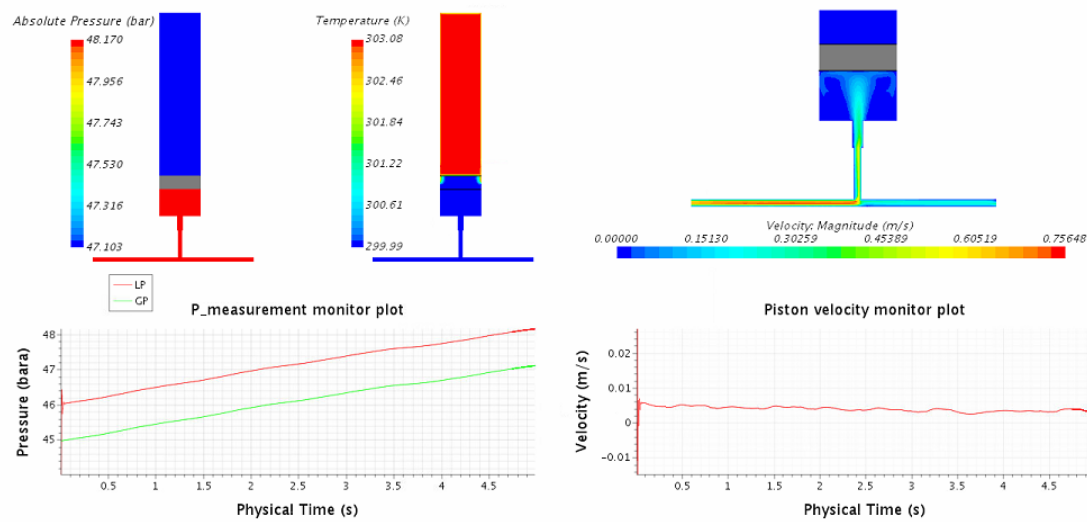
Figure 4.3: Recording scene showing scenes with pressure, temperature and velocity, and plots of pressure and piston velocity during charging of the single accumulator model.

4.1.1   Simulation 1:   Single accumulator model 39 barg without friction

The first simulation that has been run for the sensitivity analysis is a simulation with zero friction force. The simulation was set up with an initial pressure of 44 bara in both gas and liquid, and the placement of the piston was adjusted accordingly. The simulation was run and stopped automatically when the pressure in the liquid reached 47 bara. From here, the inlet boundary was changed from velocity inlet to wall, and the simulation was further run until the time reached 11 s. Fig. 4.4 shows the pressure development of the liquid and gas in the accumulator with a black line and black dotted line, respectively.
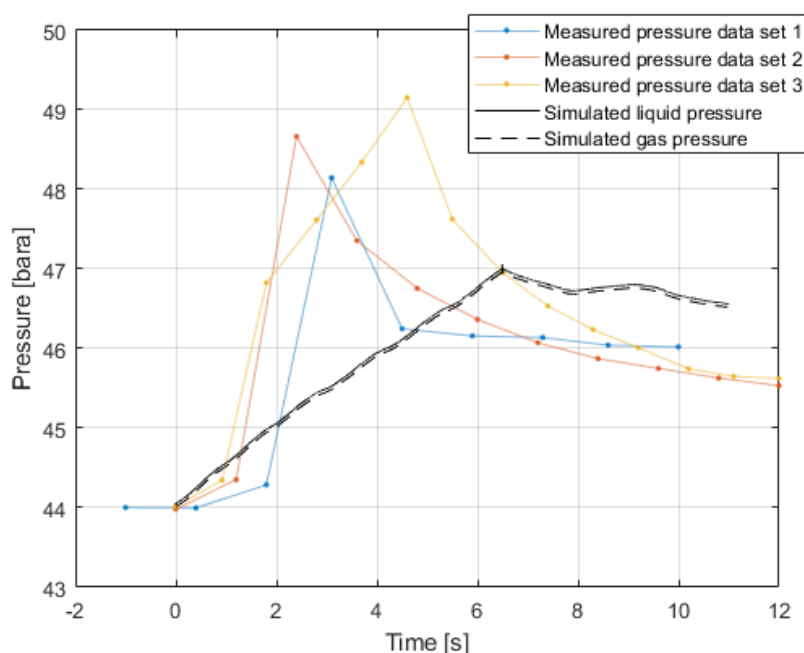
Figure 4.4: Graph showing the measured data sets together with the simulated liquid pressure and gas pressure in the single accumulator model without friction during the charging process.

It can be seen from Fig. 4.4 that for this simulation, the pressure never reached the higher pressure points of the measured data sets. This is due to the stop criterion at 47 bara, where the inlet was closed. Also, there is no pressure drop at the 47 bara point, the pressure in the liquid and gas follow each other in a parallel manner, only separated by the pressure difference caused by the mass of the piston. It was found that the pressure drop does not occur since the friction force is not present in the simulation. Due to these findings, a second simulation was set up as the first simulation, but also accounting for the friction force.

4.1.2   Simulation 2: Single accumulator model 39 barg with 616 N friction

The second simulation has been set up with a constant friction force of 616 N. The initial pressure was set to the same value as in simulation 1, where the pressure in both gas and liquid were set equal to 44 bara. The stopping criterion of 47 bara was kept. When the pressure in the liquid reached this stopping criterion, the velocity inlet was changed to a wall condition, and the direction of the friction was changed from negative to positive in an exponential manner by applying the constants $a = 3$, t_0 as the start time the function, and the slope constant $w = 0.1$, to Eqn.(3.6.5). The simulation was again run until it reached 11 s. The pressure development from this simulation has been plotted, as seen in the figure below.
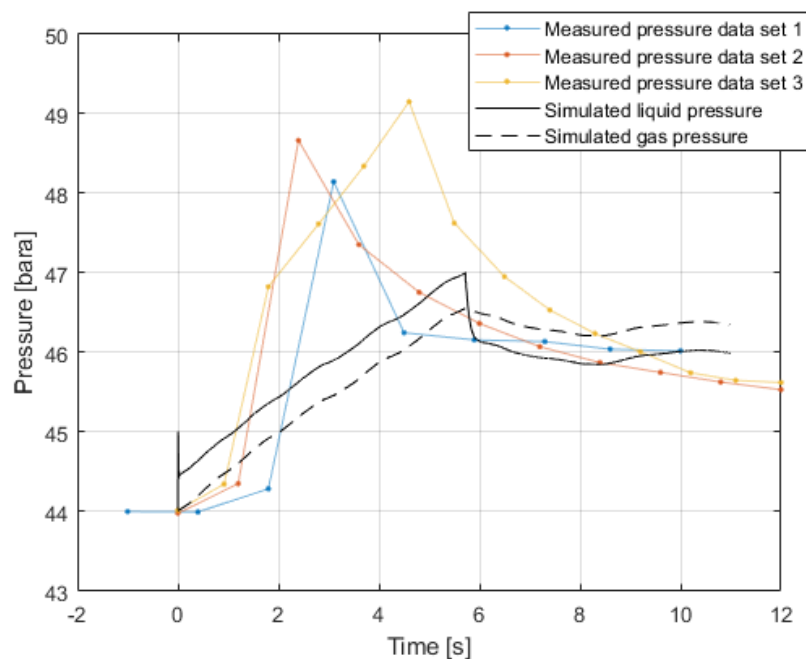
Figure 4.5: Graph showing the measured data sets together with the liquid pressure and gas pressure in the single accumulator model with a friction force of 616 N during the charging process.

From Fig. 4.5, it can be seen that the pressure in the liquid drops down two times the pressure difference corresponding to the friction force when reaching the 47 bara criterion, while the gas pressure slowly starts to decrease without any sudden drop in pressure. This shows the impact of the friction force on the pressure in the system. When comparing the simulated pressure from this simulation with simulation 1, the difference between the liquid pressure and the gas pressure has increased with ≈ 0.5 bar, this pressure difference is due to the applied friction force. When looking at the start of the simulation, a sudden pressure increase together with large oscillations can be seen. This was seen as a consequence of starting the simulation with an incorrect pressure in the gas and liquid.

From this simulation, it was found that the initial pressure of the gas and liquid should not be equal. When the charging process starts, the pressure in the liquid is 43 barg. At this point, the pressure in the gas has to be higher than the pressure in the liquid due to the friction force from the piston on its way down.

4.1.3 Simulation 3: Single accumulator model 39 barg with 1540 N friction

For this simulation, a new field function to control the individual initial pressures was made in Star CCM+. The changes that have been made are described in the previous chapter. A single accumulator model with a precharge pressure of 39 barg was set up. The friction of the piston was increased to 1540 N, and the initial pressure condition has been adjusted for this model to represent the difference in pressure between the gas and liquid at the time of simulation start.

The simulation has been divided into three cases, where all three have the same charging process, but at the time of discharge, three different friction functions have been applied. For these three cases, the pressure was built gradually towards a new stopping criterion of 48 bara, where the simulation was automatically stopped. Then the inlet boundary was closed by applying a wall condition to the boundary, and the friction function was changed from constant -1540 N to a function changing towards 1540 N by applying Eqn.(3.6.5). The first two cases was set up to change the friction function exponentially, by using the constants $a = 3$, and t_0 as the start time the function. The slope constant w was selected to 0.1 and 0.2 for the 0.5 s and 2 s friction shifts respectively. The third case was set up to change the friction function smoothly with a *tanh* function by using $a = 1$, and t_0 selected to correspond with the turning point of function. The slope constant w was selected to 0.2 to chanage the function in 2 s.

As seen in Fig. 4.6, the pressure in the low-pressure system has been plotted for all three simulated cases in the same graph together with the measured pressure data.

Figure 4.6: Graph showing the measured data sets together with the liquid pressure and gas pressure during the charging process of the single accumulator model with a friction force of 1540 N, and three different scenarios regarding the friction shift.

Similarities can be seen when comparing the simulated results with the measured pressure data in Fig. 4.6. Both the simulated pressure graphs and the measured pressure data shows a drop in pressure when the valve is closed. It can be seen from the graph that the pressure drop in the simulation is about the same as the first measured data set. The simulated pressure better fits the measured data due to the increased friction force. The shape of the pressure drop is linked to the friction force. When the inlet is being closed, and the direction of the friction force is switched, the pressure in the simulation drops down. This pressure drop is twice the pressure difference due to friction. It can also be seen that at the start of the simulation as with the previous simulation, there is still a sudden pressure increase. It was found that there should be a friction shift at the start of the simulation as well due to the initial situation. From this simulation the 2 s exponential friction shift, together with the 2 s smooth friction shift was taken further.

4.1.4   Simulation 4: Double accumulator model

The fourth simulation have been set up with a model consisting of two accumulators precharged with 39 and 55 barg of nitrogen. This to see how the second accumulator impacts the simulation, compared with the single accumulator model. The double accumulator model has been presented in the previous chapter.

As with the other simulations, a visual scene has been set up for the double accumulator model as well, and an example of the representation can be seen in Fig. 4.7.
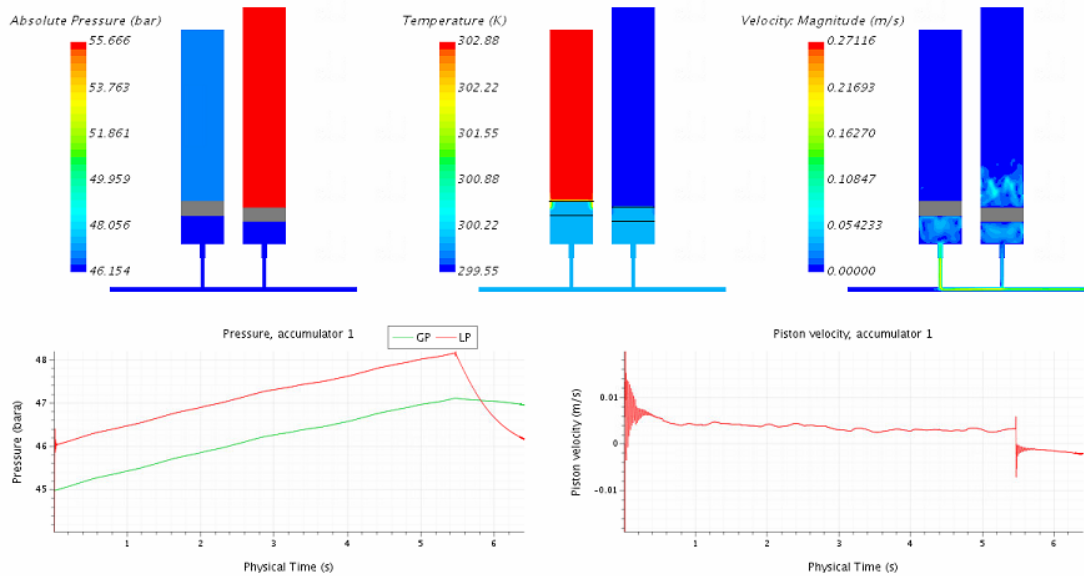
Figure 4.7: Recording scene showing the charging of the double accumulator model precharged with 39 and 55 barg.

The double accumulator model was set up the same way as the third simulation with an exponential friction shift of 2 s. The simulation has been compared with the third simulation with exponential friction shift of 2 s by plotting the pressure from both simulations in the same graph as seen in the figure below.
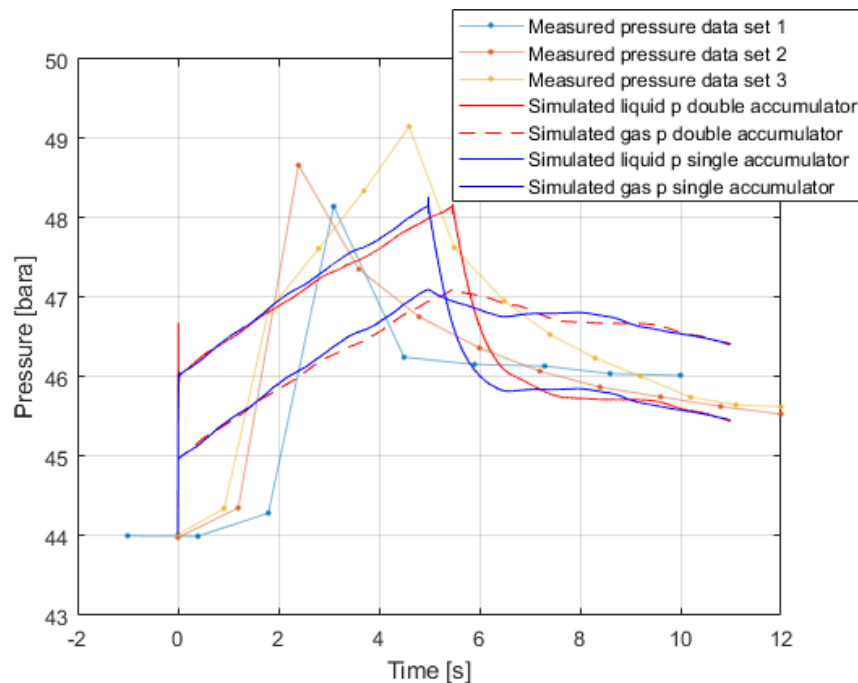
Figure 4.8: Graph showing the measured pressure data sets together with the liquid pressure and gas pressure during the charging process for both the double accumulator model and the single accumulator model with the same exponential friction shift.

It can be seen from Fig. 4.8, that there is a small offset between the two simulations. The

charging of the double accumulator model is ≈ 0.5 s slower than the single accumulator model. The reason for this small offset in charging time is possibly due to the virtual volume that was added to the simulation together with the extra volume from the fluid port of the second accumulator. There was no movement of the piston in the second accumulator during the whole simulation. The results shows that the system is not affected allot by the second accumulator.

4.2   Simulation 5: Improved single accumulator model

In the four previous simulations, the charging process was started suddenly, and the change in friction force direction was not accounted for. For this simulation, it was desired to model this behavior as well. Due to the results from the double accumulator model with 39 and 55 barg, an improved version of the one accumulator model was developed, and the improvements have been shown in the previous chapter. The inlet velocity and pressure outlet boundaries have been adjusted in an attempt to better meet the pressure development in the actual system.

The simulation was set up with the initial conditions of 43.0 barg pressure in the barrier fluid, and ≈ 44.0 barg in the gas. The subsea pressure was set to a constant value of 58.8 barg, and the simulation was run with the inlet closed until the pressure in the barrier fluid dropped down to 42.99 barg to get a stable simulation. During this period, the friction force was kept constant at 1540 N. At the moment when the pressure in the barrier fluid reached 42.99 barg, the simulation was automatically stopped. From here, two scenarios were set up, one with exponential friction shift, and one with a smooth friction shift. The following simulation parameters where changed:

1. Inlet boundary was changed from wall to velocity inlet

2. Direction of friction force was changed exponentially and smoothly in ≈ 2 s for the two simulations.

3. The subsea pressure in the function for the smart pressure outlet was changed from constant 58.8 barg to a quadratic function based on the subsea pressure from the data sets as presented in the previous chapter.

With these changes made to the simulation, the simulation was again started to simulate the charging of the accumulator. A scene showing the charging of the improved model can be seen in Fig. 4.9
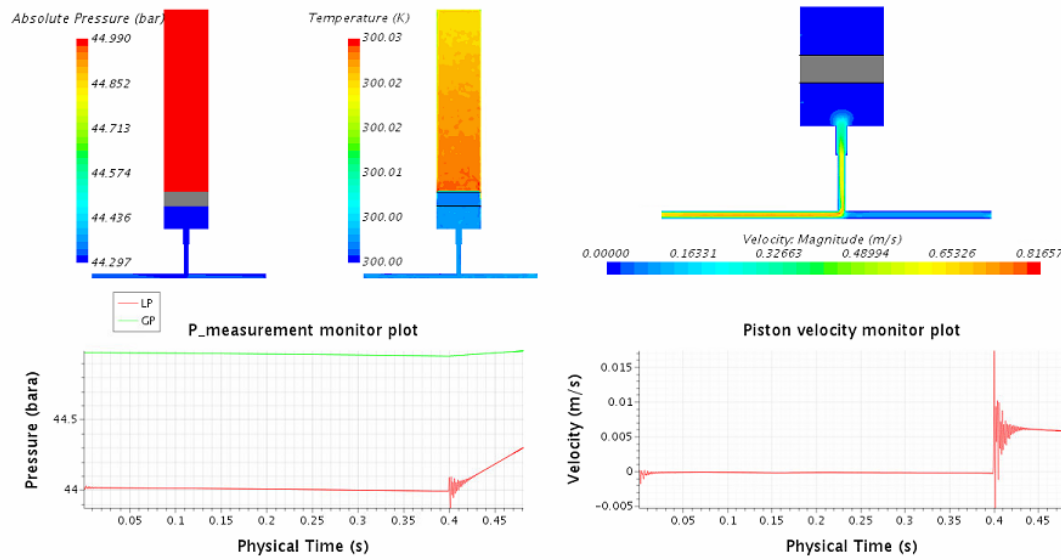
Figure 4.9: Recording scene showing the charging of the improved accumulator model precharged with 39 barg.

The simulation was again automatically stopped when pressure had reached 47.15 barg so that the simulation parameters could be changed for the discharge process.

1. Inlet boundary was changed back from velocity inlet to wall.

2. Direction of friction force was changed exponentially and smoothly in ≈ 2 s for the two simulations.

The simulation was run further to simulate the discharge of the system. 50 s from the start point of charge the subsea pressure switches from the quadratic function to a linear function that slowly brings the subsea pressure down, but the simulation was stopped at 11 s as the other simulations. The simulation results from the two cases are shown in the the following.

4.2.1 Pressure results

For the improved simulation of the single accumulator model, two cases were set up, where the following figure shows the scenario with exponential friction shift:
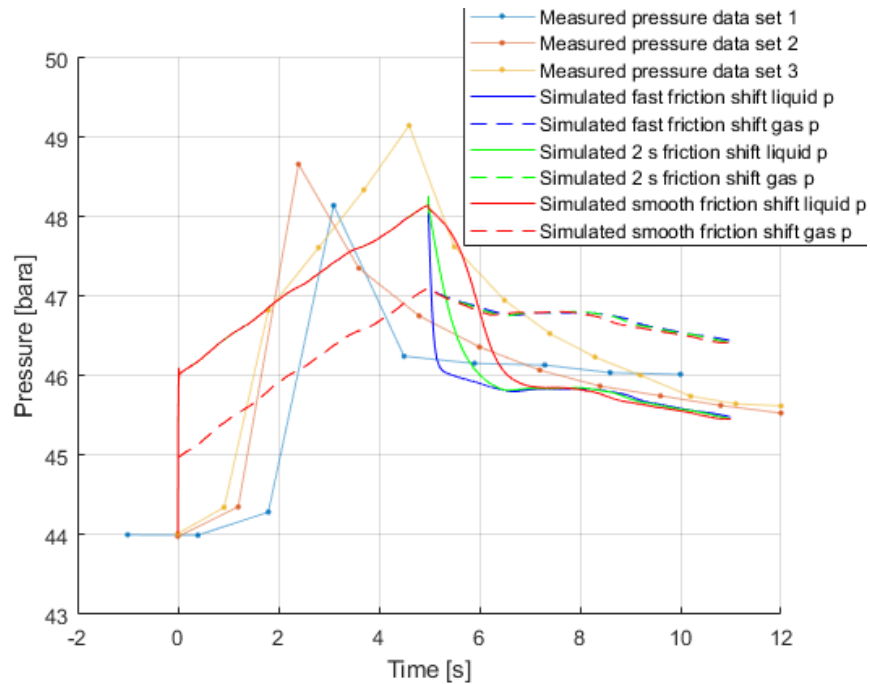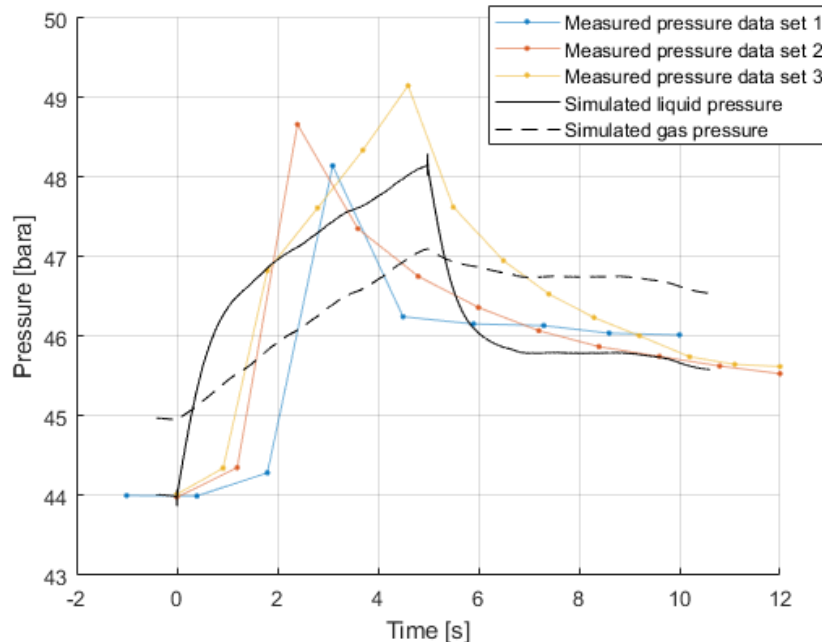

Figure 4.10: Graph showing the measured data sets together with the liquid pressure and gas pressure during the charging process for the improved simulation with exponential friction shift.

From Fig. 4.10 it can be seen that the liquid pressure is kept at 44 bara for a short period before the charging starts at time = 0 s. When the charging begins, the pressure does not longer jump up, due to the applied friction shift at the start of charging, the pressure changes exponentially. When the simulation results are compared with the measured pressure data, it can be seen that the liquid pressure changes too fast and is far from the measured pressure data points at the start of the charging process. The average discrepancy between the simulated liquid pressure and the three data sets has been calculated to ≈ 1.64 %, with measured data set 3 as the best fit with an average discrepancy of ≈ 1.41 %.

The second scenario that has been modeled with a smooth friction-shift is shown in the following figure:
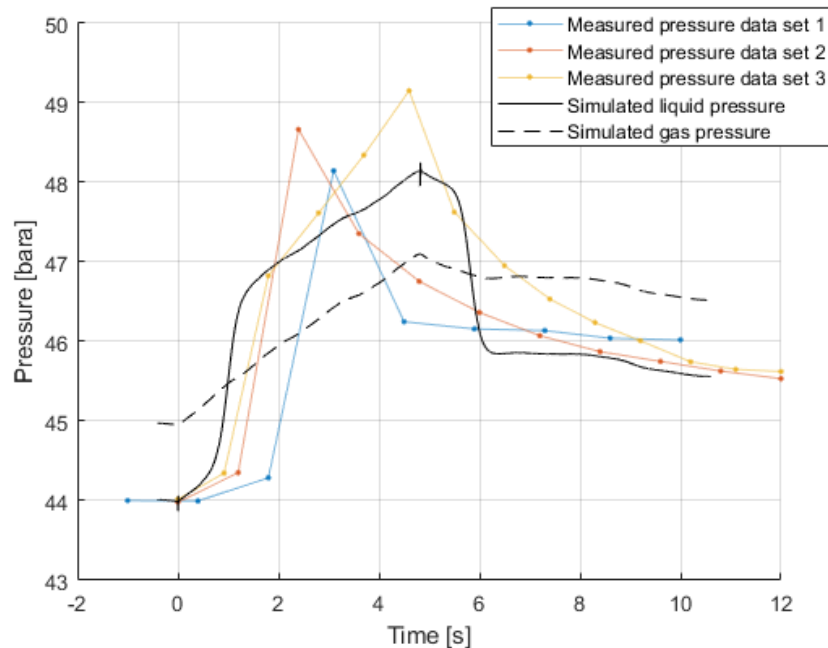
Figure 4.11: Graph showing the measured data sets together with the liquid pressure and gas pressure during the charging process for the improved simulation with smooth friction shift.

As shown in Fig. 4.11, the simulated liquid pressure stretches towards the measured pressure data during the charging. This is due to the smooth friction shift that has been applied to the piston. When comparing the charging time with simulation 3, both simulations take 4.96 s to charge, even though the volume flow was changed at both the inlet and outlet for this last simulation. When looking at the difference between the three measured pressure data sets and the pressure in the liquid for this scenario, the average discrepancy has been calculated to ≈ 1.43 %, with the best fit compared with the measured pressure data set 3 with an average discrepancy of ≈ 1.06 %. From these discrepancies, it is shown that the scenario with a smooth friction shift shows the best fit, with the measured data set 3 as the closest.

From the measured pressure data set 3, it can be seen that the friction shift at the start and after charging should not be equal. This may be due to the difference between the amount of incoming volume flow during charging, and outgoing volume flow during the discharge process. For further improvements, the friction shift should be adjusted for the first friction shift to make the pressure curve stretching slightly forward. Also, the second friction shift should be adjusted to stretch even further out. At the end of this chapter, the functions that control the friction shift have been described.

4.2.2   Preliminary temperature analysis

For the second scenario with smooth friction-shift, additionally, a preliminary temperature analysis was carried out, to see how temperature affects the pressure. A scalar scene showing the temperature distribution in the accumulator during the charging and discharge process has been recorded. As described in Section 3.7 in Chapter 3 Modeling setup, a heat transfer coefficient of 3.0 W/m^2·K have been added to the walls of the accumulator, and heat transfer through the piston has been set with a thermal conductivity of 50 W/m·K. In the following figure, the temperature has been monitored during the charge.

(a) t=0.38 s (Just before charge)

(b) t=1.0 s

(c) t=4 s

(d) t=5.2 s (Just before discharge)
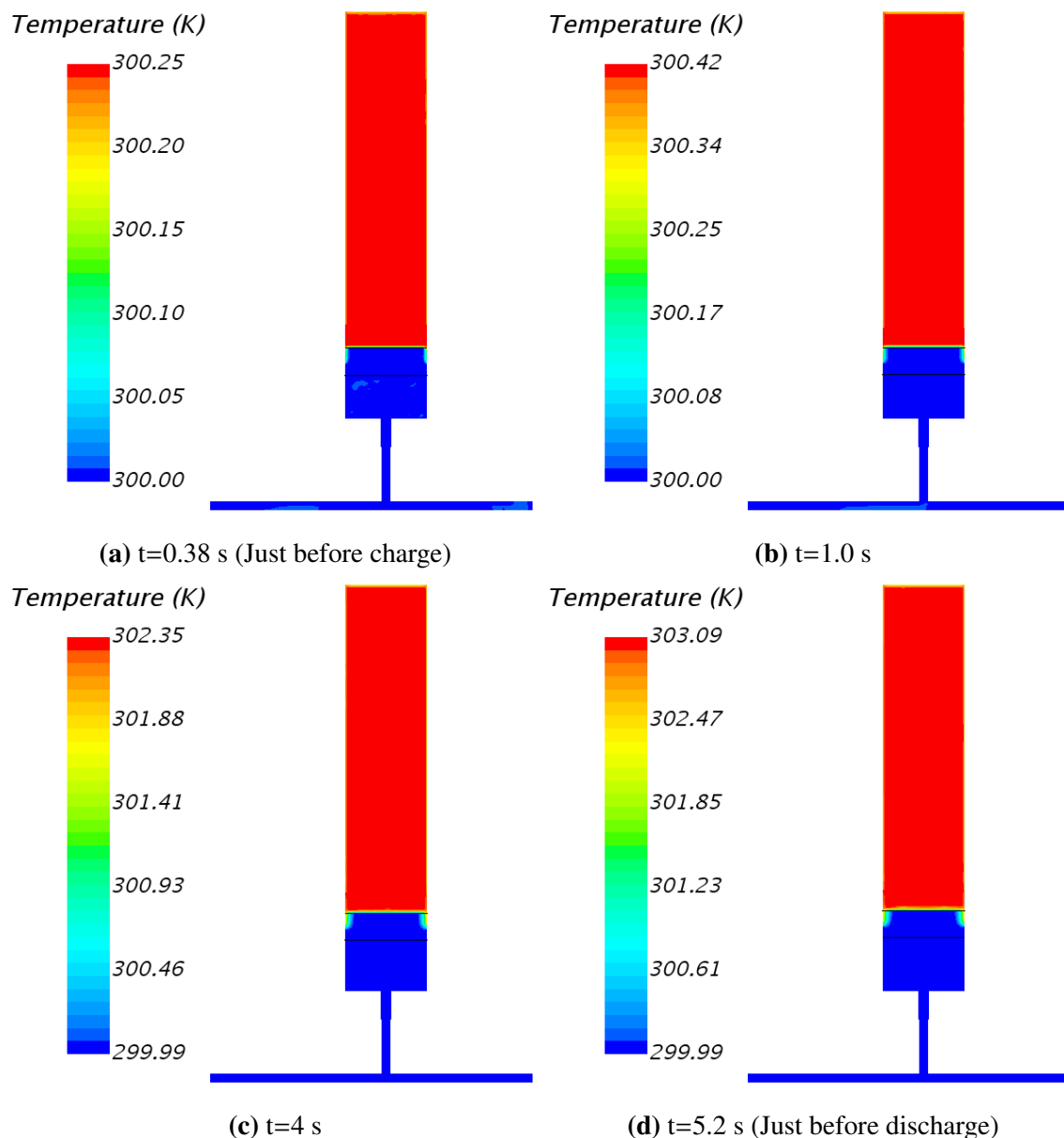
Figure 4.12: Scalar scenes showing the temperature distribution in the accumulator during the charging process.

Fig. 4.12a shows the temperature right before the charging starts, with the gas temperature at 300.25 K, when the pressure increase towards 47.15 barg, the gas temperature has

increased 2.84 K to 303.09 K. This is not a significant increase in temperature, and have a minimal effect on the pressure during the charging of the accumulators. The next figure shows the discharge process from the point where the accumulator has just started to discharge. For this part of the analysis, the simulation was run for an extended time period.

(a) t=5.22 s (Just after discharge)

(b) t=6.0 s

(c) t=8.0 s

(d) t=19.18 s
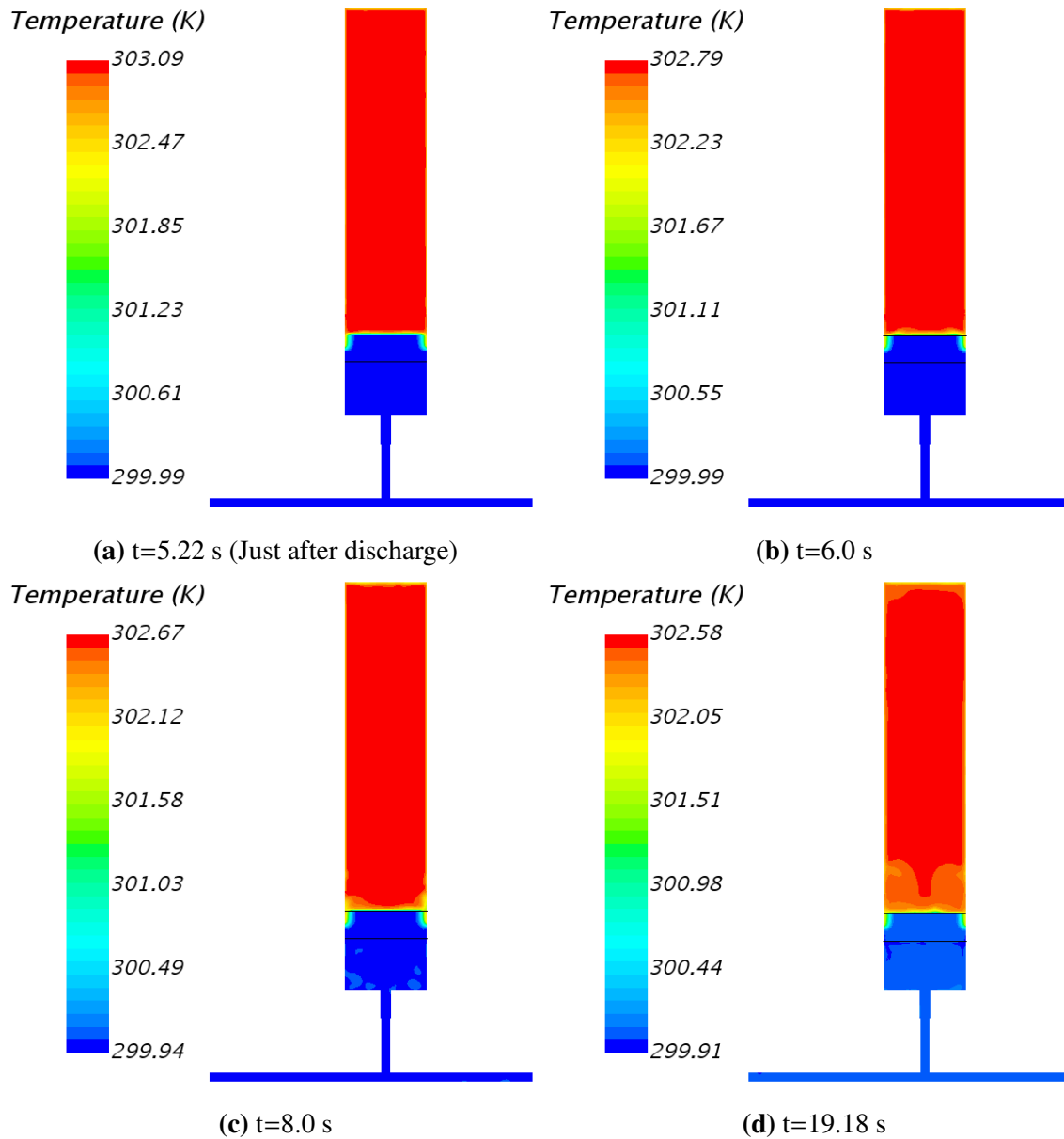
Figure 4.13: Scalar scenes showing the temperature distribution in the accumulator during the discharge process.

From Fig. 4.13a it can be seen that the temperature monotonically decreases with the discharge process. The temperature dropped by 0.51 K in $\approx$ 14 s. For this simulation, there has not been induced any heat from the piston friction, and the only source of heat comes from compression/ expansion of the nitrogen gas.

4.3   Overall discussion

As seen from the first three simulations apart from the first with no friction force, a sudden pressure increase happens at the start of the simulation. This is due to the initial pressure difference between the gas and liquid side of the piston in connection with the direction and magnitude of the friction force. For these three simulations, the simulations where started with a constant friction force in negative z-direction, assuming the piston was on its way up. At the same time, it was assumed that the pressure was higher in the gas than that of the liquid. These two assumptions did not add up, and therefore, the pressure in the liquid jumped up to the pressure that corresponded with the applied friction force. For the fifth simulation, the initial pressure was set as the third and fourth simulation, but the initial friction force was here set in the positive z-direction. The simulation was run, and the friction function was gradually shifted from positive to negative, which also smoothly changed the liquid pressure.

When comparing the pressure results from the second scenario of the last simulation with the measured pressure data set 3 in Fig. 4.11, three major differences are seen:

1. At the start of the charging process, the simulated pressure curve does not meet the first measured pressure points.

2. The measured pressure data set 3 goes higher than the simulated results and in a shorter time interval.

3. The last major difference is at the beginning of the discharge process, where the measured pressure data set 3 drops down in a much slower rate than that of the simulated pressure development.

The functions related to these differences have been looked at, and the impact of the different model parameters have been discussed to give an understanding of how to control the model and further improve the virtual digital twin. In Appendix A, a description by the author of this thesis has been attached, which shows how to run the simulations.

For point 1 and 3 in the list above, the friction force function plays an important role. The friction function that has been used for the second scenario in the last simulation have been based on Eqn.(3.6.5), and have been written in Star CCM+ syntax as follows:

$$1540*tanh((\${Time\}-(\${\_time\_of\_friction\_shift\}+1))/0.2)$$

Where 1540 is the friction force, and the *tanh* function shifts this friction force from a negative to a positive value. For the two friction shifts that occur in the process, the first

one shifts direction from positive to negative, whereas the second friction shift shifts from negative to positive. ${Time}$ is the proceeding time in the simulation, ${\_time\_of\_friction\_shift}$ is the time where the friction should start to change, and when the latter is added by 1, it defines the time of the turning point of the function. This yields when the desired friction shift is 2 s. The expression inside the *tanh* function is divided by 0.2, which controls the slope of the function.   This function should be changed individually for the two friction shifts, to meet the measured data set 3 better.

For the second point in the list, the rate of incoming and outgoing fluid is seen as the main driver. In the final simulation, the inlet and outlet flow were adjusted in an attempt to decrease the charging time of the system. There was no visual change in the charging speed. In order to make the system charge faster, the inlet velocity should be even higher, or the outlet pressure needs to be higher to make the outlet velocity lower. When doing this, the physical system should also be analyzed more in detail to make sure all pressure losses are accounted for.

Chapter 5

Conclusion

In this project, a digital twin of a hydraulic accumulator in a hydraulic system has been developed. The digital twin was modeled with the CFD software Simcenter STAR-CCM+.

Four simulations were run in a sensitivity analysis to study different parameters that impact the behavior of the model, including a sudden pressure drop occurring after the charging of the system. In this sensitivity analysis, first, a simulation with a single accumulator model without friction was run, but this simulation did not show any pressure drop after the charging process. A second simulation with constant friction of 616 N was then set up, and a connection between the pressure drop and the friction was established. It was found that the pressure drop in the liquid was caused by the change in friction direction, where the pressure drop corresponded with two times the pressure difference between the liquid and gas due to the friction. It was discovered some irregularities with the initial pressures that had to be adjusted prior to the third simulation.

For the third simulation, the friction force was increased to 1540 N, and the initial pressure distribution in the gas and liquid was changed to correspond with the applied friction force. In this simulation, different functions for the friction shift was tested out. It was seen that the pressure drop was about the same as the measured pressure data, more specific measured pressure data set 1.

The model setup was taken further and compared with a double accumulator model similar to the actual system. These simulations were compared, and the two models showed the same behavior, only small differences were seen in the charging time, where the double accumulator model charged ≈ 0.5 s slower than the single accumulator model. The additional charging time was seen as a consequence of the extra added volume to the second accumulator.

After the sensitivity analysis, two cases were brought further, where the single accumulator model with a friction force of 1540 N and a smooth change in friction force was seen as the best model to represent the physical system. For this final simulation, the model had been improved with a smooth friction force at the beginning of the charging process. This model followed the pressure pattern of the acquired measured data sets with an average discrepancy of ≈ 1.43 %, where the measured pressure data set 3, showed best similarities with an average discrepancy of ≈ 1.06 %. The relationship between the simulated pressure and the measured pressure data provided by OneSubsea showed good correlation. Hence, this model can be recommended for further development of the virtual digital twin to be used for leak detection assignments.

For this simulation, a preliminary temperature analysis was also conducted, this to see how the temperature developed in the system, and to see if the temperature had any impact on the pressure. Based on this preliminary analysis on temperature, the results show that the temperature has little effect on the pressure. The heat potentially induced from the piston friction has also been brought to light, which should be included in further improvements of the model by, e.g., introducing a constant heat source on the piston. From both the temperature and pressure analysis, further improvements have been suggested for the model to make it an even closer representation of the actual system.

5.1   Future work

In future work regarding the digital twin, the following should be included:

- Increase the inlet velocity and increase the outlet pressure, to achieve a faster charging process and meet the measured data.

- Adjust the friction function for the start of the charging process and at the beginning of the discharge to better represent the actual system. Dynamic friction could also be implemented to include stick-slip phenomenon to the model. Here the coefficients for friction should be based on friction analysis.

- To simulate the generated heat from friction, a constant temperature source could be added to the piston.

- Develop a faster model that can be run simultaneously with the physical system. This can be done e.g. by modeling a section of the accumulator, and then use symmetry to represent the whole accumulator. A mesh independence study should also be performed to find the best possible grid size of the mesh.

References

[1] Shell, "Technical Data Sheet Shell Morlina S2 BL 5," pp. 1–2, 2014.

[2] J. Anderson, G. Degres, J. Degroote, E. Dick, R. Grundmann, and J. Vierendeels, *Computational Fluid Dynamics An Introduction*, 3rd ed., J. F. Wendt, Ed. Belgium: Springer, 2009.

[3] Siemens, "STAR-CCM+® Documentation," 2018.

[4] B. H. Armstrong, P. Dupont, and C. C. De Wit, "A Survey of Models , Analysis Tools and Compensation Methods for the Control of Machines with Friction," vol. 30, no. 7, pp. 1083–1138, 1994.

[5] S. Andersson, A. Söderberg, and S. Björklund, "Friction models for sliding dry, boundary and mixed lubricated contacts," *Tribology International*, vol. 40, no. 4, pp. 580–587, 2007.

[6] HAWE, "Pressure drop-flow rate chart for valves," 2019. [Online]. Available: https://www.hawe.com/fluid-lexicon/pressure-drop-flow-rate-chart-for-valves/

[7] T. Stordal, "Resource Report. Exploration 2018," *Norwegian Petroleum Directorate*, pp. 62–63, 2018. [Online]. Available: http://www.npd.no/Global/Engelsk/3-Publications/Resource-report/Resource-report-2018/Hele-rapporten-engelsk.PDF

[8] T. N. Bakke, J. H. Klungsøyr, and S. I. Sanni, *Langtidsvirkninger av utslipp til sjø fra petroleumsvirksomheten - Resultater fra ti års forskning*, 2012.

[9] Oljedirektoratet, "Miljø og teknologi - Utslipp til sjø," 2018. [Online]. Available: https://www.norskpetroleum.no/miljo-og-teknologi/utslipp-til-sjo/

[10] E. Tangeraas, "Pipeguard," 2017. [Online]. Available: https://www.tu.no/artikler/enkelt-men-genialt-slik-klarer-badminton-flua-a-oppdage-lekkasjer-i-ror/398170

[11] E. C. Hiis, "Master Thesis," *Norwegian University of Science and Technology*, 2018.

[12] V. Irizar, P. Windfeld Rasmussen, O. Doujoux Olsen, and C. Schousboe Andreasen, "Modeling and Verification of Accumulators using CFD," *Proceedings of 15:th Scandinavian International Conference on Fluid Power, 15th Scandinavian International Conference on Fluid Power, Fluid Power in the Digital Age, SICFP'17, June 7-9 2017 - Linköping, Sweden*, vol. 144, pp. 340–350, 2018.

[13] Simens, "Digital Twin." [Online]. Available: https://www.plm.automation.siemens.com/global/en/our-story/glossary/digital-twin/24465

[14] OneSubsea, "Multiphase Subsea Pump." [Online]. Available: https://www.onesubsea.slb.com/processing-systems/subsea-pumps/multiphase-subsea-pump

[15] T. Larsen, *Pumpe staabi*, 3rd ed. Kbh.: Ingeniøren-bøger, 2000.

[16] K. Brautaset, *Innføring i oljehydraulikk.* Oslo: Gyldendal Norsk Forlag, 2013.

[17] J. F. Gülich, *Centrifugal Pumps*, 2nd ed. Berlin: Springer, 2010.

[18] Y. A. Çengel and M. A. Boles, *Thermodynamics: An Engineering Approach.* McGraw-Hill Education, 2014. [Online]. Available: https://books.google.no/books?id=c1qFoAEACAAJ

[19] Wandfluh, "Technical Explanations Hydraulic Valves," pp. 1–9, 2019. [Online]. Available: http://alt.wandfluh.com/fileadmin/user_upload/files/A_Dok/reg_1_0/1_0_100_e.pdf

[20] HAWE, "Throttles type ED Restrictor check valves type RD and RDF," no. March, pp. 4–6, 2004.

[21] R. A. Serway and J. W. Jewett, *Physics for Scientists and Engineers*, 6th ed., Unknown, 2004.

[22] G. Koreisovà, "Identification of viscous damping coefficient of hydraulic motors," *Scientific papers of the university of pardubice Series B*, 2006.

Appendix

Appendix A

Instructions for digital twin

Instructions for the digital twin

Author: Otto Andreas Moe

These instructions show how to run simulations with the accumulator models, and how to set up the model. The instruction starts with an explanation of how the model is set up.

Notes made regarding the Geometry>3D-CAD model:

If any changes need to be done on the geometry, there is a possibility that the regions must be created once again, by first making a copy of the .sim file, then clearing all generated meshes, deleting the regions and parts, and then following these steps.

1. The piston has been modeled in the center of the accumulator and is later moved to the initial placement. If it is moved in the 3D-CAD model the simulation will later not function properly.

2. The piston and the two overset over and under the piston are made as three individual parts, by applying body interaction > "none" in the 3D-CAD model.

3. After creating a "new geometry part for all the parts," select the parts overset and overset2, right click and select "combine."

4. Now there are three parts, Background, Overset, and Solid_Piston, make sure that the parts surfaces have been defined, this has been done in the 3d-geometry. Select the three parts, right click and select "Assign parts to regions" and select, as shown below:
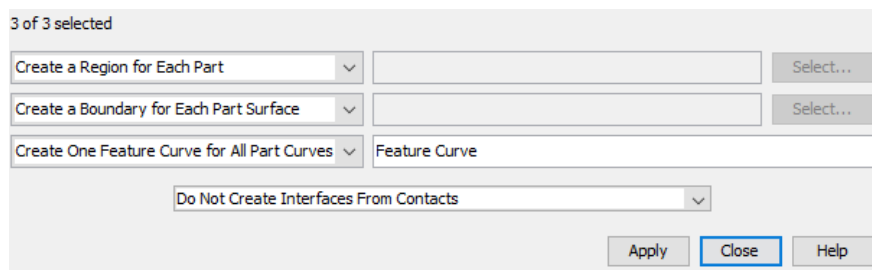
Notes on preparing the model for simulation:

Open the copy that was made earlier, go through and compare the two files

1. Geometry>Operations (go through a,b,c,d before returning to this)

2. Continua

3. Regions

4. Interfaces

Is made by:

a. Selecting the Region> Overset and background, right click and create interface>Overset mesh,

b. Selecting the Region>Overset>Wall and Region>Solid_piston>Default, right click and create an interface, repeat with Wall 2.

5. DFBI

6. Derived parts

7. Solvers

8. Construct the mesh

Running the simulation is done in three steps

Make the simulation ready for simulation

1.) Move piston into initial placement, by selecting Regions>Solid_piston and Regions>Overset, right click and select Transform>translate, and set the initial height. That is the height from the center of the accumulator to the center of the piston.

2.) DFBI>6-DOF Bodies>Body>Force 1, select the field function "_friction_force_piston"

3.) Go to field functions, and set the constant friction force that is desired for "_friction_force_piston."

4.) Go to the field functions "_outlet_pressure_with_loss," and make sure that the first term after the question mark links to the field function "_subsea_pressure_initial" (This will keep the subsea pressure constant in this initial phase)

5.) Go to Regions>Background>Boundaries>Inlet and set the type to "wall."

6.) Set Stopping Criteria>LP Criterion that is a maximum criterion to "not active," and set Stopping Criteria>LP Criterion2 that is a minimum criterion to "active."

7.) Set Maximum Physical time to the desired time, for this project, 11 s have been used to make the plots stopping at this time.

8.) Run the simulation, and the simulation will automatically stop when "Lp Criterion2" is reached

Make the simulation ready for the charge

1.) DFBI>6-DOF Bodies>Body>Force 1, select the field function "_friction_force_47_barg"

2.) Go to field functions, and set the friction force you want "_friction_force_47_barg" (piston changes from down to up movement=> friction from up to down direction).

3.) Go to field function "_friction_time_of_friction_shift", and set the time that is right now, inside the previous function I have linked to this function and have added +1s. This sets the turning point of the tanh function (The time right now can be found by open the

pressure plot and navigate to the plot>pressures>Bottom Axis. Make sure you have zoomed entirely out on the plot, and then copy the value for Maximum value)

4.) Also, go to the field function "_time_of_first_friction_shift," and paste the time here as well (this will be linked to the subsea pressure that is the next number on this list)

5.) Go to the field function "_outlet_pressure_with_loss," and change the first term after the question mark to link to the field function "_subsea_pressure_charge_or_linear." This will change the subsea pressure from a constant value to an increasing function, so that subsea pressure increases as the accumulator pressure increase, this is a quadratic function, that first will increase to 50s and after this automatically shift to a linear function that decreases.

6.) Go to Regions>Background>Boundaries>Inlet, and set type to "velocity inlet," make sure that the field function "_inlet velocity" is selected

7.) Set Stopping Criteria>LP Criterion that is a maximum criterion to "active," and set Stopping Criteria>LP Criterion2 that is a minimum criterion to "not active."

8.) Run the simulation, and the simulation will automatically stop when Lp Criterion is reached

Make the simulation ready for discharge

1.) DFBI>6-DOF Bodies>Body>Force 1, keep the field function "_friction_force_47_barg"

2.) Go to field functions and change the "_friction_force_47_barg", to switch in the opposite direction. (piston changes from up to down movement=> friction from down to up direction)

3.) Go to field function "_friction_time_of_friction_shift," and set the time for the time of your new friction shift

4.) Go to Regions>Background>Boundaries>Inlet and set type to "wall."

5.) Set Stopping Criteria>LP Criterion that is a maximum criterion to "not active," and perhaps you want to set Stopping Criteria>LP Criterion2 that is a minimum criterion to "active."

6.) Run the simulation, and the simulation will automatically stop when "Lp Criterion2" is reached, or when the criterion for "maximum physical time" is reached.

Description of the self-made field functions in same order as seen in Star CCM+:

_density_oil – The density of the Morlina S2 BL5 barrier fluid

_density_oil_changing_with_pressure – this is the density changing with pressure

_friction force_47_barg – function to shift the direction of the friction force, in this project a tanh function has been modified by using matlab as a visualization tool:

For a smooth friction shift the following equation have been used:

$$F \cdot \tanh\left(\frac{t - t_0}{w}\right) = \frac{F \cdot \exp\left(\frac{t - t_0}{w}\right) - F \cdot \exp\left(\frac{t_0 - t}{w}\right)}{\exp\left(\frac{t - t_0}{w}\right) + \exp\left(\frac{t_0 - t}{w}\right)}$$

where F is the friction, t is the time, t_0 is the turning point of the friction, t_0=_friction_time_of_frictionshift + (some value), I have used (some value)=1 s, w is a value to control the slope, the constant w was in this project set to w=0.2, these parameters changes the friction force direction in about two seconds.

For an exponential friction shift the following have been used:

$$\frac{F \cdot \exp\left(\frac{t - t_0}{w}\right) - 3 \cdot F \cdot \exp\left(\frac{t_0 - t}{w}\right)}{\exp\left(\frac{t - t_0}{w}\right) + \exp\left(\frac{t_0 - t}{w}\right)}$$

Multiplying the second term in the previous equation with 3 makes t_0=_friction_time_of_frictionshift. The slope value w was changed to see the effect, 0.1 changes the friction quickly, and 0.6 changes the friction in about two seconds.

_friction_force_piston -constant value to be used in the initial phase where piston is gong down=> direction is up

_friction_time_of_friction_shift – the time where the friction shift takes place

_HP – The pressure in the high-pressure system that delivers barrier fluid to the model

_Initial_pressure_distribution – the pressure in the gas and liquid is different from each other due to friction and mass of piston

_Inlet_velocity -the inlet velocity is applied to the inlet boundary. The function is based on the function Q_nozzle that again is based on the _HP function

_K_dir_valve – this is a valve coefficient for the solenoid valve

_kinematic_viscosity_oil – the kinematic viscosity of the barrier fluid Morlina S2 BL5

_L -this is a coefficient for the orifice

_lambda_turbulent_laminar – the friction coefficient, it is a function that changes between two functions based on if the flow is laminar or turbulent.

_Outlet_volume_flow – The outlet volume flow is calculated in a plane at the outlet pipe with an average velocity magnitude. This function is used to calculate the different pressure losses in the piping and umbilical (the velocity magnitude has been tried changed to velocity in "i" direction to account for the direction of flow without luck)

_outlet_pressere_with_loss – This is a smart boundary that is applied to the outlet boundary. It is a function based on the subsea pressure, and all losses in the piping calculating back to the pressure at the outlet.

_piston_direction (not used delete if you want)

_Q_nozzle- The volume flow at the inlet based on the pressure at the high-pressure system (_HP) and the pressure in the accumulator liquid pressure (LP), together with all the pressure losses in the valves and orifice between the two systems.

_Re_outlet -Reynolds number calculated at the outlet, to switch if the flow is turbulent or laminar

_subsea_pressure_charge – a quadratic function based on data sets required from OneSubsea

_subsea_pressure_charge_or_linear – a function that is applied in the second phase when charging starts. The subsea pressure will change from a constant value (same as _ subsea_pressure_initial) to a quadratic function "_subsea_pressure_charge" by using a tanh function. The pressure will then rise according to the quadratic function, and when 50 s is reached, the function automatically switches to a linear function "_subsea_pressure_linear", bringing the pressure down

_subsea_pressure_initial – constant value for the subsea pressure that is used in the initial phase

_subsea_pressure_linear – linear function that brings the subsea pressure down during discharge

_tempereature_piston_wall – a function that moves with the piston, to define the wall temperature of the piston and hence simulate heat transfer through the piston. This function is applied to the Region>solid_piston_default_pysics values>static_temperature – scalar function

_time_of_first_frictionshift – the time of the first friction shift is put in here and added by +1 since this field function actually is the time of the **turning point** of the tanh function function in the subsea pressure. The subsea pressure then changes from a constant value to a quadratic function in about 2 s.

Initial distribution – This function sets the initial placement of oil (where oil and gas are separated). The initial height is measured from the center of the accumulator to the center of the piston, and the value should therefore be the same as the initial placement of the piston

Initial distribution (nitrogen) – this function sets the initial placement of gas, and is automatically changed based on the previous function

Appendix B

Matlab script

Matlab script for:

1. Simulation 1: Single accumulator model 39 barg without friction

2. Simulation 2: Single accumulator model 39 barg with 616 N friction

3. Simulation 3: Single accumulator model 39 barg with 1540 N friction

4. Simulation 4: Double accumulator model

5. Simulation 5: Improved single accumulator model

6. Script to plot the measured pressure data

7. Script for finding the function for friction shift

8. Script for finding the function for the pressure in the high pressure system

9. Script to find the function for the subsea pressure

```matlab
%Simulation 1: Single accumulator model 39 barg without friction
clear all
close all
clc
%Author: Otto Andreas Moe

A = importdata('01_without_friction.csv',',',1); %importer data filnavn,
delimiterIn '\t' (for tab), headerlinesIn 22
A = A.data;
timea = A(:,1);%s
lpa = A(:,2);%bar
gpa = A(:,3);%bar


[~, ~, raw1, dates1] = xlsread('C:\Users\Otto\Desktop\OneSubsea Master
project\Matlab\Data_OneSubsea\Brenda_data_april.xlsx','Sheet2','E9:F41','',@co
nvertSpreadsheetExcelDates);
raw1 = raw1(:,2);
dates1 = dates1(:,1);
data1 = reshape([raw1{:}],size(raw1));
Brendadataapril = table;
realtime1 = datetime([dates1{:,1}].', 'ConvertFrom', 'Excel');
LPbarg1 = data1(:,1);

[~, ~, raw2, dates2] = xlsread('C:\Users\Otto\Desktop\OneSubsea Master
project\Matlab\Data_OneSubsea\Brenda_data_april.xlsx','Sheet2','L9:M36','',@co
nvertSpreadsheetExcelDates);
raw2 = raw2(:,2);
dates2 = dates2(:,1);
data2 = reshape([raw2{:}],size(raw2));
Brendadataapril_2 = table;
realtime2 = datetime([dates2{:,1}].', 'ConvertFrom', 'Excel')
LPbarg2 = data2(:,1)

[~, ~, raw0_0, dates0_0] = xlsread('C:\Users\Otto\Desktop\OneSubsea Master
project\Matlab\Data_OneSubsea\data.xlsx','Sheet2','C2:C41','',@convertSpreadsh
eetExcelDates);
[~, ~, raw0_1, dates0_1] = xlsread('C:\Users\Otto\Desktop\OneSubsea Master
project\Matlab\Data_OneSubsea\data.xlsx','Sheet2','D2:D41','',@convertSpreadsh
eetExcelDates);
raw3 = [raw0_0,raw0_1];
dates3 = [dates0_0,dates0_1];
raw3 = raw3(:,2);
dates3 = dates3(:,1);
data3 = reshape([raw3{:}],size(raw3));
realtime3 = datetime([dates3{:,1}].', 'ConvertFrom', 'Excel');
LPbarg3 = data3(:,1);

LPbarg3 = LPbarg3(2:10);
Lp3=LPbarg3+1;
realtimelp3=realtime3(2:10);
t3=[-1,0.4,1.8,3.1,4.5,5.9,7.3,8.6,10];
figure();

plot3 = plot(t3,Lp3,'.-');
plot3.Color(4) = 0.5;
```

```matlab
hold on

LPbarg1 = LPbarg1(13:23);
Lp1=LPbarg1+1;
realtimelp1=realtime1(13:23);
t1=[0,1.2,2.4,3.6,4.8,6,7.2,8.4,9.6,10.8,12];


plot1 = plot(t1,Lp1,'.-');
plot1.Color(4) = 0.5;

LPbarg2 = LPbarg2(3:16);
Lp2=LPbarg2+1;
realtimelp2=realtime2(3:16);
t2=[0,0.92,1.8,2.8,3.7,4.6,5.5,6.5,7.4,8.3,9.2,10.2,11.1,12];
plot2 = plot(t2,Lp2,'.-');
plot2.Color(4) = 0.5;

plot(timea,lpa,'k -')
plot(timea,gpa,'k --')

xlabel('Time [s]');
ylabel('Pressure [bara]');
legend('Measured pressure data set 1','Measured pressure data set 2','Measured
pressure data set 3','Simulated liquid pressure','Simulated gas pressure')
grid on
```

```matlab
%Simulation 2: Single accumulator model 39 barg with 616 N friction
clear all
close all
clc
%Author: Otto Andreas Moe

A = importdata('02_with_616N_at11s.csv',',',1); %importer data filnavn,
delimiterIn '\t' (for tab), headerlinesIn 22
A = A.data;
timea = A(:,1);%s
lpa = A(:,2);%bar
gpa = A(:,3);%bar


[~, ~, raw1, dates1] = xlsread('C:\Users\Otto\Desktop\OneSubsea Master
project\Matlab\Data_OneSubsea\Brenda_data_april.xlsx','Sheet2','E9:F41','',@co
nvertSpreadsheetExcelDates);
raw1 = raw1(:,2);
dates1 = dates1(:,1);
data1 = reshape([raw1{:}],size(raw1));
Brendadataaapril = table;
realtime1 = datetime([dates1{:,1}].', 'ConvertFrom', 'Excel');
LPbarg1 = data1(:,1);

[~, ~, raw2, dates2] = xlsread('C:\Users\Otto\Desktop\OneSubsea Master
project\Matlab\Data_OneSubsea\Brenda_data_april.xlsx','Sheet2','L9:M36','',@co
nvertSpreadsheetExcelDates);
raw2 = raw2(:,2);
dates2 = dates2(:,1);
data2 = reshape([raw2{:}],size(raw2));
Brendadataaapril_2 = table;
realtime2 = datetime([dates2{:,1}].', 'ConvertFrom', 'Excel')
LPbarg2 = data2(:,1)

%% Import the data, extracting spreadsheet dates in Excel serial date format
[~, ~, raw0_0, dates0_0] = xlsread('C:\Users\Otto\Desktop\OneSubsea Master
project\Matlab\Data_OneSubsea\data.xlsx','Sheet2','C2:C41','',@convertSpreadsh
eetExcelDates);
[~, ~, raw0_1, dates0_1] = xlsread('C:\Users\Otto\Desktop\OneSubsea Master
project\Matlab\Data_OneSubsea\data.xlsx','Sheet2','D2:D41','',@convertSpreadsh
eetExcelDates);
raw3 = [raw0_0,raw0_1];
dates3 = [dates0_0,dates0_1];
raw3 = raw3(:,2);
dates3 = dates3(:,1);
data3 = reshape([raw3{:}],size(raw3));
realtime3 = datetime([dates3{:,1}].', 'ConvertFrom', 'Excel');
LPbarg3 = data3(:,1);

LPbarg3 = LPbarg3(2:10);
Lp3=LPbarg3+1;
realtimelp3=realtime3(2:10);
t3=[-1,0.4,1.8,3.1,4.5,5.9,7.3,8.6,10];

figure();
plot3 = plot(t3,Lp3,'.-');
```

```matlab
plot3.Color(4) = 0.5;
hold on

LPbarg1 = LPbarg1(13:23);
Lp1=LPbarg1+1;
realtimelp1=realtime1(13:23);
t1=[0,1.2,2.4,3.6,4.8,6,7.2,8.4,9.6,10.8,12];

plot1 = plot(t1,Lp1,'.-');
plot1.Color(4) = 0.5;

LPbarg2 = LPbarg2(3:16);
Lp2=LPbarg2+1;
realtimelp2=realtime2(3:16);
t2=[0,0.92,1.8,2.8,3.7,4.6,5.5,6.5,7.4,8.3,9.2,10.2,11.1,12];
plot2 = plot(t2,Lp2,'.-');
plot2.Color(4) = 0.5;

plot(timea,lpa,'k')

plot(timea,gpa,'k --')

xlabel('Time [s]');
ylabel('Pressure [bara]');
legend('Measured pressure data set 1','Measured pressure data set 2','Measured
pressure data set 3','Simulated liquid pressure','Simulated gas pressure')
grid on
```

```matlab
%Simulation 3: Single accumulator model 39 barg with 1540 N friction
clear all
close all
clc
%Author: Otto Andreas Moe


A = importdata('01_fast_pressure_a_0.1.csv',',',1); %importer data filnavn,
delimiterIn '\t' (for tab), headerlinesIn 22
A = A.data;
timea = A(:,1);%s
lpa = A(:,2);%bar
gpa = A(:,3);%bar


B = importdata('01_slow_2s_pressure.csv',',',1); %importer data filnavn,
delimiterIn '\t' (for tab), headerlinesIn 22
B = B.data;
timeb = B(:,1);%s
lpb = B(:,2);%bar
gpb = B(:,3);%bar


C = importdata('01_smooth_pressure.csv',',',1); %importer data filnavn,
delimiterIn '\t' (for tab), headerlinesIn 22
C = C.data;
timec = C(:,1);%s
lpc = C(:,2);%bar
gpc = C(:,3);%bar

[~, ~, raw1, dates1] = xlsread('C:\Users\Otto\Desktop\OneSubsea Master
project\Matlab\Data_OneSubsea\Brenda_data_april.xlsx','Sheet2','E9:F41','',@co
nvertSpreadsheetExcelDates);
raw1 = raw1(:,2);
dates1 = dates1(:,1);
data1 = reshape([raw1{:}],size(raw1));
Brendadataaapril = table;
realtime1 = datetime([dates1{:,1}].', 'ConvertFrom', 'Excel');
LPbarg1 = data1(:,1);

figure();
plot(realtime1,LPbarg1);

[~, ~, raw2, dates2] = xlsread('C:\Users\Otto\Desktop\OneSubsea Master
project\Matlab\Data_OneSubsea\Brenda_data_april.xlsx','Sheet2','L9:M36','',@co
nvertSpreadsheetExcelDates);
raw2 = raw2(:,2);
dates2 = dates2(:,1);
data2 = reshape([raw2{:}],size(raw2));
Brendadataaapril_2 = table;
realtime2 = datetime([dates2{:,1}].', 'ConvertFrom', 'Excel')
LPbarg2 = data2(:,1)

figure();
plot(realtime2,LPbarg2);
%% Import the data, extracting spreadsheet dates in Excel serial date format
```

```matlab
[~, ~, raw0_0, dates0_0] = xlsread('C:\Users\Otto\Desktop\OneSubsea Master
project\Matlab\Data_OneSubsea\data.xlsx','Sheet2','C2:C41','',@convertSpreadsh
eetExcelDates);
[~, ~, raw0_1, dates0_1] = xlsread('C:\Users\Otto\Desktop\OneSubsea Master
project\Matlab\Data_OneSubsea\data.xlsx','Sheet2','D2:D41','',@convertSpreadsh
eetExcelDates);
raw3 = [raw0_0,raw0_1];
dates3 = [dates0_0,dates0_1];
raw3 = raw3(:,2);
dates3 = dates3(:,1);
data3 = reshape([raw3{:}],size(raw3));
realtime3 = datetime([dates3{:,1}].', 'ConvertFrom', 'Excel');
LPbarg3 = data3(:,1);
figure()
plot(realtime3,LPbarg3);


LPbarg1 = LPbarg1(13:23);
Lp1=LPbarg1+1;
realtimelp1=realtime1(13:23);
t1=[0,1.2,2.4,3.6,4.8,6,7.2,8.4,9.6,10.8,12];

LPbarg3 = LPbarg3(2:10);
Lp3=LPbarg3+1;
realtimelp3=realtime3(2:10);
t3=[-1,0.4,1.8,3.1,4.5,5.9,7.3,8.6,10];

figure();
hold on;

plot3 = plot(t3,Lp3,'.-');
plot3.Color(4) = 0.5;

plot1 = plot(t1,Lp1,'.-');
plot1.Color(4) = 0.5;

LPbarg2 = LPbarg2(3:16);
Lp2=LPbarg2+1;
realtimelp2=realtime2(3:16);
t2=[0,0.92,1.8,2.8,3.7,4.6,5.5,6.5,7.4,8.3,9.2,10.2,11.1,12];

plot2 = plot(t2,Lp2,'.-');
plot2.Color(4) = 0.5;


plot(timea,lpa,'b');
plot(timea,gpa,'b--');
plot(timeb,lpb,'g');
plot(timeb,gpb,'g--');
plot(timec,lpc,'r');
plot(timec,gpc,'r--');

xlabel('Time [s]');
ylabel('Pressure [bara]');
```

```matlab
legend('Measured pressure data set 1','Measured pressure data set 2','Measured
pressure data set 3','Simulated fast friction shift LP','Simulated fast
friction shift GP','Simulated 2 s friction shift LP','Simulated 2 s friction
shift GP','Simulated smooth friction shift LP','Simulated smooth friction
shift GP');
grid on;
```

```matlab
%Simulation 4: Double accumulator model
clear all
close all
clc
%Author: Otto Andreas Moe

A = importdata('04_pressure_a_0.6.csv',',',1); %importer data filnavn,
delimiterIn '\t' (for tab), headerlinesIn 22
A = A.data;
timea = A(:,1);%s
gpa = A(:,2);%bar
lpa = A(:,3);%bar

B = importdata('01_slow_2s_pressure.csv',',',1); %importer data filnavn,
delimiterIn '\t' (for tab), headerlinesIn 22
B = B.data;
timeb = B(:,1);%s
lpb = B(:,2);%bar
gpb = B(:,3);%bar

[~, ~, raw1, dates1] = xlsread('C:\Users\Otto\Desktop\OneSubsea Master
project\Matlab\Data_OneSubsea\Brenda_data_april.xlsx','Sheet2','E9:F41','',@co
nvertSpreadsheetExcelDates);
raw1 = raw1(:,2);
dates1 = dates1(:,1);
data1 = reshape([raw1{:}],size(raw1));
Brendadataapril = table;
realtime1 = datetime([dates1{:,1}].', 'ConvertFrom', 'Excel');
LPbarg1 = data1(:,1);

%figure();
%plot(realtime1,LPbarg1);

[~, ~, raw2, dates2] = xlsread('C:\Users\Otto\Desktop\OneSubsea Master
project\Matlab\Data_OneSubsea\Brenda_data_april.xlsx','Sheet2','L9:M36','',@co
nvertSpreadsheetExcelDates);
raw2 = raw2(:,2);
dates2 = dates2(:,1);
data2 = reshape([raw2{:}],size(raw2));
Brendadataapril_2 = table;
realtime2 = datetime([dates2{:,1}].', 'ConvertFrom', 'Excel')
LPbarg2 = data2(:,1)

%% Import the data, extracting spreadsheet dates in Excel serial date format
[~, ~, raw0_0, dates0_0] = xlsread('C:\Users\Otto\Desktop\OneSubsea Master
project\Matlab\Data_OneSubsea\data.xlsx','Sheet2','C2:C41','',@convertSpreadsh
eetExcelDates);
[~, ~, raw0_1, dates0_1] = xlsread('C:\Users\Otto\Desktop\OneSubsea Master
project\Matlab\Data_OneSubsea\data.xlsx','Sheet2','D2:D41','',@convertSpreadsh
eetExcelDates);
raw3 = [raw0_0,raw0_1];
dates3 = [dates0_0,dates0_1];
raw3 = raw3(:,2);
dates3 = dates3(:,1);
data3 = reshape([raw3{:}],size(raw3));
realtime3 = datetime([dates3{:,1}].', 'ConvertFrom', 'Excel');
```

```matlab
LPbarg3 = data3(:,1);

LPbarg1 = LPbarg1(13:23);
Lp1=LPbarg1+1;
realtimelp1=realtime1(13:23);
t1=[0,1.2,2.4,3.6,4.8,6,7.2,8.4,9.6,10.8,12];

LPbarg3 = LPbarg3(2:10);
Lp3=LPbarg3+1;
realtimelp3=realtime3(2:10);
t3=[-1,0.4,1.8,3.1,4.5,5.9,7.3,8.6,10];

plot3 = plot(t3,Lp3,'.-');
plot3.Color(4) = 0.5;
grid on;
hold on;

plot1 = plot(t1,Lp1,'.-');
plot1.Color(4) = 0.5;

LPbarg2 = LPbarg2(3:16);
Lp2=LPbarg2+1;
realtimelp2=realtime2(3:16);
t2=[0,0.92,1.8,2.8,3.7,4.6,5.5,6.5,7.4,8.3,9.2,10.2,11.1,12];

plot2 = plot(t2,Lp2,'.-');
plot2.Color(4) = 0.5;

plot(timea,lpa,'r');
plot(timea,gpa,'r--');
plot(timeb,lpb,'b');
plot(timeb,gpb,'b');
xlabel('Time [s]');
ylabel('Pressure [bara]');
legend('Measured pressure data set 1','Measured pressure data set 2','Measured
pressure data set 3','Simulated LP double accumulator','Simulated GP double
accumulator','Simulated LP single accumulator','Simulated GP single
accumulator');
grid on;
```

```matlab
%Simulation 5: Improved single accumulator model
clear all
close all
clc
%Author: Otto Andreas Moe

A = importdata('05_pressure_smooth_increasing_subsure_pressure.csv',',',1);
%importer data filnavn, delimiterIn '\t' (for tab), headerlinesIn 22
A = A.data;
timea = A(:,1)%s
lpa = A(:,2);%bar
gpa = A(:,3);%bar

B = importdata('05_pressure_exponential_a_0.6.csv',',',1); %importer data
filnavn, delimiterIn '\t' (for tab), headerlinesIn 22
B = B.data;
timeb = B(:,1)%s
lpb = B(:,2);%bar
gpb = B(:,3);%bar

[~, ~, raw0_0, dates0_0] = xlsread('C:\Users\Otto\Desktop\OneSubsea Master
project\Matlab\Data_OneSubsea\data.xlsx','Sheet2','C2:C41','',@convertSpreadsh
eetExcelDates);
[~, ~, raw0_1, dates0_1] = xlsread('C:\Users\Otto\Desktop\OneSubsea Master
project\Matlab\Data_OneSubsea\data.xlsx','Sheet2','D2:D41','',@convertSpreadsh
eetExcelDates);
raw1 = [raw0_0,raw0_1];
dates1 = [dates0_0,dates0_1];
raw1 = raw1(:,2);
dates1 = dates1(:,1);
data1 = reshape([raw1{:}],size(raw1));
realtime1 = datetime([dates1{:,1}].', 'ConvertFrom', 'Excel');
LPbarg1 = data1(:,1);

[~, ~, raw2, dates2] = xlsread('C:\Users\Otto\Desktop\OneSubsea Master
project\Matlab\Data_OneSubsea\Brenda_data_april.xlsx','Sheet2','E9:F41','',@co
nvertSpreadsheetExcelDates);
raw2 = raw2(:,2);
dates2 = dates2(:,1);
data2 = reshape([raw2{:}],size(raw2));
Brendadataapril_2 = table;
realtime2 = datetime([dates2{:,1}].', 'ConvertFrom', 'Excel');
LPbarg2 = data2(:,1);

[~, ~, raw3, dates3] = xlsread('C:\Users\Otto\Desktop\OneSubsea Master
project\Matlab\Data_OneSubsea\Brenda_data_april.xlsx','Sheet2','L9:M36','',@co
nvertSpreadsheetExcelDates);
raw3 = raw3(:,2);
dates3 = dates3(:,1);
data3 = reshape([raw3{:}],size(raw3));
Brendadataapril_3 = table;
realtime3 = datetime([dates3{:,1}].', 'ConvertFrom', 'Excel')
LPbarg3 = data3(:,1)

LPbarg1 = LPbarg1(2:10);
Lp1=LPbarg1+1;
```

```matlab
realtimelp1=realtime1(2:10);
t1=[-1,0.4,1.8,3.1,4.5,5.9,7.3,8.6,10];
figure();
hold on;

LPbarg2 = LPbarg2(13:23);
Lp2=LPbarg2+1;
realtimelp2=realtime2(13:23);
t2=[0,1.2,2.4,3.6,4.8,6,7.2,8.4,9.6,10.8,12];

LPbarg3 = LPbarg3(3:16);
Lp3=LPbarg3+1;
realtimelp3=realtime3(3:16);
t3=[0,0.92,1.8,2.8,3.7,4.6,5.5,6.5,7.4,8.3,9.2,10.2,11.1,12];

plot1 = plot(t1,Lp1,'.-');
plot1.Color(4) = 0.5;
plot2 = plot(t2,Lp2,'.-');
plot2.Color(4) = 0.5;
plot3 = plot(t3,Lp3,'.-');
plot3.Color(4) = 0.5;
plot(timea-0.39784000000003644,lpa,'k');
plot(timea-0.39784000000003644,gpa,'k--');
xlabel('Time [s]');
ylabel('Pressure [bara]');
legend('Measured pressure data set 1','Measured pressure data set 2','Measured
pressure data set 3','Simulated liquid pressure','Simulated gas pressure');
grid on;

figure()
hold on
plot1 = plot(t1,Lp1,'.-');
plot1.Color(4) = 0.5;
plot2 = plot(t2,Lp2,'.-');
plot2.Color(4) = 0.5;
plot3 = plot(t3,Lp3,'.-');
plot3.Color(4) = 0.5;
plot(timeb-0.39784000000003644,lpb,'k');
plot(timeb-0.39784000000003644,gpb,'k--')
xlabel('Time [s]');
ylabel('Pressure [bara]');
legend('Measured pressure data set 1','Measured pressure data set 2','Measured
pressure data set 3','Simulated liquid pressure','Simulated gas pressure');
grid on;

%finding discrepancy between the measured pressure data
%(t1 & Lp1,t2 & Lp2,t3 & Lp3) and the "smooth" simulated pressure (timea &
lpa)

%Measured pressure data set 1 (t1 & Lp1) and "smooth" simulated pressure
(timea & lpa)
for n = 2:1:9
    idx1 = find(abs(timea-(t1(n)+0.4))<=0.00115)
lpa1(n-1)=lpa(idx1);
end
lpa1=lpa1'
```

```matlab
dis1a=Lp1(2:9)-lpa1
figure()
plot(t1(2:9),dis1a)
grid on
dis1a=(abs(dis1a)./Lp1(2:9)).*100;


avgdis1a=sum(dis1a)/8%average discrepancy in percentage



%Measured pressure data set 2 (t2 & Lp2) and "smooth" simulated pressure
(timea & lpa)
for n = 1:1:9
    idx2a = find(abs(timea-(t2(n)+0.4))<=0.00115)
   lpa2(n)=lpa(idx2a);
end
lpa2=lpa2'
dis2a=Lp2(1:9)-lpa2
figure()
plot(t2(1:9),dis2a)
grid on
dis2a=(abs(dis2a)./Lp2(1:9)).*100
avgdis2a=sum(dis2a)/9%average discrepancy in percentage

%Measured pressure data set 3 (t3 & Lp3) and "amooth" simulated pressure
(timea & lpa)
for n = 1:1:12
    idx3a = find(abs(timea-(t3(n)+0.4))<=0.00115)
 lpa3(n)=lpa(idx3a);
end
lpa3=lpa3'
dis3a=Lp3(1:12)-lpa3
figure()
plot(t3(1:12),dis3a)
grid on
dis3a=(abs(dis3a)./Lp3(1:12)).*100
avgdis3a=sum(dis3a)/12%average discrepancy in percentage



overalldis_a=(avgdis1a+avgdis2a+avgdis3a)/3%overall discrepancy in percentage

%finding discrepancy between the measured pressure data
%(t1 & Lp1,t2 & Lp2,t3 & Lp3) and the "exponential" simulated pressure (timeb
& lpb)

%Measured pressure data set 1 (t1 & Lp1) and "exponential" simulated pressure
(timeb & lpb)
for n = 2:1:9
    idx1b = find(abs(timeb-(t1(n)+0.4))<=0.00115)
lpb1b(n-1)=lpb(idx1b);
end
lpb1b=lpb1b'
dis1b=Lp1(2:9)-lpb1b
figure()
plot(t1(2:9),dis1b)
grid on
```

```matlab
dis1b=(abs(dis1b)./Lp1(2:9)).*100
avgdis1b=sum(dis1b)/8%average discrepancy in percentage


%Measured pressure data set 2 (t2 & Lp2) and "exponential" simulated pressure
(timeb & lpb)
for n = 1:1:9
    idx2b = find(abs(timeb-(t2(n)+0.4))<=0.00115)
   lpb2b(n)=lpb(idx2b);
end
lpb2b=lpb2b'
dis2b=Lp2(1:9)-lpb2b
figure()
plot(t2(1:9),dis2b)
grid on
dis2b=(abs(dis2b)./Lp2(1:9)).*100
avgdis2b=sum(dis2b)/9%average discrepancy in percentage

%Measured pressure data set 3 (t3 & Lp3) and "exponential" simulated pressure
(timeb & lpb)
for n = 1:1:12
    idx3b = find(abs(timeb-(t3(n)+0.4))<=0.00115)
 lpb3b(n)=lpb(idx3b);
end
lpb3b=lpb3b'
dis3b=Lp3(1:12)-lpb3b
figure()
plot(t3(1:12),dis3b)
grid on
dis3b=(abs(dis3b)./Lp3(1:12)).*100
avgdis3b=sum(dis3b)/12%average discrepancy in percentage


overalldis_b=(avgdis1b+avgdis2b+avgdis3b)/3%overall discrepancy in percentage
```

```matlab
%Script to plot the measured pressure data
clear all
close all
clc
%Author: Otto Andreas Moe

[~, ~, raw1, dates1] = xlsread('C:\Users\Otto\Desktop\OneSubsea Master
project\Matlab\Data_OneSubsea\Brenda_data_april.xlsx','Sheet2','E9:F41','',@co
nvertSpreadsheetExcelDates);
raw1 = raw1(:,2);
dates1 = dates1(:,1);
data1 = reshape([raw1{:}],size(raw1));
Brendadataaapril = table;
realtime1 = datetime([dates1{:,1}].', 'ConvertFrom', 'Excel');
LPbarg1 = data1(:,1);

figure();
plot(realtime1,LPbarg1,'.');

[~, ~, raw2, dates2] = xlsread('C:\Users\Otto\Desktop\OneSubsea Master
project\Matlab\Data_OneSubsea\Brenda_data_april.xlsx','Sheet2','L9:M36','',@co
nvertSpreadsheetExcelDates);
raw2 = raw2(:,2);
dates2 = dates2(:,1);
data2 = reshape([raw2{:}],size(raw2));
Brendadataaapril_2 = table;
realtime2 = datetime([dates2{:,1}].', 'ConvertFrom', 'Excel')
LPbarg2 = data2(:,1)

figure();
plot(realtime2,LPbarg2,'.');
%% Import the data, extracting spreadsheet dates in Excel serial date format
[~, ~, raw0_0, dates0_0] = xlsread('C:\Users\Otto\Desktop\OneSubsea Master
project\Matlab\Data_OneSubsea\data.xlsx','Sheet2','C2:C41','',@convertSpreadsh
eetExcelDates);
[~, ~, raw0_1, dates0_1] = xlsread('C:\Users\Otto\Desktop\OneSubsea Master
project\Matlab\Data_OneSubsea\data.xlsx','Sheet2','D2:D41','',@convertSpreadsh
eetExcelDates);
raw3 = [raw0_0,raw0_1];
dates3 = [dates0_0,dates0_1];
raw3 = raw3(:,2);
dates3 = dates3(:,1);
data3 = reshape([raw3{:}],size(raw3));
realtime3 = datetime([dates3{:,1}].', 'ConvertFrom', 'Excel');
LPbarg3 = data3(:,1);
figure()
plot(realtime3,LPbarg3,'.-');
xlabel('Time');
ylabel('Pressure [barg]');
grid on
%legend('Measured pressure data set 1')

LPbarg1 = LPbarg1(13:23);
Lp1=LPbarg1+1;
realtimelp1=realtime1(13:23);
t1=[0,1.2,2.4,3.6,4.8,6,7.2,8.4,9.6,10.8,12];
```

```matlab
LPbarg3 = LPbarg3(2:10);
Lp3=LPbarg3+1;
realtimelp3=realtime3(2:10);
t3=[-1,0.4,1.8,3.1,4.5,5.9,7.3,8.6,10];
figure();
plot(t3,Lp3,'.-');
grid on;
hold on;

plot(t1,Lp1,'.-');

LPbarg2 = LPbarg2(3:16);
Lp2=LPbarg2+1;
realtimelp2=realtime2(3:16);
t2=[0,0.92,1.8,2.8,3.7,4.6,5.5,6.5,7.4,8.3,9.2,10.2,11.1,12];
plot(t2,Lp2,'.-');

xlabel('Time [s]');
ylabel('Pressure [bara]');
legend('Measured pressure data set 1','Measured pressure data set 2','Measured
pressure data set 3');
grid on;
```

```matlab
%Script for finding the function for friction shift
clear all
clc
close all
%Author Otto Andreas Moe


F=1540
c=6;
r=20;
x1=0.39784000000003644
a1=0.1
a2=0.6
a3=0.8

time=0:0.01:5;
figure()
f1=(-1540.*exp((time-x1)./a1)+3.*1540.*exp((-time+x1)./a1))./(exp((time-
x1)./a1)+exp((-time+x1)./a1));
plot(time,f1,'k')
hold on
f2=(-1540.*exp((time-x1)./a2)+3*1540.*exp((-time+x1)./a2))./(exp((time-
x1)./a2)+exp((-time+x1)./a2));
plot(time,f2,'k')
f3=(-1540.*exp((time-x1)./a3)+3.*1540.*exp((-time+x1)./a3))./(exp((time-
x1)./a3)+exp((-time+x1)./a3));
plot(time,f3,'k')

%Guidelines
constant=time*0+1540;
plot(time,constant,'r--')
plot(time,-constant,'r--')
line([0.39784000000003644 0.39784000000003644], [-1540 1540])
line([7+1 7+1], [-1540 1540])

figure()
fyo=-1540.*tanh((time-(x1+1.76))./0.12)
plot(time,fyo,'k')
xlabel('time [s]')
ylabel('Force [N]')

%Guidelines
line([0.39784000000003644 0.39784000000003644], [-1540 1540])
line([0.92+0.39784000000003644 0.92+0.39784000000003644],[-1540 1540])
line([1.8+0.39784000000003644 1.8+0.39784000000003644],[-1540 1540])
line([2+0.39784000000003644 2+0.39784000000003644],[-1540 1540])
legend('tanh function','start of friction shift','still 1540','-1540
accieved','2 s from start of friction shift')
grid on
```

```matlab
%Script for finding the function for the pressure in the high pressure system
clear all
close all
clc
%Author Otto Andreas Moe

[~, ~, raw0_0, dates0_0] = xlsread('C:\Users\Otto\Desktop\OneSubsea Master
project\Matlab\Data_OneSubsea\data.xlsx','Sheet2','E2:E94','',@convertSpreadsh
eetExcelDates);
[~, ~, raw0_1, dates0_1] = xlsread('C:\Users\Otto\Desktop\OneSubsea Master
project\Matlab\Data_OneSubsea\data.xlsx','Sheet2','F2:F94','',@convertSpreadsh
eetExcelDates);
raw = [raw0_0,raw0_1];
dates = [dates0_0,dates0_1];
raw = raw(:,2);
dates = dates(:,1);

data = reshape([raw{:}],size(raw));

VarName3 = datetime([dates{:,1}].', 'ConvertFrom', 'Excel');
hp1 = data(:,1);
hp1=hp1(2:8)+1

[~, ~, raw0_0, dates0_0] = xlsread('C:\Users\Otto\Desktop\OneSubsea Master
project\Matlab\Data_OneSubsea\Brenda_data_april.xlsx','Sheet2','I9:J57','',@co
nvertSpreadsheetExcelDates);
[~, ~, raw0_1, dates0_1] = xlsread('C:\Users\Otto\Desktop\OneSubsea Master
project\Matlab\Data_OneSubsea\Brenda_data_april.xlsx','Sheet2','P9:Q57','',@co
nvertSpreadsheetExcelDates);
raw = [raw0_0,raw0_1];
dates = [dates0_0,dates0_1];
raw(cellfun(@(x) ~isempty(x) && isnumeric(x) && isnan(x),raw)) = {''};
raw = raw(:,[2,4]);
dates = dates(:,[1,3]);

R = cellfun(@(x) ~isnumeric(x) && ~islogical(x),raw); % Find non-numeric cells
raw(R) = {NaN}; % Replace non-numeric cells
R = cellfun(@(x) ~isnumeric(x) && ~islogical(x),dates); % Find non-numeric
cells
dates(R) = {NaN}; % Replace non-numeric Excel dates with NaN

data = reshape([raw{:}],size(raw));

BrendadataaprilS1 = table;

time_hp_2 = datetime([dates{:,1}].', 'ConvertFrom', 'Excel')
hp2 = data(:,1);
time_hp_3 = datetime([dates{:,2}].', 'ConvertFrom', 'Excel')
hp3 = data(:,2);

hp2=hp2(1:7)+1
time2=[0,3,3,4,5,6,7]
hp3=hp3(1:5)+1
time3=[0,1,3,3,4]
```

```
t=[0,1,3,4,5,6,7]
t=t'
plot(t,hp1,'k o');
xlabel('Time [s]');
ylabel('Pressure [barg]');
legend('Pessure data points')
grid on
hold on
plot(time2,hp2,'*')
plot(time3,hp3,'x')
x_mean=(sum(hp1)+sum(hp2)+sum(hp3))./19
plot(t,t*0+x_mean)
```

```matlab
%Script to find the function for the subsea pressure
clear all
clc
close all
%Author: Otto Andreas Moe

[~, ~, raw, dates] = xlsread('C:\Users\Otto\Desktop\OneSubsea Master
project\Matlab\Data_OneSubsea\Brenda_data_april.xlsx','Sheet2','N9:O133','',@c
onvertSpreadsheetExcelDates);
raw = raw(:,2);
dates = dates(:,1);
data = reshape([raw{:}],size(raw));
BrendadataaprilS1 = table;
time = datetime([dates{:,1}].', 'ConvertFrom', 'Excel')
pressure_data = data(:,1)

clearvars data raw dates;
plot(time,pressure_data,'k')
hold on
timedischarge=time(1:74);
pressuredischarge=pressure_data(1:74);
timecharge=time(65:125);
timecharge_s=-10:1:50;
pressurecharge=pressure_data(65:125);
figure()
plot(timecharge_s,pressurecharge,'k *');

[~, ~, raw, dates] = xlsread('C:\Users\Otto\Desktop\OneSubsea Master
project\Matlab\Data_OneSubsea\Brenda_data_april.xlsx','Sheet2','G9:H92','',@co
nvertSpreadsheetExcelDates);
raw = raw(:,2);
dates = dates(:,1);
data = reshape([raw{:}],size(raw));
BrendadataaprilS1 = table
time2 = datetime([dates{:,1}].', 'ConvertFrom', 'Excel')
pressure_data2 = data(:,1)

clearvars data raw dates;

figure()
plot(time2,pressure_data2,'k')


timedischarge2=time2(1:42);
pressuredischarge2=pressure_data2(1:42);

timecharge2=time2(32:84);
timecharge_s2=-10:1:42;
pressurecharge2=pressure_data2(32:84);

figure()
plot(timecharge_s,pressurecharge,'k x')
hold on
plot(timecharge_s2,pressurecharge2,'k *')
```

```matlab
%Plot of all measured data and the curve fit together
figure
plot(timecharge_s,pressurecharge,'.')
hold on
plot(timecharge_s2,pressurecharge2,'.')

x1=0
w1=0.3
w2=0.5
a=58.8
b=59.9
t_stop=-1
t_0=t_stop+1


t=-10:0.01:200
0;

%The initial pressure is constant pressure 58.8 barg
plot(t,t*0+58.8)

% The curvefit of function the first pressure data
p11 = -0.0014173
p22 = 0.10996
p33 = 59.101
y2 = p11.*(t).^2+p22.*(t)+p33
plot(t,y2)

% The curvefit of function the second pressure data
p1 = -0.00079268;
p2 = 0.061048
p3 = 59.68
y = p1.*(t).^2+p2.*(t)+p3

plot(t,y)

%function to connect the constant function with the quadratic function
f1=1/2.*((a+(p1.*(t-t_0).^2+p2.*(t-t_0)+p3))+((p1.*(t-t_0).^2+p2.*(t-t_0)+p3)-
a).*(exp((t-t_0)./w1)-exp((-t+t_0)./w1))./(exp((t-t_0)./w1)+exp((-
t+t_0)./w1)));
plot(t,f1,'k')

%Linear function from max down to min
linear=60.7507-0.02*(t-(50+t_0))
plot(t,linear)

 xlabel('Time [s]')
 ylabel('Pressure [barg]')
 legend('Measured subsea pressure data set 1','Measured subsea pressure data
set 2','Initial pressure constant at 58.8 barg','Curvefit of measured data set
1','Curvefit of measured data set 2','Function that connects the initial
pressure and curvefit of data set 2','Linear function')
 grid on
 xlim([-10 150]);
 ylim([58 64]);
```

```matlab
figure()
subsea_pressure=(1/2.*((a+(p1.*(t-t_0).^2+p2.*(t-t_0)+p3))+((p1.*(t-
t_0).^2+p2.*(t-t_0)+p3)-a).*(exp((t-t_0)./w1)-exp((-t+t_0)./w1))./(exp((t-
t_0)./w1)+exp((-t+t_0)./w1)))).*10^5;
plot(t,subsea_pressure,'k')
```

Appendix C

Excel spreadsheet

Spreadsheet with calculations of flow coefficients for the system components, together with estimation of system parameters according to pressure data.

Solenoid			LP (barg)	LP (bara)	
18-Jul-18 22:55:00	150	18-Jul-18 22:54:11	43.097637	44.09764	Lpmean
18-Jul-18 22:55:36	150	18-Jul-18 22:55:35	43.002235	44.00224	4404994
18-Jul-18 22:55:37	180	18-Jul-18 22:55:35	42.996933	43.99693	4399958
18-Jul-18 22:55:38	180	18-Jul-18 22:55:36	43.288422	44.28842	4414268
18-Jul-18 22:55:39	150	18-Jul-18 22:55:37	47.146732	48.14673	4621758
18-Jul-18 22:57:00	150	18-Jul-18 22:55:39	45.249378	46.24938	4719806
		18-Jul-18 22:55:40	45.159279	46.15928	4620433
150-close		18-Jul-18 22:55:41	45.138084	46.13808	4614868
200-open		18-Jul-18 22:55:45	45.042686	46.04269	4609039
		18-Jul-18 22:55:46	45.021488	46.02149	4603209
		18-Jul-18 22:55:48	44.936687	45.93669	4597909
		18-Jul-18 22:55:49	44.904884	45.90488	4592079
		18-Jul-18 22:55:51	44.830688	45.83069	4586779
		18-Jul-18 22:55:52	44.777695	45.77769	4580419
		18-Jul-18 22:55:52	44.714092	45.71409	4574589
		18-Jul-18 22:55:53	44.61869	45.61869	4566639
		18-Jul-18 22:55:53	44.507401	45.5074	4556305
		18-Jul-18 22:55:55	44.438496	45.4385	4547295
		18-Jul-18 22:55:56	44.380207	45.38021	4540935
		18-Jul-18 22:55:57	44.295403	45.2954	4533780
		18-Jul-18 22:55:57	44.253006	45.25301	4527420
		18-Jul-18 22:55:59	44.162907	45.16291	4520796
		18-Jul-18 22:56:00	44.13641	45.13641	4514966
		18-Jul-18 22:56:03	44.046303	45.0463	4509136
		18-Jul-18 22:56:04	44.019814	45.01981	4503306
		18-Jul-18 22:56:07	43.935009	44.93501	4497741
		18-Jul-18 22:56:08	43.919117	44.91912	4492706
		18-Jul-18 22:56:13	43.82901	44.82901	4487406
		18-Jul-18 22:56:14	43.81311	44.81311	4482106
		18-Jul-18 22:56:22	43.723022	44.72302	4476807
		18-Jul-18 22:56:22	43.712418	44.71242	4471772
		18-Jul-18 22:56:31	43.622318	44.62232	4466737
		18-Jul-18 22:56:32	43.606419	44.60642	4461437
		18-Jul-18 22:56:44	43.526924	44.52692	4456667
		18-Jul-18 22:56:45	43.505722	44.50572	4451632
		18-Jul-18 22:57:05	43.410332	44.41033	4445803
		18-Jul-18 22:57:06	43.405018	44.40502	4440767
		18-Jul-18 22:57:28	43.320225	44.32022	4436262
		18-Jul-18 22:57:30	43.304325	44.30433	4431227
		18-Jul-18 22:58:15	43.208931	44.20893	4425663
			43.203629	44.20363	4420628
					2210181

	HP (barg)	HP (bara)		time LP, s	timeHP, s	HP	LP
18-Jul-18 22:55:34	163.330414	164.3304	HPmean,Pa	0	84	dP/dt, Pa/s	dP/dt, Pa/s
18-Jul-18 22:55:36	163.298615	164.2986	16431451	84	86.00	-1589.966	-113.5735
18-Jul-18 22:55:37	160.791794	161.7918	16304520	85	87.00	-250682.1	-530.2429
18-Jul-18 22:55:39	162.726227	163.7262	16275901	86	89.00	96721.649	29148.865
18-Jul-18 22:55:40	163.796814	164.7968	16426152	87	90.00	107058.72	385831.07
18-Jul-18 22:55:41	164.983978	165.984	16539040	89	91.00	118716.43	-94867.71
18-Jul-18 22:55:42	166.028046	167.028	16650601	90	92.00	104406.74	-9009.933
18-Jul-18 22:55:43	167.103928	168.1039	16756599	91	93.00	107588.2	-2119.446
18-Jul-18 22:55:44	168.227493	169.2275	16866571	95	94.00	112356.57	-2384.949
18-Jul-18 22:55:44	169.260971	170.261	16974423	96	95.00	103347.78	-2119.827
18-Jul-18 22:55:45	170.26265	171.2626	17076181	98	96.00	100167.85	-4240.036
18-Jul-18 22:55:45	171.343811	172.3438	17180323	99	97.00	108116.15	-3180.313
18-Jul-18 22:55:46	172.297791	173.2978	17282080	101	98.00	95397.949	-3709.793
18-Jul-18 22:55:47	173.288879	174.2889	17379333	102	99.00	99108.887	-5299.377
18-Jul-18 22:55:47	173.590958	174.591	17443992	103	100.00	30207.825	-6360.245
18-Jul-18 22:55:48	173.46907	174.4691	17453001	104	101.00	-12188.72	-9540.176
18-Jul-18 22:55:49	173.341873	174.3419	17440547	105	102.00	-12719.73	-11129
18-Jul-18 22:55:50	173.246475	174.2465	17429417	107	103.00	-9539.795	-3445.244
18-Jul-18 22:55:50	173.166992	174.167	17420673	108	104.00	-7948.303	-5828.857
18-Jul-18 22:55:51	173.098068	174.0981	17413253	109	105.00	-6892.395	-8480.453
18-Jul-18 22:55:52	173.03978	174.0398	17406892	110	106.00	-5828.857	-4239.655
18-Jul-18 22:55:52	172.981476	173.9815	17401063	112	107.00	-5830.383	-4504.967
18-Jul-18 22:55:53	172.928482	173.9285	17395498	113	108.00	-5299.377	-2649.689
18-Jul-18 22:55:53	172.864883	173.8649	17389668	116	108.00	#DIV/0!	-3003.565
18-Jul-18 22:55:55	172.81189	173.8119	17383839	117	110.00	-2649.689	-2648.926
18-Jul-18 22:55:56	172.764191	173.7642	17378804	120	111.00	-4769.897	-2826.818
18-Jul-18 22:55:56	172.711197	173.7112	17373769	121	112.00	-5299.377	-1589.203
18-Jul-18 22:55:57	172.615799	173.6158	17366350	126	113.00	-9539.795	-1802.139
18-Jul-18 22:55:58	172.57338	173.5734	17359459	127	114.00	-4241.943	-1589.966
18-Jul-18 22:55:59	172.477997	173.478	17352569	135	116.00	-4769.135	-1126.099
18-Jul-18 22:56:00	172.440887	173.4409	17345944	136	117.00	-3710.938	-1060.486
18-Jul-18 22:56:02	172.3508	173.3508	17339584	145	119.00	-4504.395	-1001.104
18-Jul-18 22:56:02	172.308395	173.3084	17332960	146	120.00	-4240.417	-1589.966
18-Jul-18 22:56:04	172.228912	173.2289	17326865	158	121.00	-7948.303	-662.454
18-Jul-18 22:56:05	172.191803	173.1918	17321036	159	122.00	-3710.938	-2120.209
18-Jul-18 22:56:06	172.10701	173.107	17314941	179	123.00	-8479.309	-476.9516
18-Jul-18 22:56:06	172.069916	173.0699	17308846	180	124.00	-3709.412	-531.3873
18-Jul-18 22:56:08	171.990402	172.9904	17303016	203	126.00	-3975.677	-368.6656
18-Jul-18 22:56:09	171.953308	172.9533	17297186	204	127.00	-3709.412	-1589.966
18-Jul-18 22:56:11	171.85791	172.8579	17290561	249	129.00	-4769.897	-211.987
18-Jul-18 22:56:11	171.826111	172.8261	17284201	250	130.00	-3179.932	-530.2429
18-Jul-18 22:56:13	171.751907	172.7519	17278901		131.00	-7420.349	17681.451

	ThermEstHP	Orifice				OrificeEst	
Q, m3/s	Q, l/min	v, m/s	Re	mu_cap	HP-LP	Q, m3/s	Q, l/min
1.90302E-06	0.114180976	2.42E+00	4.85E+02	6.48E-01	1.20E+02	9.58E-05	5.75E+00
0.000304055	**18.24327364**	3.87E+02	7.75E+04	7.98E-01	1.14E+02	9.32E-05	5.59E+00
-0.00011767	-7.060105279	-1.50E+02	3.00E+04	7.88E-01	1.17E+02	9.48E-05	5.69E+00
-0.00012821	ThermEstLP						

Q, m3/s	Q, l/min	v, m/s	Re	lambd	dP_umb, bar	
-0.00014051						
-0.00012216	-2.549186338	2.14E-01	6.81E+02	9.40E-02	1.14E+01	
-0.00012452	-31.18743806	2.62E+00	8.33E+03	7.68E-03	1.39E+02 ????	
-0.00012859	**7.397276948**	6.21E-01	1.98E+03	3.24E-02	3.31E+01	
-0.00011699	0.728647591	6.12E-02	1.95E+02	3.29E-01	3.26E+00	
-0.00011224	0.171757401	1.44E-02	4.59E+01	1.40E+00	7.68E-01	v, m/s
-0.00011988	0.193692705	1.63E-02	5.17E+01	1.24E+00	8.66E-01	6.06E-01
-0.00010472	0.172534912	1.45E-02	4.61E+01	1.39E+00	7.72E-01	
-0.00010775	0.345783084	2.90E-02	9.23E+01	6.93E-01	1.55E+00	
-3.2633E-05	0.259925397	2.18E-02	6.94E+01	9.22E-01	1.16E+00	
1.31555E-05	0.303800365	2.55E-02	8.11E+01	7.89E-01	1.36E+00	
1.37455E-05	0.435007169	3.65E-02	1.16E+02	5.51E-01	1.95E+00	
1.03204E-05	0.523231131	4.39E-02	1.40E+02	4.58E-01	2.34E+00	
8.60607E-06	0.787174754	6.61E-02	2.10E+02	3.04E-01	3.52E+00	
7.46824E-06	0.92184431	7.74E-02	2.46E+02	2.60E-01	4.12E+00	
6.3198E-06	0.286348654	2.40E-02	7.65E+01	8.37E-01	1.28E+00	
6.32509E-06	0.485624488	4.08E-02	1.30E+02	4.93E-01	2.17E+00	
5.75218E-06	0.708451596	5.95E-02	1.89E+02	3.38E-01	3.17E+00	
#DIV/0!	0.355031357	2.98E-02	9.48E+01	6.75E-01	1.59E+00	
2.8794E-06	0.378196959	3.18E-02	1.01E+02	6.34E-01	1.69E+00	
5.18599E-06	0.222936921	1.87E-02	5.95E+01	1.07E+00	9.97E-01	
5.76452E-06	0.253271457	2.13E-02	6.76E+01	9.46E-01	1.13E+00	
1.03847E-05	0.223862898	1.88E-02	5.98E+01	1.07E+00	1.00E+00	
4.62079E-06	0.239403612	2.01E-02	6.39E+01	1.00E+00	1.07E+00	
5.1986E-06	0.134848492	1.13E-02	3.60E+01	1.78E+00	6.03E-01	
4.04776E-06	0.153226506	1.29E-02	4.09E+01	1.56E+00	6.85E-01	
4.91633E-06	0.135460674	1.14E-02	3.62E+01	1.77E+00	6.06E-01	
4.63124E-06	0.096135249	8.07E-03	2.57E+01	2.49E+00	4.30E-01	
8.6861E-06	0.090708679	7.62E-03	2.42E+01	2.64E+00	4.06E-01	
4.05775E-06	0.08579497	7.21E-03	2.29E+01	2.79E+00	3.84E-01	
9.27734E-06	0.136538286	1.15E-02	3.65E+01	1.76E+00	6.11E-01	
4.06097E-06	0.056992635	4.79E-03	1.52E+01	4.20E+00	2.55E-01	
4.35499E-06	0.18276087	1.53E-02	4.88E+01	1.31E+00	8.17E-01	
4.06567E-06	0.041205435	3.46E-03	1.10E+01	5.82E+00	1.84E-01	
5.23144E-06	0.04599759	3.86E-03	1.23E+01	5.21E+00	2.06E-01	
3.48983E-06	0.031967762	2.68E-03	8.54E+00	7.50E+00	1.43E-01	
8.14777E-06	0.138137882	1.16E-02	3.69E+01	1.73E+00	6.18E-01	

Ffr_estimate   1.54E+03

High pressure accumulator

Initial volume		Precharge volume	
V1, m3	2.75E-02	V0, m3	3.12E-02
p1, Pa	1.64E+07	p0, Pa	1.45E+07
T0, K	293		

Low Pressure accumulator

Initial volume		Precharge volume	
V1, m3	8.99E-03	V0, m3	9.95E-03
p1, Pa	4.43E+06	p0, Pa	4.00E+06

Shell Morlina S2 BL 5

dens	869
visc.kin, m2/s	5.00E-06
visc.dyn., Pas	4.35E-03
adiab. Index	1.4
p_hydr_stat, bar	17.81702

Inlet:

Orifice

assume l nozzle = 2 d nozzle	
mu_cap_ave	7.45E-01
A, m2	7.85E-07
Л	1.27E+15

Solenoid valve

Q, l/min	dP, bar	K (SI)
2	0.36	3.24E+13
4	1.43	3.218E+13
6	3.39	3.39E+13
8	5.71	3.212E+13
10	9.68	3.485E+13
12	15	3.75E+13
14	22.07	4.054E+13
K_ave		3.578E+13

Ball valve — 1/2" NPT

Cv gpm	4.2
kv, bar*m^3/h	3.6
K_ballvave (SI)	8.69E+10

Outlet:

Plattform Pipe

l, m	80
d, m	0.014
A, m^2	0.000154
ε	0.05
λ	0.027826
λ_turbulent	0.036174
K_platform	3.79E+12

Coupling

d_1	0.014
d_2	0.0159
ζ	0.0504965

Ball valve — 1/2" NPT

Cv	4.2
kv	3.6
K_ballvave (SI)	8.69E+10

Umbillical

h, m	209
l, m	9474
l_total, m	9683
d, m	0.0159
A, m^2	0.000199
ε	0.005
λ	0.027826
K_umbillical	1.87E+14
dP_hyd, Pa	1781702

Tank

ζ	1
Density	869
Q, l/h	0.5
Q, m^3/s	1.389E-07
d, m	0.0159
A, m^2	0.0001986
K_tank	1.102E+10

Appendix D

Barrier fluid Morlina data sheet

Bulk modulus table for Tellus Oil 15, equivalent for Morlina S2 BL 5. Provided by Univar AS, the Shell lubricants distributor in Norway.
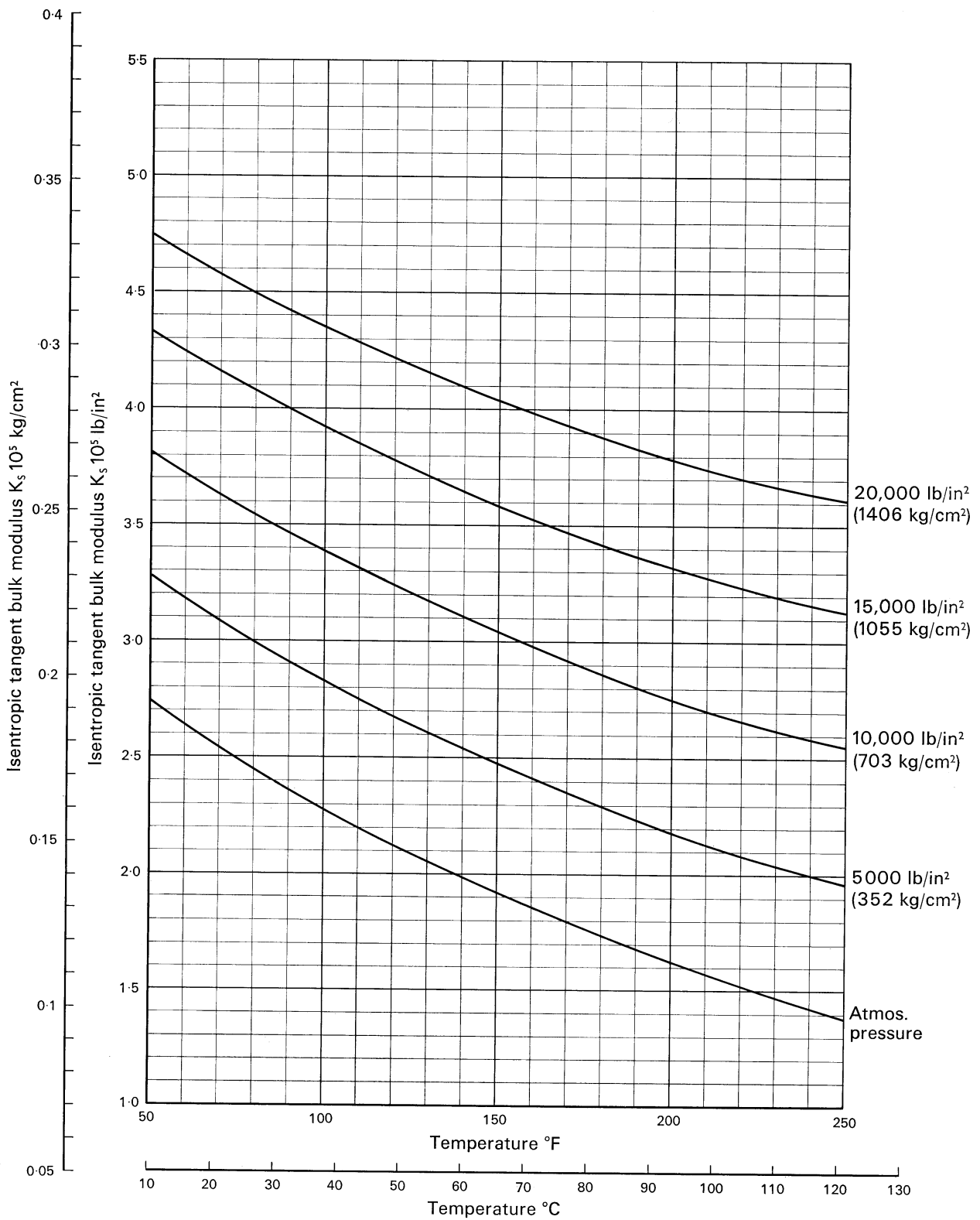
Fig. 20 Isentropic tangent bulk modulus against temperature and pressure for Shell Tellus Oil 15

Appendix E

Orifice data sheet

Throttles type ED
Restrictor check valves type RD and RDF

Operating pressure p_{max} = 500 bar
Flow Q_{max} = 70 lpm

Other valves with same design
Type ED, RD, and RDF (11 ... 51) acc. to D 7540

1. General

According to DIN standard 1219-1, restrictor valves belong to the flow control group of valves. In hydraulic installations they are used as resistance valves. By adjustment of the restriction area, their flow resistance is changed, which together with the actuator back pressure, causes a pressure limiting valve at the inlet side to crack, part of the pump delivery flow (residual flow) is bypassed via this valve, whereas only the remaining partial flow reaches the actuator via the restrictor as effective flow. If the actuator back pressure changes, the flow changes in turn, the setting of the restrictor valve remaining the same. Combined restrictor and check valves allow free flow in the opposite direction.

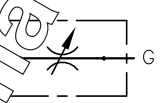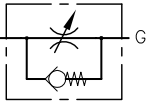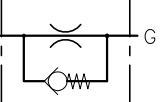## 2. Available versions, main data

Order examples:

ED 1   Throttle
RDF 2/1,0   Restrictor check valve

Table 2: Non-adjustable throttle with type RDF../..

∅ (mm)	0.6	0.8	1.0	1.2	1.4	1.6	1.8	2.0	2.5	3.0	4.0
Coding	0,6	0,8	1,0	1,2	1,4	1,6	1,8	2,0	2,5	3,0	4,0
	Carburetor jet CO SOLEX M 5 x ...										without [1]

[1] The throttle hole ∅4 is identical with the core diameter for M5.

Table 1: Basic type , size

Version		Coding	Ports acc. to ISO 228/1 (BSPP) G and F	Pressure p_{max} (bar)	Flow Q_{max} approx. (lpm)	Mass (weight) approx. (g)
Restrictor valve		**ED 1**	G 1/4	500	15	360
Restriction preferable G → F		**ED 2**	G 3/8		25	450
		ED 3	G 1/2		40	400
		ED 4	G 3/4		70	530
Restrictor check valve		**RD 1**	G 1/4	500	15	360
G → F throttled flow F → G free flow		**RD 2**	G 3/8		25	450
		RD 3	G 1/2		40	400
		RD 4	G 3/4		70	530
Restrictor check valve		**RDF 1/..**	G 1/4	500	15	360
Non-adjustable throttle G → F throttled flow F → G free flow		**RDF 2/..**	G 3/8		25	450
		RDF 3/..	G 1/2		40	400
		RDF 4/..	G 3/4		70	530

2.4

March 2004-00

3.   Additional characteristic data

|	
Design	Poppet restrictor valve - Type ED..
	Poppet restrictor valve with bypass check valve - Type RD..
	Fixed restrictor valve with bypass check valve - Type RDF..
Installed position	as desired
Pressure fluid	Fluids acc. to DIN 51524 table 1 to 3; ISO VG 10 to 68 acc. to DIN 51519
	Viscosity range: min. approx. 4; max. approx. 1500 mm^2/sec;
	Optimal operation range: approx. 10...500 mm^2/sec
	Also suitable are biologically degradable pressure fluids of the type HEPG (Polyalkylenglycol) and HEES (synth. Ester) at operation temperatures up to approx. +70°C.
Temperature	Ambient: approx. -40 ... +80°C
	Fluid: -25...+80°C; take note of viscosity ranges!
	Start temperature down to -40°C are allowable (Pay attention to the viscosity range during start!), as long as the operation temperature during subsequent running is at least 20 K (Kelvin) higher. Biological degradable pressure fluids: Pay attention to manufacturer's information. With regard to the compatibility with sealing materials do not exceed +70°C.

Δp-Q-characteristics

Throttle direction G → F   Throttle direction F → G
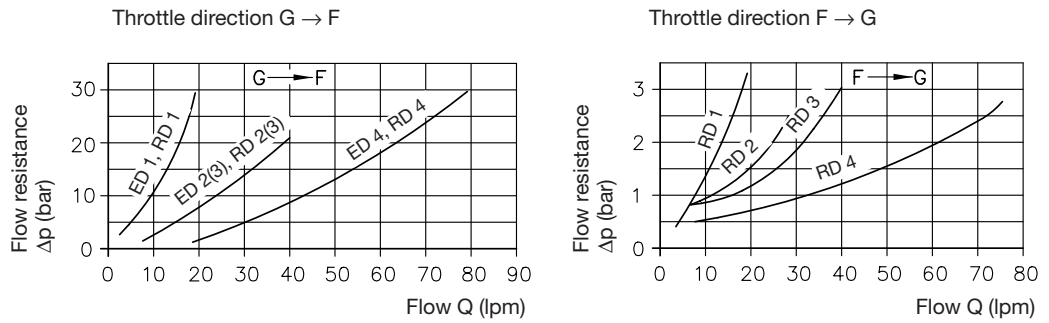
Oil viscosity during test approx. 50 mm^2/s

Attention: The throttles show a certain viscosity dependence, the Δp-Q curves can differ more or less strongly when used beyond the optimal range.

4.   Unit dimensions   All dimensions in mm, subject to change without notice!
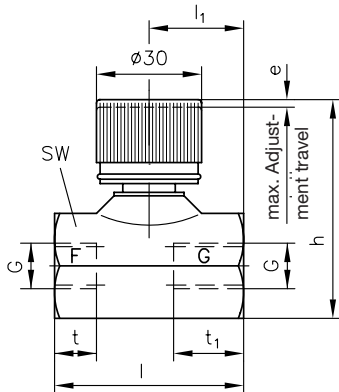
Type ED.. and RD..   **Type RDF..**
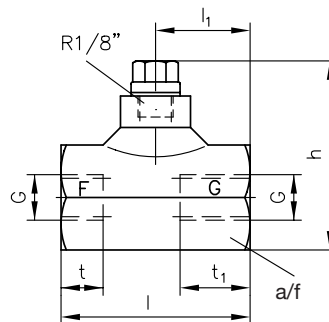
Type	Ports ISO 228/1 (BSPP) F and G	l	l1	h approx.	t	t1	a/f	Travel e approx.
ED 1 and RD 1	G 1/4	54	27	65	12	21	30	4
ED 2 and RD 2	G 3/8	62	31	67	12	24	32	3.5
ED 3 and RD 3	G 1/2	62	31	67	14	23	32	3.5
ED 4 and RD 4	G 3/4	78	39	74	18	25	36	4
RDF 1	G 1/4	54	27	55	12	21	30	--
RDF 2	G 3/8	62	31	57	12	24	32	--
RDF 3	G 1/2	62	31	57	14	23	32	--
RDF 4	G 3/4	78	39	61	18	25	36	--

5.   Appendix

5.1   Determining fixed restrictor bore

For hydraulic oil ρ = 870 ... 900 kg/m^3 and given flow Q (lpm) and desired flow resistance Δp (bar)

$$d \approx 1{,}2 \sqrt{\frac{Q}{\alpha \sqrt{\Delta p}}}$$

d (mm) = Fixed restrictor bore
α (-)   Flow coeefficient
          = 0.82 to approx. 2.5 dia.

The α values have been determined experimentally with hydraulic oil, viscosity 36 mm^2/s at 50°C and apply only to type RDF.
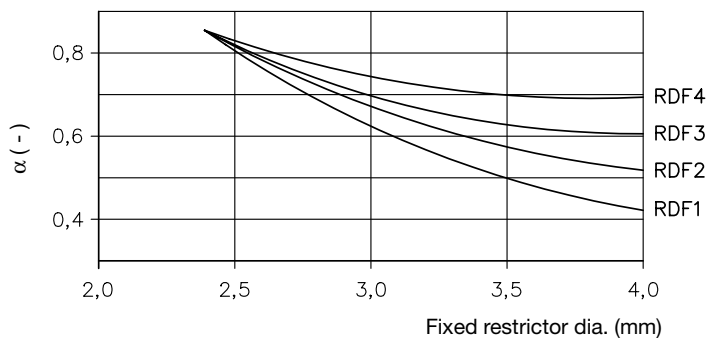
5.2   Quick selection
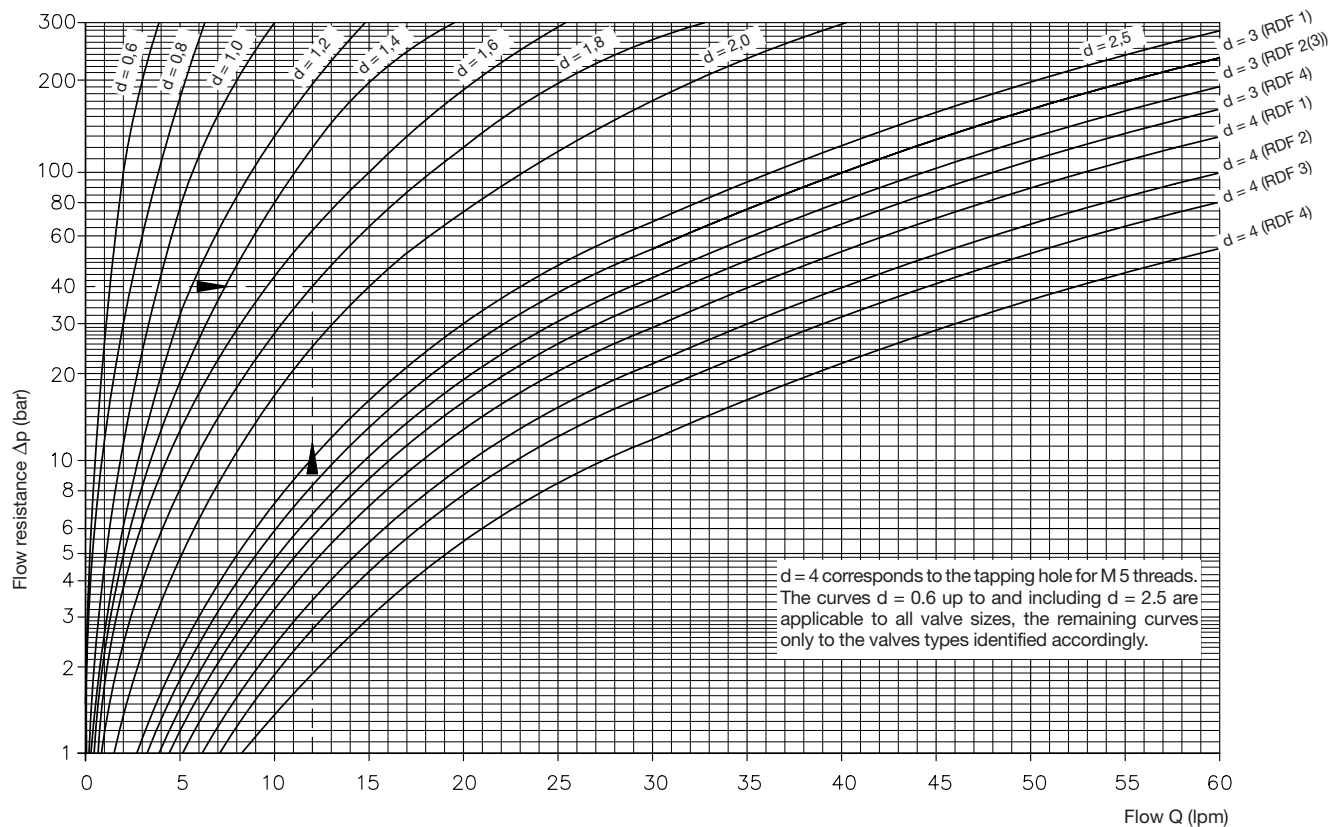
Example: For a gliven flow of 12 lpm a flow resitance of Δp = 40 bar is required.
          The necessary fixed restrictor bore is d = 1.8 mm.

Appendix F

Solenoid data sheet

Solenoid poppet valve
- 2/2-, 3/2- and 3/4-way type
- Q_{max} = 15 l/min
- p_{max} = 350 bar

NG4-Mini®

II 2 G / II 2 D
EEx em II

DESCRIPTION

Direct opperated poppet valve flange type NG4-Mini. Activated with explosion proof solenoid.
EEx: in accordance with european standards EN 50014, EN 50019, EN 50028
e: increased safety
m: encapsulation
Group II:
for all applications except mining
Zone 1 / 21 (and 2 / 22):
explosive mixtures present intermittently
EC-type examination certificate:
PTB 01 ATEX 2129 X
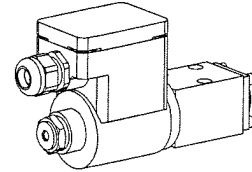
FUNCTION

The central functioning element of all directly controlled poppet valves is the poppet valve cartridge NG4. The valve is operated by a explosion proof type solenoid which in turn either opens or closes the poppet. The design of the poppet spool, which is equal in surface area on both sides and thus pressure balanced, means there are no undue opening and closing hydraulic forces. Due to this the oil flow through the poppet valve is possible in both directions. The valve is tight in both flow directions.

APPLICATION

Wandfluh poppet valves can be used anywhere absolutely leak tight closing functions are important. Completely sealed loading, gripping and clamping operations are all important functions which Wandfluh poppet valves can perform. From a mechanical and functional point of view, poppet valves can replace slide valves at any time. These valves are suitable for hazardeous areas in off-shore and shipbuilding applications as well as in chemical, oil and gas industry.

TYPE CODE

2/2- or 3/2-way construction				B	EX ☐	2	04	☐ - S1788 -	☐	/	☐	# ☐
3/4-way construction				B	EX 3	4	04	- S1788 -	☐	/	☐	# ☐

Mounting interface
Explosion proof solenoid
2-way (connections) — 2
3-way (connections) — 3
2 position
4 position
Nominal size 4-Mini
Normally closed, solenoid on A-Side — 1a
Normally open, solenoid on B-Side — 0b
Terminal box with out cable
Standard nominal voltage U_N: 24 VDC G24   115 VAC R115   230 VAC R230
Execution: T4   T6 (on request)
Design-Index (Subject to change)
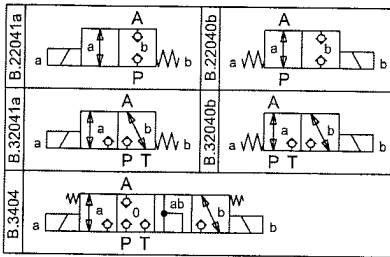
GENERAL SPECIFICATIONS

Description	2/2-, 3/2-and 3/4-way poppet valve
Nominal size	NG4-Mini acc. to Wandfluh standard
Construction	Direct operated poppet valve
Operations	Solenoid
Mounting	Flange
	3 mounting holes for cyl. screws M5x40
	M5x50 with distance plate BDP4/12
Connections	Threaded connection plates
	Multi-flange subplates
	Longitudinal stacking system
Admissible ambient temp.	-20...+40° C
Mounting position	any, preverable horizontal
Fastening torque	M_D = 5,5 Nm (quality 8,8)
Weight: 2/2-, 3/2-way	m = 2,0 kg
3/4-way	m = 2,9 kg
Volume flow direction	any (see characteristics)

HYDRAULIC SPECIFICATIONS

Fluid	Mineral oil, other fluid on request
Contamination efficiency	ISO 4406:1999, class 20/18/14
	(Required filtration grade ß10...16≥75)
	refer to data sheet 1.0-50/2
Viscosity range	12 mm²/s ... 320 mm²/s
Admissible fluid temp.	-20 ... +40° C
Working pressure	p_{max} = 350 bar
Max. volume flow	Q_{max} = 15 l/min see characteristics

ELECTRICAL CONTROL

Construction	Solenoid, wet pin push, pressure tight
Standard-nominal voltage	U_N = 24 VDC
	U_N = 115 VAC, U_N = 230 VAC
	DC = Ripple component 20%;
	wired with VDR
	AC = 50 to 60 Hz ±2%;
	with integrated half wave
	rectifier and recovery diode
Voltage tolerance	±10% of nominal voltage
Protection class	IP65 acc. to EN 60 529
Relative duty factor	100% DF
Switching cycles	12'000/h
Operating life	10⁷ (number of switching cycles, theoretically)
Connection/Power supply	Through cable entry for cable
	diameter 6...12 mm
Execution:	T4 = II 2 G EEx em II T4 (for gas)
(acc. to EN 50 014)	T4 = II 2 D IP65 T130°C (for dust)
	T6 (on request) = II 2 G EEx em II T4 (for gas)
	T6 (on request) = II 2 D IP65 T80°C (for dust)
Nominal power:	T4 = 17 W (DC), 23 VA (AC)
	T6 (on request) = 7 W (DC), 11 VA (AC)

Wandfluh AG   *Tel.* +41 33 672 72 72   *E-mail:* sales@wandfluh.com   *Illustrations not obligatory*   *Data sheet no.*
Postfach   *Fax* +41 33 672 72 12   *Internet:* www.wandfluh.com   *Data subject to change*   **1.11-3130E** 1/2
CH-3714 Frutigen   *Edition 05 02*

SYMBOLS

START-UP

1. In the power supply for each solenoid a fuse of an appropriate rating (max. 3 times I_B of solenoid, DIN 41571 or IEC 127) respectivly a motor circuit breaker with electromagnetic an thermal interruption must be installed. The fuse may be located in the power supply unit for the solenoid or between power supply and solenoid. The voltage rating for the fuse must be equal or higher than the one for the solenoid.

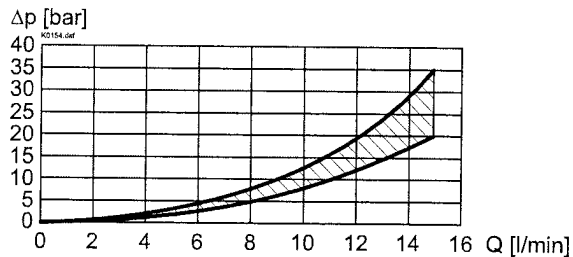2. Solenoid coils may only be mounted on those valves assigned to.

CHARACTERISTICS (T6 on request) Oil viscosity υ = 30 mm²/s

$p = f(Q)$ Performance limits with standard voltage -10%

p [bar]
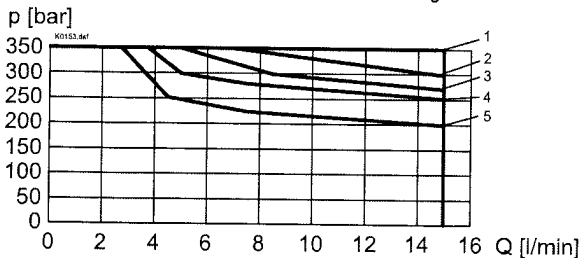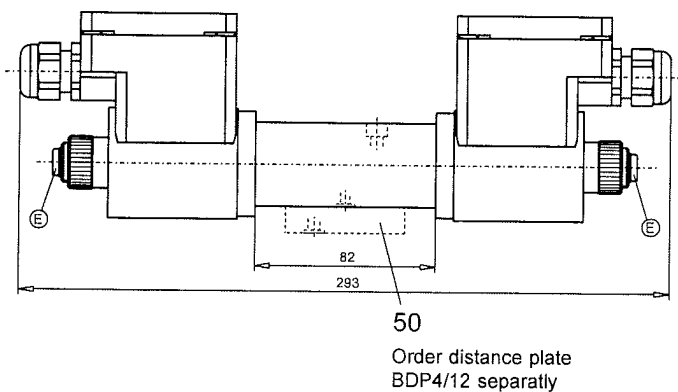

Type	Flow direction			
	P - A	A - T	A - P	T - A
BEX22041a	1	-	2	-
BEX22040b	1	-	4	-
BEX32041a	1	3	5	1
BEX32040b	1	4	5	1
BEX3404	1	1	2	2

$\Delta p = f(Q)$ Pressure drop volume flow characteristics

Δp [bar]

DIMENSIONS

3/4-way poppet valve

82
293

50

Order distance plate
BDP4/12 separatly

2/2-way poppet valve
3/2-way poppet valve

159,5   B..22041a
169,5   B..32041a
169,5   B..32040b,B..22040b
(Magnet auf B-Seite)
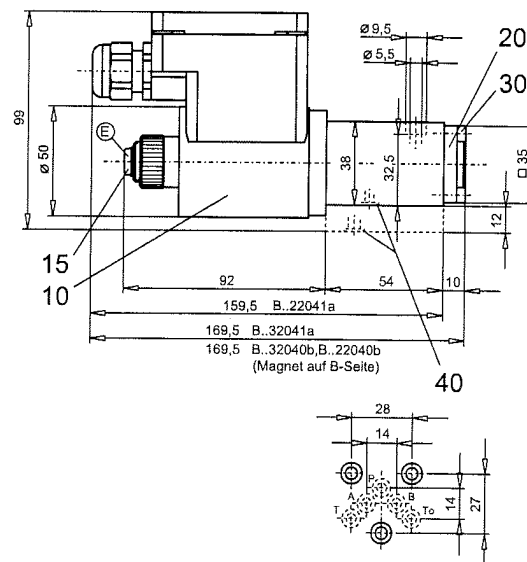
PARTS LIST

Position	Article	Description
10	207.5 ...	Coil type EExem
15	239.2033	Plug HB0 (incl. seal)
20	057.4202	Cover
30	246.1112	Socket head cap screw M4x12 DIN 912
40	160.2052	O-ring ID 5,28x1,78
50	173.1450	Distance plate BDP4/12

ACCESSORIES

Threaded connecting plates, Multi-flange subplates and
Longitudinal stacking system   see Reg. 2.9

Technical explanation see data sheet 1.0-100E

Wandfluh AG   Tel. +41 33 672 72 72   E-mail: sales@wandfluh.com   *Illustrations not obligatory*   *Data sheet no.*
Postfach   Fax +41 33 672 72 12   Internet: www.wandfluh.com   *Data subject to change*   *1.11-3130E 2/2*
CH-3714 Frutigen   *Edition 05 02*

Appendix G

Ball Valve data sheet

UB Series

General Information

Heavy duty high pressure ball valve 10,000 psi rated

Alco are aware of the ever increasing operating pressures demanded by industry, and for this reason have developed the "UB" range of valves to accommodate these stringent requirements. The UB series high pressure valve has a working pressure of 10,000 psi with a body test at (15,000 psi). The UB Series is a tried and tested rugged design for high pressure applications. It comes with panel mounting holes and stainless steel handle as standard. Service / repair kits are available to prolong service / field life. Many options available such as locking device.

Design Features

- 2 piece design for safety.
- Quick 90° operation, lever handle standard.
- Bi-directional floating ball design to ensure leak-proof shut-off on pressure or vacuum.
- Anti-blowout stem for safety.
- End pinned, stopping accidental removal or loosening by vibration.
- Available with 4-panel mounting holes M4 x 10 deep, can be actuated (if specified)
- Available in 316ss / Duplex / Monel.

- Pressure / Temperature rating -20°C to 250°C
- Available loose with socket weld or butt weld ends.
- Renewable seats and seals for long life.
- Repair kits available to prolong valve life.
- Floating ball design for first time seal.
- Available FULL bore or STANDARD bore.
- Full material traceability.
- 100% Hydrostatic testing.
- Materials of construction can be supplied to meet the requirements of NACE MR-01-75 latest revision.

VALVE SIZE	F	G	H	I
1/4"-3/4"	27	24	5	27
4 – off M4 x 10 Mounting Holes				

Stainless steel handle as standard

90°   0°
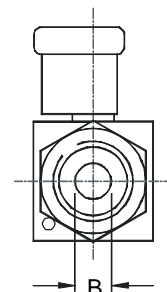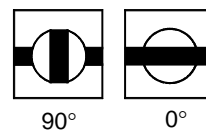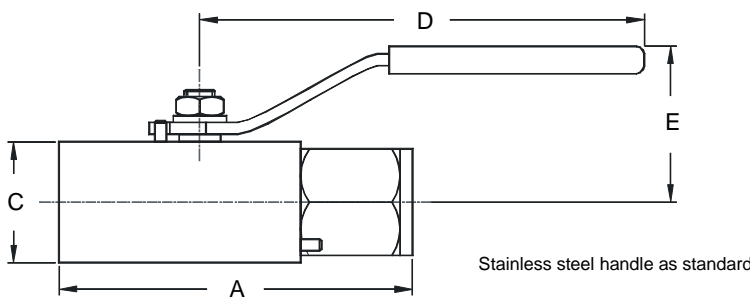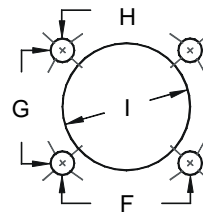
Part Numbers

St/St Part No.	Connections Size	A	B (Bore)	C	D	E	Cv	Kv	Weight (kgs)
UB2NS	1/4" NPT	89	10	32	115	36	2.5	2.2	0.7
UB3NS	3/8" NPT	92	10	32	115	36	3.0	2.6	0.7
UB4NS	1/2" NPT	95	10	32	115	36	4.2	3.6	0.7
UB6NS	3/4" NPT	110	13	38	140	40	7.8	6.7	1.0

For BSPT threads change 'N' to 'T' i.e. UB4TS
For BSPP version change "N" to "P" i.e.UB4PS
Note: check the international standards for pressure limitations of certain threads
before you specify a thread form or end connection
Seat materials: 10,000psi = Peek®   Seal materials: Body = PTFE - Stem = Peek

Dims are in mm (Appx)

See technical section for important additional valve data.

© 1999

Alco Valves
Industrial Valve Manufacturers
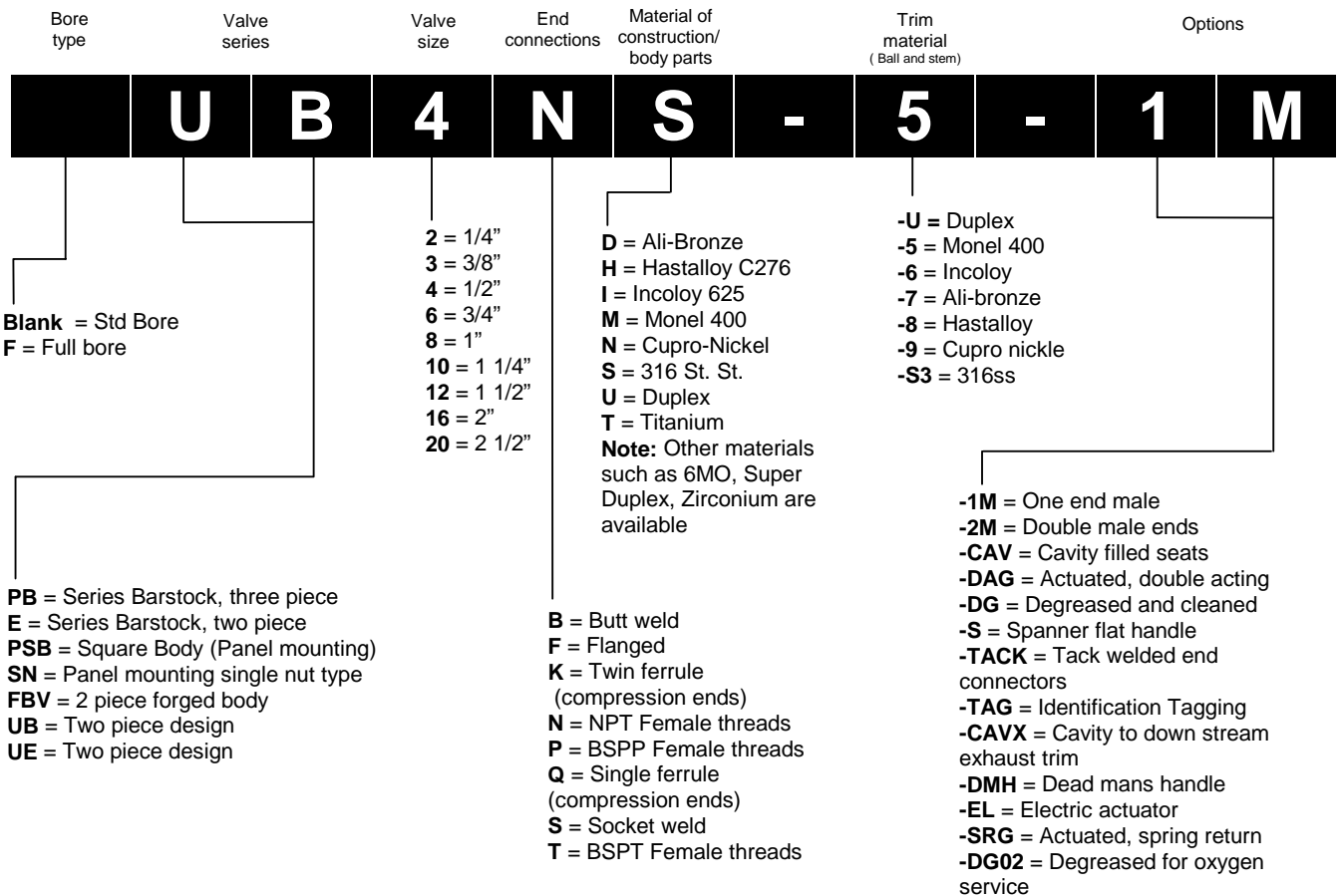
REF: AVCAT2K032

REV: 00

How to order valves 3,000 to 10,000 psi

Our part number system is made up of alphanumeric / generic code system as explained below.
An example is :-

1/2" NPT male x female 316ss 'UB' series ball valve, Monel® trim, lever handle rated 690 BAR (10,000 psi)

The part number shown below is made up using the following system:-

Bore type	Valve series	Valve size	End connections	Material of construction/ body parts	Trim material (Ball and stem)	Options

U B 4 N S - 5 - 1 M

2 = 1/4"
3 = 3/8"
4 = 1/2"
6 = 3/4"
8 = 1"
10 = 1 1/4"
12 = 1 1/2"
16 = 2"
20 = 2 1/2"

D = Ali-Bronze
H = Hastalloy C276
I = Incoloy 625
M = Monel 400
N = Cupro-Nickel
S = 316 St. St.
U = Duplex
T = Titanium
Note: Other materials such as 6MO, Super Duplex, Zirconium are available

-U = Duplex
-5 = Monel 400
-6 = Incoloy
-7 = Ali-bronze
-8 = Hastalloy
-9 = Cupro nickle
-S3 = 316ss

Blank = Std Bore
F = Full bore

-1M = One end male
-2M = Double male ends
-CAV = Cavity filled seats
-DAG = Actuated, double acting
-DG = Degreased and cleaned
-S = Spanner flat handle
-TACK = Tack welded end connectors
-TAG = Identification Tagging
-CAVX = Cavity to down stream exhaust trim
-DMH = Dead mans handle
-EL = Electric actuator
-SRG = Actuated, spring return
-DG02 = Degreased for oxygen service

PB = Series Barstock, three piece
E = Series Barstock, two piece
PSB = Square Body (Panel mounting)
SN = Panel mounting single nut type
FBV = 2 piece forged body
UB = Two piece design
UE = Two piece design

B = Butt weld
F = Flanged
K = Twin ferrule (compression ends)
N = NPT Female threads
P = BSPP Female threads
Q = Single ferrule (compression ends)
S = Socket weld
T = BSPT Female threads

Socket weld and butt weld end connectors may be extended for thermal protection of the valve internals

NOTE 1: The pressure ratings quoted within our literature are maximum hydrostatic pressure ratings for the valves. Certain options available are the products / designs of other manufacturers, Alco valves cannot accept any responsibility for these products unsuitability or failure in service.

NOTE 2: It is always advisable to refer to specific product literature or contact our technical sales department when ordering valves as some of these options are available only on certain styles of valves. Any special end connections such as compression ends or butt / socket weld may limit the rated working pressure of the valve or component supplied in accordance with the relevant specification of design or use of that method of connection. The valve or component will still carry the maximum working pressure markings in accordance with the valve or component design not the connection method as they vary.